NTNU
Norwegian University of
Science and Technology

Characterization of the Uptake and Trafficking of A_vB_3-targeted and Non-targeted Nanoemulsions in Human Endothelial Cells in vitro

Emily Helgesen

Nanotechnology
Submission date: June 2011
Supervisor: Catharina de Lange Davies, IFY

Norwegian University of Science and Technology
Department of Physics

Emily Helgesen

Characterization of the Uptake and Trafficking of $\alpha_v\beta_3$-targeted and Non-targeted Nanoemulsions in Human Endothelial Cells *in vitro*

Master thesis, Spring 2011

Faculty of Natural Sciences and Technology
Department of Physics

Preface

This master thesis at the Norwegian University of Science and Technology was carried out at the Department of Physics, Spring 2011.

I would like to thank my supervisors Catharina de Lange Davies and Sjoerd Hak for superior guidance and assistance throughout the thesis work. Furthermore, I wish to thank Kristin G. Sæterbø for advice and guidance with HUVEC culturing and flow cytometry, Astrid Bjørkøy for technical assistance with the confocal laser scanning microscope, and Øyvind Halaas for advice concerning cellular endocytic processes.

Abstract

RGD-functionalized and non-functionalized oil-in-water nanoemulsions of approximately 100 nm containing DSPC, PEGylated DSPE, cholesterol and Gd-DTPA-DSA at a molar ratio of 1.1/0.15/1/0.75 were prepared. *In vitro* uptake and trafficking in HUVECs of the nanoemulsions was characterized using confocal laser scanning microscopy and flow cytometry. The RGD peptide recognizes $\alpha_v\beta_3$ and $\alpha_v\beta_5$ integrin receptors, which play central roles in angiogenesis. Moreover, the $\alpha_v\beta_3$ integrin receptor is overexpressed in the endothelium of angiogenic tumor vasculature. It was found that the RGD-emulsion showed a remarkably high uptake in HUVECs expressing $\alpha_v\beta_3$ integrins compared to its non-conjugated control version. Furthermore, the RGD-emulsion was able to evade the lysosomes at least within the first 3 hours of incubation, while the control-emulsion was not. The uptake of both emulsions was mainly facilitated by caveolae-mediated endocytosis, but also to a lesser extent by clathrin-mediated endocytosis and other unknown mechanisms. It was shown that RGD and control-emulsions were internalized or sorted into distinct vesicles. Both emulsions bypassed the early endosomes, and it was hypothesized that they were mainly trafficked to caveosomes before subsequent trafficking of control-emulsion to late endosomes/lysosomes and of RGD-emulsion to cis-Golgi or endoplasmatic reticulum. The results suggest that the RGD-emulsion has promising feasibility as a site-specific targetable delivery system.

Contents

1 Introduction **1**

2 Theory **3**

2.1 Nanoparticle Systems and Applications . . . 3
   2.1.1 Drug delivery . . . 6
   2.1.2 Gene Delivery . . . 7
   2.1.3 Photothermal Therapy . . . 8
   2.1.4 Imaging . . . 9
   2.1.5 Multifunctional Nanoparticles . . . 10
2.2 Lipid-based Nanoparticles . . . 11
   2.2.1 Self-assembly Mechanisms of Amphiphiles . . . 11
   2.2.2 Liposomes . . . 12
   2.2.3 Micelles . . . 13
   2.2.4 Oil-in-water Nanoemulsions . . . 14
   2.2.5 Stabilization of Lipid-based Nanoparticles . . . 16
2.3 Nanoparticles and Cancer . . . 17
   2.3.1 The EPR Effect: Passive Targeting . . . 17
   2.3.2 Angiogenesis . . . 18
   2.3.3 The Integrin Receptor and Interaction with RGD-peptides . . . 20
   2.3.4 Increasing Specificity: Active Targeting . . . 22
   2.3.5 The ECM Diffusion Problem . . . 23
2.4 Uptake Mechanisms and Intracellular Trafficking Pathways . . . 24
   2.4.1 Clathrin-mediated Endocytosis . . . 25
   2.4.2 Caveolae-mediated Endocytosis . . . 25
   2.4.3 Macropinocytosis . . . 27
   2.4.4 Clathrin and Caveolae Independent Endocytosis . . . 27
   2.4.5 Uptake and Trafficking of Nanoparticles . . . 28
2.5 Tools for Studying Nanoparticle Cellular Uptake and Trafficking . . . 29
   2.5.1 The use of Fluorophore Markers . . . 29
   2.5.2 Colocalization Coefficients . . . 30
   2.5.3 The use of Endocytic Inhibitors . . . 31
2.6 Experimental Techniques . . . 32
   2.6.1 Dynamic Light Scattering . . . 32

2.6.2 Confocal Laser Scanning Microscopy 33
2.6.3 Flow Cytometry 36

3 Materials and Methods 39
3.1 Materials 39
3.1.1 Nanoemulsions 39
3.1.2 Fluorescent Cell Markers 39
3.1.3 Endocytic Inhibitors 39
3.1.4 Cell Culture 39
3.2 Cell Cultivation 40
3.3 Gelatin Coating 40
3.4 Preparation and Characterization of Nanoemulsions 41
3.4.1 Synthesis 41
3.4.2 RGD-conjugation 42
3.4.3 Characterization by DLS 42
3.4.4 Calculating Concentrations 43
3.5 Experimental Assays and Setup for CLSM 44
3.5.1 Test Experiment for Studying Emulsion Uptake in Cells 44
3.5.2 Investigating Optimal Incubation Times for RGD versus Control Emulsions 45
3.5.3 Lysosome Staining Using LysoTracker 45
3.5.4 Early Endosome Staining Using CellLight Rab5-GFP 46
3.5.5 Early Endosome Staining Using Transferrin-Alexa Fluor 488 . . . 46
3.5.6 Cells Incubated with Both Emulsion Types Simultaneously 46
3.6 Experimental Assays and Setup for Flow Cytometry 47
3.6.1 Investigating the Effect of RGD-dialysis 47
3.6.2 Chlorpromazine and Genistein Endocytic Inhibition 47
3.7 Data Analysis and Image Handling 49
3.7.1 ImageJ 49
3.7.2 Amira 49
3.7.3 Kaluza 49
3.7.4 Statistics 49

4 Results 51
4.1 Characterization by DLS 51
4.2 CLSM Experiments 53
4.2.1 Test Experiment for Studying Emulsion Uptake in Cells 53
4.2.2 Investigating Optimal Incubation Times for RGD versus Control Emulsions 55
4.2.3 Lysosome Staining Using LysoTracker 58
4.2.4 Early Endosome Staining Using CellLight Rab5-GFP 62
4.2.5 Early Endosome Staining Using Transferrin-Alexa Fluor 488 . . . 63
4.2.6 Cells Incubated with Both Emulsion Types Simultaneously 66
4.3 Flow Cytometry Experiments 70

4.3.1 Investigating the Effect of RGD-Dialysis 70
4.3.2 Chlorpromazine and Genistein Endocytic Inhibition 72

5 Discussion 77
5.1 Characterization by DLS 77
5.2 CLSM Experiments 78
5.2.1 Investigating Optimal Incubation times of RGD versus Control Emulsions 78
5.2.2 Trafficking to Lysosomes 79
5.2.3 Trafficking to Early Endosomes 81
5.2.4 Cells Incubated with Both Emulsion Types Simultaneously 83
5.3 Flow Cytometry Experiments 85
5.3.1 Investigating the Effect of RGD-Dialysis 85
5.3.2 Chlorpromazine and Genistein Endocytic Inhibition 85
5.4 Overview of Possible Trafficking Pathways 87
5.5 Implications and Further Work 89

6 Conclusion 91

Bibliography 93

Appendix 103

List of Figures

2.1 Illustration of *some* typical NP platforms [5]. 4
2.2 Common limitations associated with delivery of free drugs, and suggestions of how drug delivery systems (DDS) may offer possible solutions [28]. 7
2.3 Schematic illustration of multifunctional NP with iron oxide nanocrystals encapsulated within mesoporous silica, hydrophobic anticancer drug stored inside the pores, and surface modifications with phosphonate and folic acid targeting ligands [34]. 10
2.4 The molecular structure of a typical phospholipid. 12
2.5 Illustration of some of the aggregates lipids can form. 12
2.6 Schematic illustration of how the shape of a lipid can be used to predict what kind of aggregate it will form. 13
2.7 Illustration of the process of making an o/w nanoemulsion [55]. 14
2.8 Multifunctional o/w NP with DSPC, DSPE-PEG and cholesterol surrounding an oil core. Fluorescent probes NIR and Rhodamine are included, and also some percentage of gadolinium conjugated lipids (Gd-DTPA-DSA). Fluorescent probes enable visualization in optical microscopes, and the latter in MRI. Additionally, an RGD peptide is displayed on the surface, to obtain increased specificity towards endothelial cells in cancer tissue [56]. 15
2.9 Schematic illustration of how increased amounts of angiogenic factors from cancer cells activate normal endothelial cells, which onsets a process that further stimulate tumor growth and angiogenesis. Paracrine stimulation: stimulation by nearby cells, autocrine stimulation: stimulation by the cells own growth factors. VEGF = vascular endothelial growth factor; FGF = fibroblast growth factor; PDGF = platelet-derived growth factor [66]. . . 19
2.10 Integrins expressed in tumour cells contribute to tumour progression and metastasis by increasing tumour cell migration, invasion, proliferation and survival [69]. 20
2.11 Illustration of how circulating NPs in plasma may extravasate into tumor tissue through leaky vasculature and further enter specific cells via ligand tags. By using NPs as carriers, the intracellular concentration of the drug may become high enough to overcome drug resistance by efflux pumps [26]. 22

2.12 Illustration of the different types of known entry portals into mammalian cells. Essentially, the endocytic pathways differ for vesicles with different formation mechanisms and sizes, and with different types of content [80]. 24

2.13 Intracellular pathways of various substances after uptake in caveolae and clathrin-coated pits. The trafficking depends on the substance internalized, and question marks indicate that there is a large uncertainty concerning other possible pathways for caveosome sorting. 26

2.14 Schematic diagram of the optical pathway and principal components in a confocal laser scanning microscope [102]. 34

2.15 Image aquired by a conventional optical microscope (a) versus a confocal laser scanning microscope (b) [102]. 35

2.16 Schematic diagram of the optical pathway and principal components in a flow cytometer [106]. 37

2.17 A typical histogram for the logarithmic fluorescence intensity in a population, compared autofluorescence of the control population. The y-axis represents the number of objects (counts), while the x-axis represents the fluorescence intensity. 38

4.1 A typical size distribution curve for an emulsion of 100 nm expected size, aquired from the DLS software system. 52

4.2 CLSM images of HUVECs with cell membrane staining (green), nucleus staining (blue) and emulsion (red). (a): RGD-emulsion, (b): control-emulsion, (c) and (d): overlays of cell membrane and nucleus staining, (e) and (f): overlays of cell membrane staining, nucleus staining and emulsion for RGD and control-emulsions respectively. The green "vesicles" seen near the nucleus in (c) and (e) are parts of the cell membrane containing CellMask Orange that have been internalized after incubation. Both emulsions were incubated with cells for 3 hours, and it is clear that the uptake of RGD-emulsion is substantially larger than for control-emulsion. 54

4.3 Cells incubated with control-emulsion for 20 minutes, 1 hour, 2 hours, 2.5 hours and 3 hours. It can be seen that the uptake amount is substantial after approximately 2.5 - 3 hours. 56

4.4 HUVECs incubated with RGD-emulsion for 10 minutes, 20 minutes, 40 minutes and 1 hour. The uptake was substantial already after 20 minutes. 57

4.5 Representative images taken 5 minutes, 1 hour, 2 hours and 24 hours after incubation time with RGD and control-emulsions. The red spots represent the emulsions, whereas the green spots represent lysosomes stained by LysoTracker. A high degree of colocalization (yellow spots) can be seen for control-emulsions already 5 minutes after incubation. After 24 hours the colocalization of the RGD-emulsion in lysosomes is similar to that of control-emulsion. An image that show the RGD-emulsion 3 hours after incubation is also included, in order to compare it with that of control-emulsions imaged shortly after incubation (as the emulsions have been trafficked inside the cells for the same amount of time at this point). . . 59

4.6 3-dimensional images generated from Z-stacks of imaged cells incubated with LysoTracker plus RGD-emulsion and control-emulsion respectively. The images were taken directly after incubation. The emulsions can be seen in red, whereas lysosomes are marked as green. The control-emulsion seem to be more closely associated with the lysosomes. The bottom row shows images of the same cells as the first row, only zoomed in at areas near the nucleus. 60

4.7 Quantitative analysis of colocalization of emulsion in lysosomes (M1), and lysosomes in emulsion (M2). Manders coefficient values were averaged over a selection of 18 images. 1 represent perfect colocalization overlap, whereas 0 represent no colocalization. The control-emulsion is colocalized with lysosomes (and vice versa) to a larger extent than the RGD-emulsion in the first 3 hours after incubation. After 24 hours the colocalization is more similar for both emulsion types. T-testing showed that the difference in RGD-emulsion colocalization between the two time periods was significant (p-value of 0.041), while the difference for control-emulsion was not (p-value of 0.273). 61

4.8 CLSM images of HUVECs with Rab5-GFP staining of early endosomes (green) and emulsion (red). (a): cells incubated with RGD-emulsion (20 min), (b): cells incubated with control-emulsion (3 h). Almost no uptake of RGD-emulsion was observed. 62

4.9 CLSM images of HUVECs with transferrin-Alexa Fluor 488 staining of early endosomes (green) and emulsion (red). (a): RGD-emulsion and transferrin-Alexa Fluor (10 μg/ml) with corresponding DIC image (b), (c): control-emulsion and transferrin-Alexa Fluor (10 μg/ml) with corresponding DIC image (d). Two lower concentrations of transferrin-Alexa Fluor 488 were used along with a higher concentration of emulsion (2mM) for samples with control-emulsion, in order to incubate the cells with control-emulsion and staining for the same time period (45 minutes). (e): control-emulsion and transferrin-Alexa Fluor (2.5 μg/ml), (f):control-emulsion and transferrin-Alexa Fluor (5 μg/ml). 64

4.10 Quantitative analysis of colocalization of emulsion in early endosomes (M1), and early endosomes in emulsion (M2). Manders coefficient values were averaged over a selection of 14 images. 1 represent perfect colocalization overlap, whereas 0 represent no colocalization. The colocalization of both emulsions in early endosomes was low. T-testing showed that the difference in RGD and control-emulsion in early endosomes was not significant (p-value of 0.771). 65

4.11 CLSM images of cells incubated with RGD (red) and control-emulsion (green) simultaneously. Little colocalization was seen visually directly after incubation, but increased with time. 2 hours after incubation, it was possible to see that vesicles of RGD and control-emulsion were fusing together, as highlighted by pink squares. 67

4.12 3-dimensional images generated from Z-stacks of cells incubated with RGD (red) and control-emulsion (green) simultaneously. The control-emulsion is localized to the periphery of the cell to a larger degree than the RGD-emulsion. Image (a) shows an overview over the cell, while the periphery of the cell is zoomed in in image (b). In image (c), vesicles of RGD and control-emulsion near the perinuclear region are seen. They seem to be associated. 68

4.13 Quantitative analysis of colocalization of RGD-emulsion in control-emulsion (M1), and of control-emulsion in RGD-emulsion (M2). The analysis was done of images from two different time periods: 0-45 minutes after incubation and 2 hours after incubation. Manders coefficient values averaged over a selection of 5 images were used to generate the charts. 1 represent perfect colocalization, whereas 0 represent no colocalization. From t-tests it was found that the colocalization of RGD-emulsion in control-emulsion increased substantially with time. 69

4.14 Uptake amount of dialyzed versus non-dialyzed RGD-emulsion. The values of the columns represent the average fluorescence intensity medians from flow cytometry experiments, normalized by the fluorescence intensity median of untreated cells (autofluorescence). Columns for uptake in all cells and in positive cells (cells with emulsion uptake) can be seen separately. 70

4.15 Representative logarithmic histograms obtained in flow cytometry from samples with dialyzed and non-dialyzed RGD-emulsion. The cellular uptake of dialyzed RGD-emulsion is approximately 1.6 times higher than the non-dialyzed RGD-emulsion. 71

4.16 Uptake studies of cells incubated with emulsions and endocytic inhibitors. The values of the columns represent the average fluorescence intensity medians from flow cytometry experiments, normalized to the fluorescence intensity median of untreated cells (autofluorescence). Chlorpromazine is an inhibitor of clathrin-mediated uptake, whereas genistein is an inhibitor of caveolae-mediated uptake. Charts were generated for uptake in all cells (top) and in uptake positive cells (bottom)separately. 73
4.17 Representative histograms obtained in flow cytometry from cells incubated with RGD-emulsion and inhibitors (a), and control-emulsion and inhibitors (b). Histograms that show the difference in uptake of RGD and control-emulsion are also included (c). 74
4.18 The amount of positive cells in each sample type relative to the total number of cells in the sample, in %. The number of positive cells in samples with control-emulsion is more greatly affected by inhibitors than for samples with RGD-emulsions. The percentage of positive cells is reduced to 70.9 % for control-emulsion/genistein, which means that approximately 27 % of all cells are completely inhibited by genistein in this sample. . . . 75

5.1 Illustration that summarize events along the endocytosis pathways of caveolae-mediated, clathrin-mediated and clathrin and caveolae independent endocytosis. The trafficking pathways of the transferrin receptor (TfR) and $\alpha_v\beta_3$ integrin receptor are included. Abbreviations: EE=early endosomes, LE=late endosomes, ER=endoplasmatic reticulum, PNRC= perinuclear recycling compartment. 82
5.2 Illustration that summarize events along the endocytosis pathways of caveolae-mediated, clathrin-mediated and clathrin and caveolae independent endocytosis, and that indicate possible uptake and trafficking pathways for RGD and control-emulsions. The trafficking pathways of the transferrin receptor (TfR) and $\alpha_v\beta_3$ integrin receptor are included. Symbols containing an S (small) indicate that this involves only small amounts of emulsion. Abbreviations: EE=early endosomes, LE=late endosomes, ER=endoplasmatic reticulum, PNRC= perinuclear recycling compartment. 87

6.1 Scatterplot of FS vs. SS that shows how cells were gated to avoid dead cells, debris and cell clusters in results for flow cytometry experiments. Approximately 90% of all cells were gated. 103
6.2 Histograms of fluorescence intensity vs. count that show how a boundary line was set to define cells that were positive for emulsion uptake (positive cells lie within the line marked by P). The threshold for the line was set to approximately 6-7 in fluorescence intensity. Fluorescence intensity below the line was considered to be autofluorescence. 104

List of Tables

2.1 *Examples that illustrate the wide variety of NP systems in pre-clinical development.* 5

3.1 *Amounts used of the different compounds for making 100 nm sized nanoemulsions.* 41

4.1 *Values from DLS analysis of the nanoemulsions used in this thesis.* 52
4.2 *Overview over the purpose and results of different experiments conducted, with reference to correlated figures.* 76

Chapter 1

Introduction

In the past two decades, there has been a progressively increasing interest for nanoparticles (NPs) as therapeutic and diagnostic tools, and the number of commercially available products is constantly growing [1]. The interest for NPs is based on the fact that they offer possible solutions to current limitations in diagnosis, treatment and management of many human diseases [2, 3]. For example, most conventional anticancer treatments involve severe toxic side effects upon systemic administration. By incorporating anticancer agents into NPs, these side effects can become less prominent [3, 4, 5].)

In principle, the true potential of NPs lies within the fact that their size, dispersibility, specificity, blood circulation time, immunogenicity and degradation characteristics can be tuned to achieve a desired effect in a physiological system [6, 7]. In the case of drug delivery, it is important that the NPs possess characteristics that allow the drug to circulate for extended periods of time without being eliminated by the reticuloendothelial system (RES). Such properties can be achieved by functionalizing the surface of the NPs with polymers that provide colloidal stability of the NPs in plasma, and that give improved stealth properties and prevent adherence of plasma proteins. PEG (polyethylene glycol) is a polymer commonly employed for this purpose [8]. However, the NPs must also allow release of the drug at the target site, which means that the NP material should be of biodegradable character [7]. Moreover, NPs can be functionalized with targeting ligands that match disease-specific receptors on target cells. This can be useful for several purposes. For example, NPs incorporated with imaging agents can bind to disease cells and provide an early diagnostic evaluation, or NPs incorporated with drugs can ensure a more site-specific pharmaceutic effect. Additionally, several functionalities can be combined within one single construct, to yield multifunctional NPs [3, 9, 10]. One ligand commonly employed for site specific interactions are peptides containing cyclic RGD (Arg-Gly-Asp) sequences. RGD selectively recognizes $\alpha_v\beta_3$ and $\alpha_v\beta_5$ integrins, and the $\alpha_v\beta_3$ integrin is overexpressed by tumor endothelial cells [3, 10].

One type of NP currently investigated for imaging and drug delivery purposes, is lipid oil-in-water nanoemulsions. These emulsions consist of an oil core surrounded by DSPC, DSPE-PEG and cholesterol lipids. The design of the nanoemulsion allows for inclusion of various compounds, such as MRI imaging agents and/or hydrophobic drugs.

Furthermore, the lipids can be conjugated to fluorophores that enable optical imaging, or to site-specific ligands that increase the specificity of the emulsion [10, 11, 12].

In this study, the uptake and trafficking of 100 nm sized lipid oil-in-water nanoemulsions has been characterized *in vitro*. Two types of emulsions were used: one with RGD-peptides conjugated to the surface, and one non-conjugated control-emulsion. As a model system, human umbilical vein endothelial cells (HUVECs) that express $\alpha_v\beta_3$ integrins were used. The goal of the study can be divided into two aims: 1) to elucidate how the RGD-conjugation affects emulsion uptake in HUVECs compared to that of control-emulsions, and 2) what kind of endocytic uptake and trafficking pathways the two respective emulsion types employ.

Chapter 2

Theory

2.1 Nanoparticle Systems and Applications

A wide variety of nanoparticle systems are under development today, all designed with specific applications in mind. Such systems have huge potentials in the field of medical and biological technologies. One of the major advantages of NPs is their size, which per definition lies between 1 and 100 nm [3, 4, 13]. Size-effects can be exploited in several ways. For example, a typical protein is at the same size as the smallest manmade NPs (around 5 nm). This gives the opportunity to use NPs as probes for studying cellular machinery in a non-invasive way [13]. As for larger NPs, an advantageous property may be the ability to accumulate in tumor tissue, due to the leaky nature of tumor vasculature [3, 4]. Furthermore, NPs can be modified and functionalized in a number of ways to improve or introduce properties, such as specificity, stability and biocompatibility [3, 8, 13]. For example, the size, shape and charge can be tailored. Moreover, the surface can be functionalized with PEG (polyethylene glycol) to improve stability and/or ligands to improve specificity [3, 8]. Figure 1 visualizes some general NP platforms, while a list with concrete examples of systems in pre-clinical development can be seen in table 1.

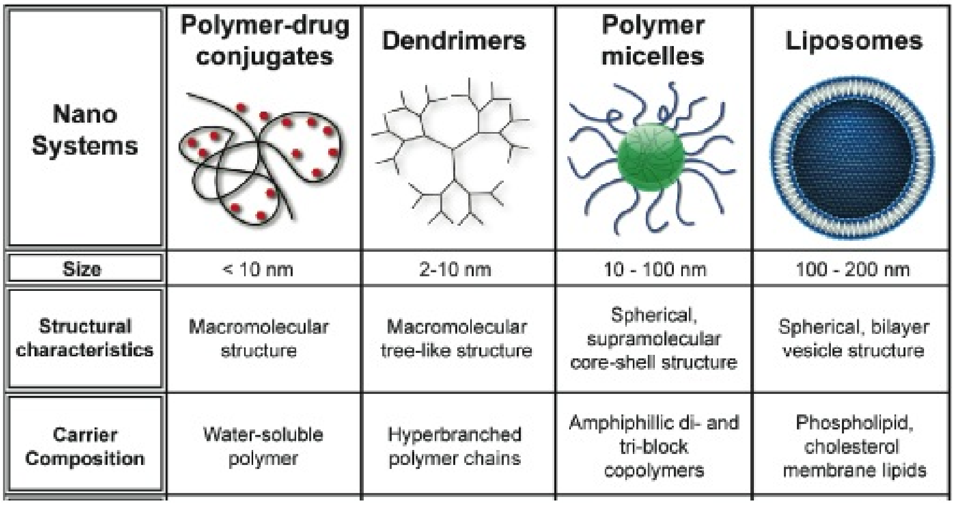

Nano Systems	Polymer-drug conjugates	Dendrimers	Polymer micelles	Liposomes
Size	< 10 nm	2-10 nm	10 - 100 nm	100 - 200 nm
Structural characteristics	Macromolecular structure	Macromolecular tree-like structure	Spherical, supramolecular core-shell structure	Spherical, bilayer vesicle structure
Carrier Composition	Water-soluble polymer	Hyperbranched polymer chains	Amphiphillic di- and tri-block copolymers	Phospholipid, cholesterol membrane lipids

Figure 2.1: Illustration of *some* typical NP platforms [5].

Table 2.1: *Examples that illustrate the wide variety of NP systems in pre-clinical development.*

Type of System	**Application**	**Target**	**Reference**
Dendrimers			
Folic acid PAMAM dendrimers	Drug delivery of Methotrexate	Epithelial cancer	[14]
Ligand conjugated PEG-Poly-L-lysine dendrimers	Drug delivery of Chloroquine Phosphate	Malaria	[15]
Polymer micelles			
Polymer-lipid NPs	Drug delivery of Doxorubicin	Solid tumors	[16]
Biotinylated antibody-conjugated polymeric micelles	Drug delivery of Daunomycin	Brain	[17]
Liposomal NPs			
CpG ODN liposomal NP	Delivery of immuno-stimulatory ODN	Immune cells	[18]
SN-38 liposomal NP	Drug delivery of SN-38	Solid tumors	[19]
Nanoemulsions			
Iron oxide core oil-in-water nanoemulsion	Targeting and Imaging	Solid tumors	[11]
Virus-based NPs			
Adenovirus captured in lipid bilayers	Gene therapy	Various	[20]
Gold-conjugated cytomegalovirus	Photothermal therapy and gene therapy	Solid tumors	[21]
DNA-NPs			
Chitosan/DNA polyplexes	Gene therapy	Various	[22]
PEG-stabilized DNA	Gene therapy	Cystic fibrosis	[23]
Metallic NPs			
Anti-HER2 antibody-targeted gold/silicon NP	Photohermal therapy	Breast cancer	[24]
Ceramic NPs			
Silica crosslinked block copolymer micelles	Imaging and chemotherapy	Various	[25]

PAMAM: polyamidoamine, PEG: polyethylene glycol, CpG: Cytosine-guanine, ODN: Oligodeoxynucleotides, SN-38: 7-ethyl-10-hydroxycamptothecin

2.1.1 Drug delivery

Drug delivery is an important application of NP systems, and approximately 76% of all nanomedicine publications deal with this topic [1]. In theory, NP drug delivery can be applied to a wide variety of disorders, but the most frequently investigated one in this aspect is cancer [3, 4, 5, 9, 10]. The goal of delivering medicines by the aid of NPs is to improve the therapeutic effect of the incorporated drug. For example, the drug can be protected against systemic degradation and elimination. In that matter, the drug can be allowed to circulate for extended periods of time and reach the target site. This means that properties needed for a specific pharmacokinetic effect are mainly dependent on the characteristics of the NP, and not limited by the drug itself [4]. When it comes to hydrophobic drugs, the protection effect is especially important because many of these drugs cannot be used effectively *in vivo* due to rapid elimination by the reticuloendothelial system [8]. Moreover, large amounts of drugs can be loaded into one particle, which can increase the local concentration of the drug at the target site [26]. Last but not least, the NPs can be surface functionalized to introduce new properties or improve already existing properties [3, 5, 9, 10].

One important surface modification that is utilized by many NP systems is the conjugation of PEG. PEG is a flexible, hydrophilic polymer that can give a brush-like effect on the surface of NPs. In that matter, it improves stealth properties of the NP and prevents plasma proteins to adhere. As adherent plasma proteins can tag the NP for destruction, the conjugation of PEG can significantly enhance NP's lifetime in circulation. PEG have shown large enhancement of circulation times for many types of NPs. PEGylated liposomes are one example of LNPs that showed increased circulation times in mice, rats, dogs and humans [8, 27].

Some drug delivery systems are already on the market, such as liposome-encapsulated doxorubicin (Doxil) [1]. Examples of drug delivery systems in development can be found in table 1. One of them is the delivery of methotrexate to tumors by the help of dendrimers. Kukowska-Latallo et al. showed that PAMAM-dendrimers conjugated to folic acid accumulated in tumors over a period of 4 days, and significantly increased the anti-tumor activity while reducing toxic side effects of methotrexate. The targeting of dendrimers by conjugation to folic acid played a central role in these experiments, as the non-targeted control version was cleared from the system after only 2 hours (not enough time for substantial tumor accumulation). The advantage of using folic acid is that the folic acid receptor is upregulated on several types of cancer cells and internalized once a ligand is bound. A more general advantage of dendrimers is that they can be made extremely small (2-10 nm). This gives them the ability to diffuse more easily in the extracellular matrix of a tumor [14].

Figure 2.2 indicate how drug delivery systems (DDS) can solve common problems associated with administration of free drugs [28].

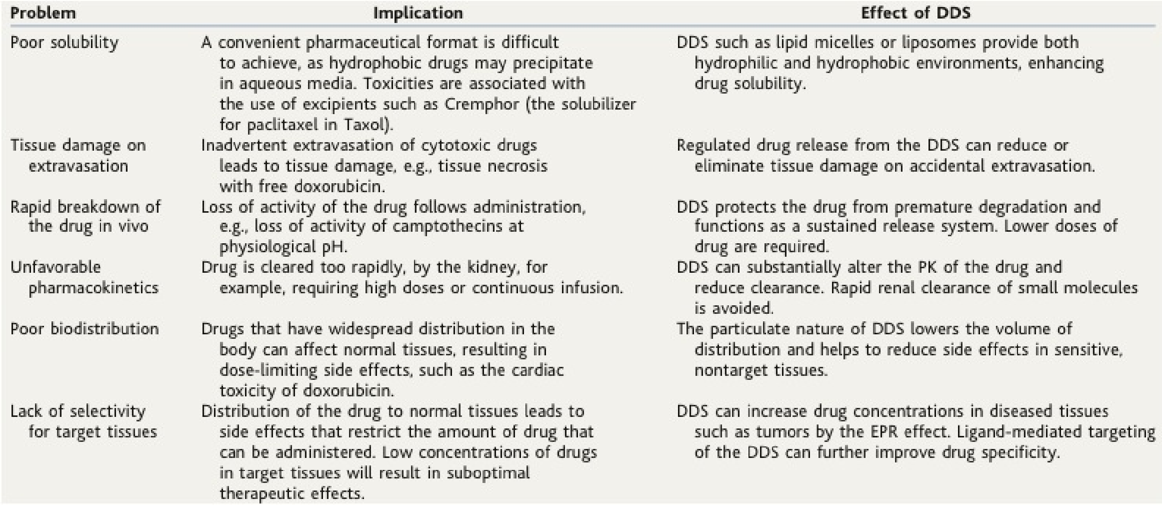

Problem	Implication	Effect of DDS
Poor solubility	A convenient pharmaceutical format is difficult to achieve, as hydrophobic drugs may precipitate in aqueous media. Toxicities are associated with the use of excipients such as Cremphor (the solubilizer for paclitaxel in Taxol).	DDS such as lipid micelles or liposomes provide both hydrophilic and hydrophobic environments, enhancing drug solubility.
Tissue damage on extravasation	Inadvertent extravasation of cytotoxic drugs leads to tissue damage, e.g., tissue necrosis with free doxorubicin.	Regulated drug release from the DDS can reduce or eliminate tissue damage on accidental extravasation.
Rapid breakdown of the drug in vivo	Loss of activity of the drug follows administration, e.g., loss of activity of camptothecins at physiological pH.	DDS protects the drug from premature degradation and functions as a sustained release system. Lower doses of drug are required.
Unfavorable pharmacokinetics	Drug is cleared too rapidly, by the kidney, for example, requiring high doses or continuous infusion.	DDS can substantially alter the PK of the drug and reduce clearance. Rapid renal clearance of small molecules is avoided.
Poor biodistribution	Drugs that have widespread distribution in the body can affect normal tissues, resulting in dose-limiting side effects, such as the cardiac toxicity of doxorubicin.	The particulate nature of DDS lowers the volume of distribution and helps to reduce side effects in sensitive, nontarget tissues.
Lack of selectivity for target tissues	Distribution of the drug to normal tissues leads to side effects that restrict the amount of drug that can be administered. Low concentrations of drugs in target tissues will result in suboptimal therapeutic effects.	DDS can increase drug concentrations in diseased tissues such as tumors by the EPR effect. Ligand-mediated targeting of the DDS can further improve drug specificity.

Figure 2.2: Common limitations associated with delivery of free drugs, and suggestions of how drug delivery systems (DDS) may offer possible solutions [28].

2.1.2 Gene Delivery

For developing gene delivery systems, viral particles have been widely used. This is because viruses cleverly enter and transfect cells with high efficiency [29]. However, viral vectors can induce severe immunological responses in the host, and deaths have occurred in human clinical trials [30]. Unwanted effects such as immune system induction need to be prevented in order to safely use viral vectors in gene therapy, and nanotechnology offers possible solutions. For example, the surface of the virus can be covered with lipid bilayers to mask the proteins that normally onset immune reactions. This has been done by Singh et al., using adenovirus particles. By simply including the virus particles when hydrating a lipid film, lipid bilayers was shown to spontaneously form around them. The transfection efficiency was delayed because the lipid bilayer inhibited binding to adenovirus receptors on cells, but the experiments demonstrate the possibility to systemically administer viral NPs without immune system induction and degradation [20].

Even though viruses efficiently deliver genetic payloads, synthetic vectors based on NP platforms may offer more controllable parameters considering safety. Strand et al. are working on developing NP systems for gene delivery based on chitosan. Chitosans are cationic polysaccharides with an excellent safety profile. They spontaneously self-assemble with nucleic acids to form NPs, and those constructs are able to induce trans-gene expression. By studying structure-function relationships of many different types of chitosans, it is possible to tailor them to exhibit optimal properties for specific applications [22].

2.1.3 Photothermal Therapy

Photothermal therapy (PTT) is investigated as a method to treat tumor tissue by inducing heat that irreversibly damages cancer cells. This is done by using electromagnetic radiation to excite a sensitive material to a vibrational state within a biological system. When relaxing from the excited state, these materials release heat that kill cancer cells locally. In contrast to conventional surgical treatment of solid tumors, PTT offers the ability to treat small, poorly defined metastases embedded within vital regions, in a non-invasive and highly specific way [31].

Electromagnetic radiation typically used for PTT is radiation in the infrared region. Previously, materials used for PTT included natural chromophores in tissue or externally added dyes. However, these materials suffered from low absorption and photobleaching [31].

Several materials are now being investigated for PTT purposes, amongst them carbon nanotubes, gold NPs, gold nanoshells and gold nanorods. The common denominator of these particles is that they readily absorb radiation in the infrared or near-infrared region, and efficiently release heat as they relax from their excited state. Additionally, they can be functionalized to increase stability and improve specificity to the target tissue [31, 32]. One example is provided by Hirsch et al. They showed that silica NPs covered by a shell of gold induced irreversible tumor damage within 4-6 minutes, when exposed to low doses of near infrared light (820 nm) *in vivo* [24]. Similarly, Zhou et al. showed that single-walled carbon nanotubes conjugated to folate effectively enhanced the photothermal destruction on tumor cells, while sparing normal cells [32].

2.1.4 Imaging

For the development of therapeutic NP delivery systems, non-invasive imaging technologies play a key role, since they allow one to follow the fate of NPs inside biological systems like cells, tissues or whole organisms. Furthermore, such technologies can allow monitoring of physiological and molecular changes for diagnostic purposes. Common technologies utilized today are molecular resonance imaging (MRI) and ultrasound [10, 33].

Nanoparticle platforms offer great advancement for non-invasive imaging technologies, although very few systems are given commercial effort compared to systems for drug delivery [1]. By incorporating contrast generating materials, such as quantum dots, paramagnetic materials, superparamagnetic materials, gas bubbles or fluorescent dyes into NPs, imaging can be done with enhanced specificity [11, 12, 33, 34]. There are a number of possibilities for these NP constructs. For MRI, aggregates consisting of gadolinium-conjugated lipids and iron oxide NPs coated with hydrophilic layers are *some* of the possibilities [12, 35]. However, encapsulating the contrast generating material in another type of NP offers additional advantages. Mulder et al. showed that by encapsulating iron oxide NPs in oil core of a lipid oil-in-water nanoemulsion, the contrast agent was rendered stabile in circulation and allowed accumulation in tumor tissue. Due to high payloads of iron oxide in the emulsion, the transverse relaxivity was high enough for T_2 weighted MRI. Additionally, the lipids on the surface could be conjugated with other substances, such as fluorophores. This enabled *in vivo* fluorescence imaging to determine pharmacokinetic profile and organ distribution [11].

For ultrasound, examples such as lipid coated perfluorocarbon nanodroplets, acoustic liposomes, microbubbles, PLA nanobubbles and solid PLA NPs can be mentioned [33, 36, 37, 38]. Nanosized particles are not theoretically as echogenic as microbubbles, but when targeted with a ligand they can be deposited as layers at the target site. This can generate sufficient contrast, and may be advantageous for localizing disease specific areas *in vivo* [33].

2.1.5 Multifunctional Nanoparticles

As indicated in previous sections, NP systems can exploit several properties and functionalities, such as the described system for drug delivery by the aid of folic acid (section 2.1.1). This means that one NP system can be used for *several* applications at the same time. For example, a NP system can actively target a disease site, deliver a drug, and contain an imaging label. NPs that combine different functionalities in a single stable construct are called multifunctional nanoparticles [39].

Liong et al. developed a multifunctional NP system based on mesoporous silica NPs, shown in figure 2.3. By incorporating iron oxide nanocrystals and anticancer drug, while functionalizing the surface of the NP with folic acid and phosphonate, both targeted drug delivery and MRI of the agent was possible. The phosphonate made the particles hydrophilic, and prevented aggregation in solution. It was also demonstrated that fluorescent molecules could be added to the system to introduce the possibility of fluorescence imaging [34].

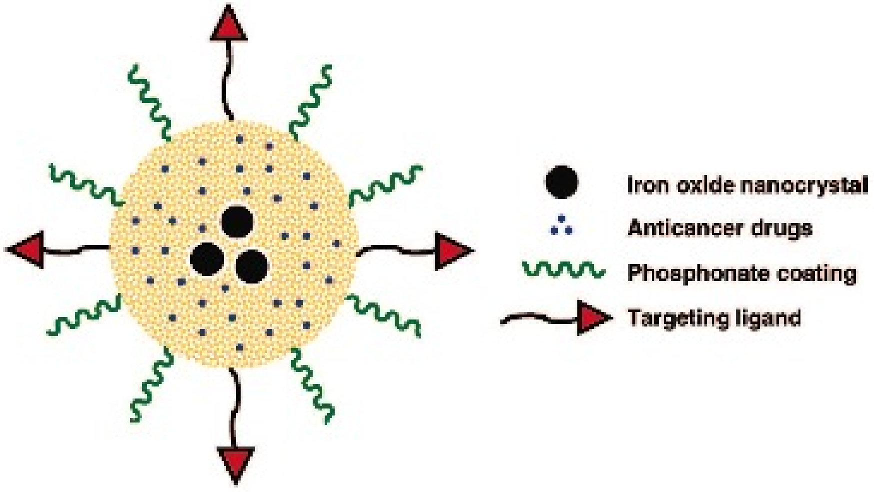

Figure 2.3: Schematic illustration of multifunctional NP with iron oxide nanocrystals encapsulated within mesoporous silica, hydrophobic anticancer drug stored inside the pores, and surface modifications with phosphonate and folic acid targeting ligands [34].

2.2 Lipid-based Nanoparticles

Lipid-based nanoparticles (LNPs) can be described as particles that consist of an outer shell of lipids. The use of lipids creates a biocompatible barrier against a physiological environment, and can significantly improve important properties of the encapsulated agent(s), such as pharmacokinetic profile and specificity. Aspects concerning LNP formation are described below. Sections 2.2.1 and 2.2.4 were taken from previously elaborated project work [40].

2.2.1 Self-assembly Mechanisms of Amphiphiles

An amphiphilic molecule is a molecule that has one hydrophilic polar end, and one hydrophobic nonpolar end. When put in contact with an aqueous liquid, such molecules tend to orient themselves so that the hydrophobic end is shielded from water. In that way, the total nonpolar surface exposed to water is reduced, and an entropy favored, spontaneous self-assembly process of amphiphiles has occurred. Phospholipids, which contain two fatty acyl chains and one phosphate head group, exist in biological membranes and are perhaps the most well known type of amphiphile. Its structure is shown in figure 2.4. However, many types of lipids and also other molecules can be involved in complex self-assembly mechanisms. In general, amphiphiles are able to form very diverse fluid crystalline structures. The type of structure formed depends largely on the shape, charge and concentration of the lipid molecules, as well as the pH and salt concentration of the solution. For example, amphiphiles can exist as single molecules when present in very low concentrations in aqueous liquid, but over a certain concentration, the critical aggregation concentration, they start to form aggregates. In very high concentrations, even cubic, lamellar and hexagonal phases are observed. In terms of lipid self-assembly, different types of NP aggregates can be micelles, liposomes and bilayers sheets, as seen in figure 2.5. More complex structures can also be formed, such as rod-like micelles and disc-like micelles [41, 42, 43].

The shape of the lipids can be used to predict what kind of aggregate they will form. For example, in order to form micelles, each lipid must fit into a cone shape so that the hydrophilic head is wider than the hydrophobic tail. When forming lipid bilayers, on the other hand, the volume of the tail region is much larger, and looks similar to the shape of a cylinder. Its circular cross section is then comparable to the cross section of the head group, as is often the case for phospholipids with two acyl chains. The shape of a micelle forming lipid and a bilayer-forming lipid is shown in figure 2.6 [44, 42, 45].

In general, the larger the volume of the tail region of an amphiphile, the higher the hydrophobic cost of exposing its surface to water. Following this, self-assembly into bilayers is more avid than self-assembly into micelles. It should be noted that aggregate prediction based on shape usually is used for single component systems, and does not necessarily work for systems containing different types of amphiphiles. As mentioned, the lipid concentration, salt concentration and pH also affect which aggregates are formed [41, 45].

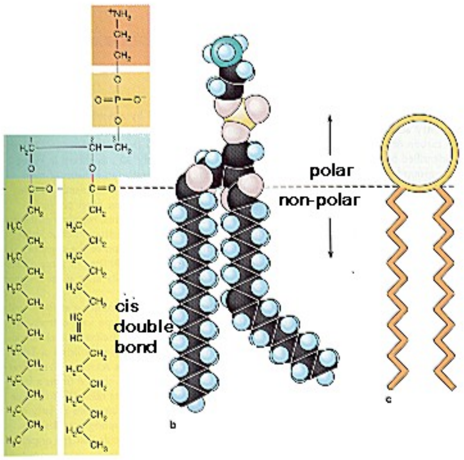

Figure 2.4: The molecular structure of a typical phospholipid.

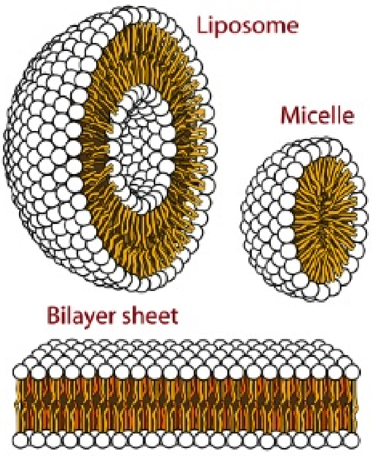

Figure 2.5: Illustration of some of the aggregates lipids can form.

2.2.2 Liposomes

Liposomes are structures that readily self-assemble due to the mechanism explained above, and can be seen in figure 2.5. Self-assembly of liposomes is a two-step process, where the lipids firstly form bilayers and then closes off to form vesicles with an aqueous core environment [46]. The diameter of liposomes normally lies between 800 and 50 nm, and they have been investigated as vehicles for transportation of various materials *in vitro* and *in vivo* since their discovery in 1965 [12, 47, 48, 49, 50, 51]. During the recent years, there have been major advances within the field of liposome- mediated delivery, and some products can be found on the market [1, 28]. The majority of liposomes on the market are liposomes that encapsulate chemotherapeutics or antifungal agents

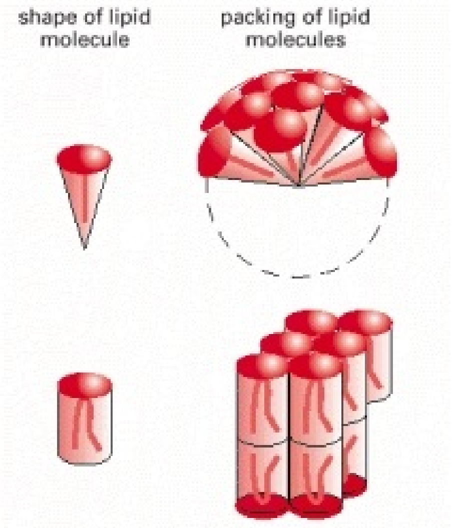

Figure 2.6: Schematic illustration of how the shape of a lipid can be used to predict what kind of aggregate it will form.

[1]. The development of sterically stabilized lipsomes is perhaps the most important reason for the progression of liposomes in clinical use, as stabilization gives prolonged circulation times of included substances [52]. One major advantage of using liposomes is that they can carry both hydrophobic and hydrophilic materials. Hydrophobic materials or amphiphatic molecules can go into the lipid bilayer, while hydrophilic substances may reside in the aqueous core [12].

2.2.3 Micelles

Micelles are self-assembled lipid structures of substantially smaller size than that of liposomes, ranging from 5 to 100 nm [53]. As explained in section 2.4.1, it is the shape of the lipids that determines what kind of structures can be obtained, and for micelles the cone-shaped lipids enables close packing into small spheres without lumen (figure 2.5). Other micelle structures can also be found, such as threads, discs and rods [12]. For carrier applications, micelles can contain amphiphatic or hydrophobic materials, and have been extensively investigated for their ability to improve pharmacokinetic properties in the same manner as for liposomes. However, micelles may offer additional advantages. It has been shown that accumulation of micelles in tumors may be larger than that of liposomes, due to tumor-dependent vascular pore cutoff size. In other words, micelles may be better suited for passive accumulation in certain tumors, such as in Lewis lung carcinomas [54].

2.2.4 Oil-in-water Nanoemulsions

Oil-in-water (o/w) nanoemulsions are NPs with an oil core and a layer of lipids as an outer shell. In contrast to micelles, a very high payload of hydrophobic materials can be incorporated into the core of such particles [11].

Emulsion LNPs do not spontaneously self-assemble in the same way as micelles and liposomes do. First of all, water and oil separates into two phases, as seen in figure 2.7 (a). This is entropically favorable because water molecules are more attracted to each other than they are to oil molecules, and vice versa. Secondly, lipids have one hydrophilic part and one hydrophobic part, and will orient themselves on the oil-water interface so that both parts are satisfied and the molecules' free energy minimized (figure 2.7 (b)). This reduces interface tension, and happens spontaneously. In other words, this is all the self-assembly that occurs in such solutions. To make particles in the nano size range, mechanical energy/shear needs to be introduced to the system. Such energy can be in the form of physical mixing movements or ultrasonic agitation, and makes the two phases mix so that the oil breaks into fine droplets (figure 2.7 (c)). The lipids will cover the outer surface of these droplets, with the polar head facing water, and in this way make them stable for extended periods of time [55]. DSPC (Distearoyl-sn-glycero-3-phosphocholine) and PEG-DSPE (distearoyl-phosphoethanol- amine-N-[methoxy(polyethylene glycol)-2000]) are lipid amphiphiles typically used to make o/w LNPs [12]. An example of a multifunctional oil-in-water nanoemulsion can be seen in figure 2.8.

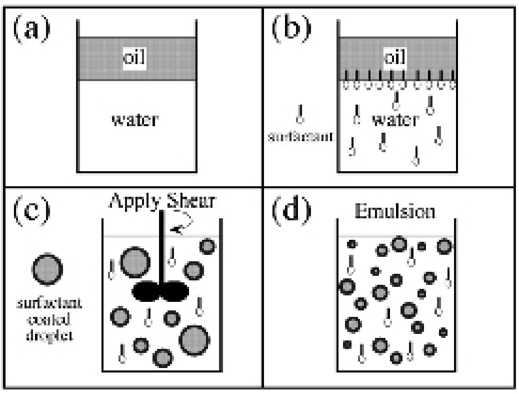

Figure 2.7: Illustration of the process of making an o/w nanoemulsion [55].

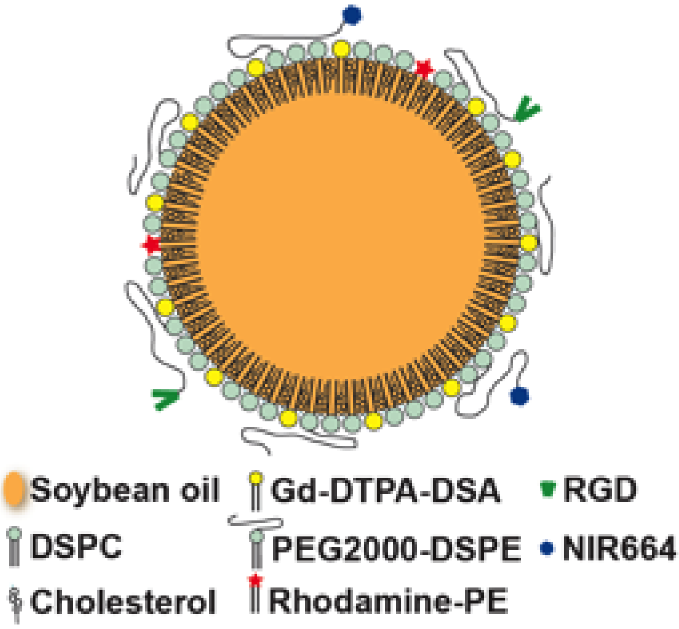
Soybean oil
Gd-DTPA-DSA
RGD
DSPC
PEG2000-DSPE
NIR664
Cholesterol
Rhodamine-PE

Figure 2.8: Multifunctional o/w NP with DSPC, DSPE-PEG and cholesterol surrounding an oil core. Fluorescent probes NIR and Rhodamine are included, and also some percentage of gadolinium conjugated lipids (Gd-DTPA-DSA). Fluorescent probes enable visualization in optical microscopes, and the latter in MRI. Additionally, an RGD peptide is displayed on the surface, to obtain increased specificity towards endothelial cells in cancer tissue [56].

2.2.5 Stabilization of Lipid-based Nanoparticles

Even though many LNPs are formed due to entropically favored reactions, they are not necessarily stabile for prolonged periods of time *in vivo*. There are basically two reasons for this: limited particle integrity and degradation by the immune system.

Firstly, LNPs rely on weak non-covalent interactions, and there exist a well-known fluidity of lipid membranes that allow lipids to diffuse laterally and occasionally also axially. Membrane fusion mechanisms, such as under the event of phagocytosis and secretion, are phenomena that rely on such lipid movements [57]. Considering this, it is likely that there is some lipid transfer between distinct LNPs, as well as between LNPs and cells. From experiments with both lipid vesicles and lipid nanoemulsions, it has been shown that this lipid transfer process is a fact [40, 58]. Physical constraints such as these compromise the general integrity of LNPs, but may also hamper specificity exerted by targeting ligands. This is because ligand conjugated lipids may be lost before the LNPs reach their target [40].

The second major stability problem for LNPs is degradation by the Reticuloendothelial System (RES). RES normally recognizes substances that are foreign to the body, and degrades them chemically [8]. For LNPs, this means that they may not be able to stay in circulation long enough to efficiently accumulate in the target tissue. One advantage of using lipids in general, is that they are said to be biocompatible, as lipids exist naturally in *in vivo* environments. However, degradation still happens to some degree when LNPs are introduced into the blood stream. As previously mentioned, plasma proteins adhere and tag particles for destruction. The amount and composition of proteins that participates in this action is dependent on the physicochemical properties of the LNPs, such as lipid composition, zeta potential and size [27].

Up to date, different ways to overcome the above explained problems have been introduced. One of them is to include cholesterol and PEG-conjugated lipids in the original lipid mixture. Cholesterol is an amphiphile that contains a hydrophobic planar steroid ring, which lowers the mobility of lipid tails when incorporated into a lipid layer. Variation in small cholesterol contents can give control of lipid layer stiffness and morphology. In that matter, cholesterol can be utilized to reduce fluidity in lipid layers, and further increase stability and specificity of LNPs [59]. An experiment that shows the significance of cholesterol in LNPs was done by Sengupta et al. The transfer rate of lipids between DPPC (dipalmitoyl-L-α-phosphatidylcholin) vesicles with and without 5 mole% of cholesterol was measured, and it turned out that the transfer rate was reduced by 50% in the case of vesicles with cholesterol [58]. PEG stabilizes the LNPs sterically, improves stealth properties and prevents plasma protein adherence as previously explained.

2.3 Nanoparticles and Cancer

Cancer therapy is one of the major fields for the use of NP systems. This is because the properties of NPs match the pathophysiology of cancerous diseases in an optimal way. The relationship between different aspects of cancer development and the use of NPs is explained below.

2.3.1 The EPR Effect: Passive Targeting

Due to an increased level of stimulatory signals in the process of angiogenesis (will be explained in section 2.3.2), tumor vasculature is known to be tortuous and poorly organized [60]. The gaps between endothelial cells are abnormally wide, and this leads to leakage of nutrients and macromolecules into tumor tissue. Additionally, tumors lack effective lymphatic drainage systems and the enhanced retention results in increased interstitial pressure. These phenomena are together called the enhanced permeability and retention (EPR) effect [61, 26].

Even though the EPR effect contributes to tumor growth, it also creates an optimal microenvironment for the passive targeting and accumulation of NPs. The size range of NP is optimal for passive diffusion through leaky endothelial junctions, and by incorporating therapeutic drugs the local drug concentration can become many times larger than after conventional systemic intravenous administration. Perhaps more importantly, the use of NP systems can significantly reduce commonly observed side effects, such as cardiotoxicity [26, 62]. NPs are therefore considered valuable tools for cancer treatment purposes. The extent of NP extravasation depends on the size of the endothelial gaps, which can vary significantly from tumor type to tumor type [63]. General observations indicate that particles with diameters less than 200 nm are the most effective for extravasation purposes, but it can be useful to further tailor the size of the NPs to specifically match the vascular cutoff pore size of the tumor in question [26, 63]. However, it should be mentioned that the vascular permeability is not necessarily homogeneous in the same tumor, which means that the passive accumulation can also vary within a tumor.

One example of a passively targeting chemotherapeutic is the already mentioned Doxil. Doxil increased the specificity of doxorubicin against tumor tissue, and showed a reduction in toxic side effects [47, 64]. The results cannot solely be explained by the EPR effect, but also by the liposome's ability to improve the circulation time of the drug. For example, the half-life of PEGylated doxil (doxil liposome stabilized by polyethylene glycol) in systemic circulation was shown to be 84 hours, which is 105 times longer than that of doxorubicin alone [26]. Increased circulation time results in increased probability of entering the target site.

2.3.2 Angiogenesis

Angiogenesis is the process of forming networks of new blood vessels from pre-existing vasculature, and plays a crucial role in several ways. For example, angiogenesis is needed for developing embryos, for the growth of a child, and for wound healing. What initiates the process is that vascular endothelial cells, which form the lining of blood vessels, receive angiogenic factors. The endothelial cells are then *activated*, and subsequently start dividing and producing metalloproteases and other cytokines [57]. A consequence of this is that receptors that interact with angiogenic factors get upregulated, such as P-selectin, VEGFR, PDGFR and $\alpha_v\beta_3$ integrins [65, 66, 67, 68]. Metalloproteases are enzymes that break down the extracellular matrix (ECM: support matrix of proteins and polysaccharides) to provide space for new blood vessels. Activated endothelial cells migrate out in degraded parts of the ECM, and further divide to form hollow tubes that originate in the major blood vessel [57].

Normally, there are more inhibitors of angiogenesis than angiogenic factors present. Production of angiogenic factors to onset division only occurs upon requirement, for example when tissue needs to be repaired [57]. However, in cancerous diseases the fine balance between angiogenic factors and inhibitors is disturbed, so that the amount of angiogenic factors always exceeds that of inhibitors. The reason for this is that a tumor requires a larger supply of blood with nutrients as it grows, and thus cancer cells release large amounts of angiogenic factors. In fact, angiogenic factors produced by cancer cells even force non-cancerous endothelial cells into producing angiogenic factors on their own, to *further* stimulate tumor growth and angiogenesis, as depicted in figure 2.9. This means that activated endothelial cells contribute to an angiogenesis process that continues in uncontrollable manner. It has been shown that tumors are not able to grow beyond 1-2 mm if deprived of blood supply, and this pinpoints the angiogenesis process as a major target for cancer therapy [57, 66].

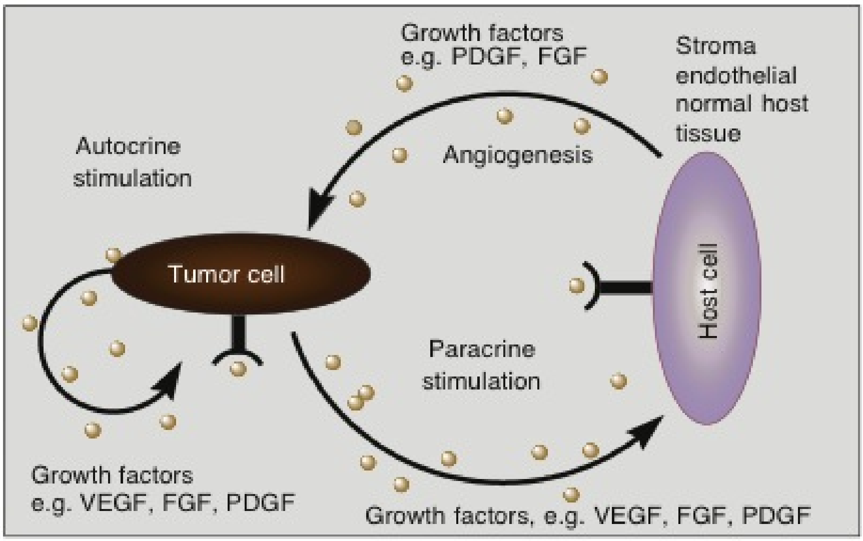
Growth factors
e.g. PDGF, FGF
Stroma
endothelial
normal host
tissue
Autocrine
stimulation
Angiogenesis
Tumor cell
Host cell
Paracrine
stimulation
Growth factors
e.g. VEGF, FGF, PDGF
Growth factors, e.g. VEGF, FGF, PDGF

Figure 2.9: Schematic illustration of how increased amounts of angiogenic factors from cancer cells activate normal endothelial cells, which onsets a process that further stimulate tumor growth and angiogenesis. Paracrine stimulation: stimulation by nearby cells, autocrine stimulation: stimulation by the cells own growth factors. VEGF = vascular endothelial growth factor; FGF = fibroblast growth factor; PDGF = platelet-derived growth factor [66].

2.3.3 The Integrin Receptor and Interaction with RGD-peptides

As mentioned, several receptors get upregulated on angiogenically activated endothelial cells, and these play important roles in the process of angiogenesis as they interact with angiogenic factors. One of them is the $\alpha_v\beta_3$ integrin receptor. Integrins are transmembrane proteins composed of an α and a β subunit in at least 24 different heterodimeric combinations. They bind to ECM proteins or cell surface ligands through short peptide sequences, and can facilitate signal transduction from the ECM to the cell interior and vice versa. Integrins are involved in processes such as cell migration, invasion and differentiation, but also participate in cell proliferation and survival [69].

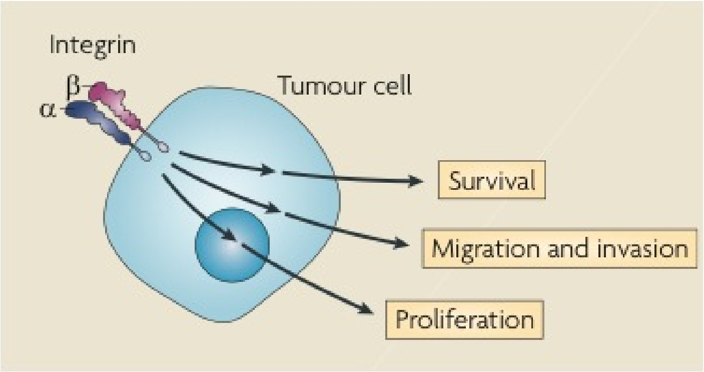

Figure 2.10: Integrins expressed in tumour cells contribute to tumour progression and metastasis by increasing tumour cell migration, invasion, proliferation and survival [69].

An interesting property of the $\alpha_v\beta_3$ integrin is its high expression level on endothelial cells in angiogenic tumor vasculature compared to that of normal vasculature [68], and this makes it useful as a target for selective therapy of tumor angiogenesis. Indeed, antagonists have been developed for the purpose of blocking the activity of integrins. Especially, peptides containing an RGD (Arg-Gly-Asp) motif have been shown to have high affinity for $\alpha_v\beta_3$ and $\alpha_v\beta_5$ integrins. This discovery led to the development of cilengitide, which was successful in blocking glioblastoma tumor activity in phase II trials [68]. However, cilengitide was co-administered with temozolomide and radiotherapy, and questions have been raised about the efficacy exerted by cilengitide alone [70].

Even though RGD-peptides intrinsically may show anti-tumor effect, they can be exploited for selective targeting of NPs to tumor blood vessels. Tumor vascular targeting may possess advantages over targeting directly to tumor cells, because the endothelium of tumor vasculature is readily accessible to circulating NPs. NPs that directly target tumor cells have to overcome the interstitial pressure in the tumors (explained in sec. 2.3.5) to reach their target cells, and this presents a large restriction in delivery effect. By using the RGD binding affinity to $\alpha_v\beta_3$ integrins, drugs, genes, imaging agents etc. can be delivered to tumor vasculature by the aid of RGD-NPs. High payloads of chemotherapeutic drugs in the vasculature of tumors may potentially increase the drug efficacy far beyond that of the above mentioned cilengitide [69]. Furthermore, the binding of

RGD-conjugated NPs to $\alpha_v\beta_3$ integrins can lead to early detection of cancer or monitor the disease progression with the use of contrast agents [10].

Researchers have shown that conjugation of RGD to NPs can increase the NP uptake amount in cells due to $\alpha_v\beta_3$ binding [71, 72]. For example, it has been shown that conjugation of RGD to PLGA NPs increased the uptake in endothelial cells by 3 times compared to the non-conjugated PLGA NP version [72].

2.3.4 Increasing Specificity: Active Targeting

As explained in the previous section, NPs accumulate in tumor tissue due to size effects combined with the EPR effect. In some cases this may be sufficient for obtaining a desired outcome. However, it is possible to make the NPs even more specific to certain types of cells. This can be done by conjugating them to ligands that bind to receptors or disease specific tags on cells in the target tissue [12, 26]. Examples of such NP systems have already been mentioned, such as PAMAM-dendrimers conjugated to folic acid, carbon nanotubes conjugated to folic acid, or polyplex micelles conjugated to RGD [14, 32, 71].

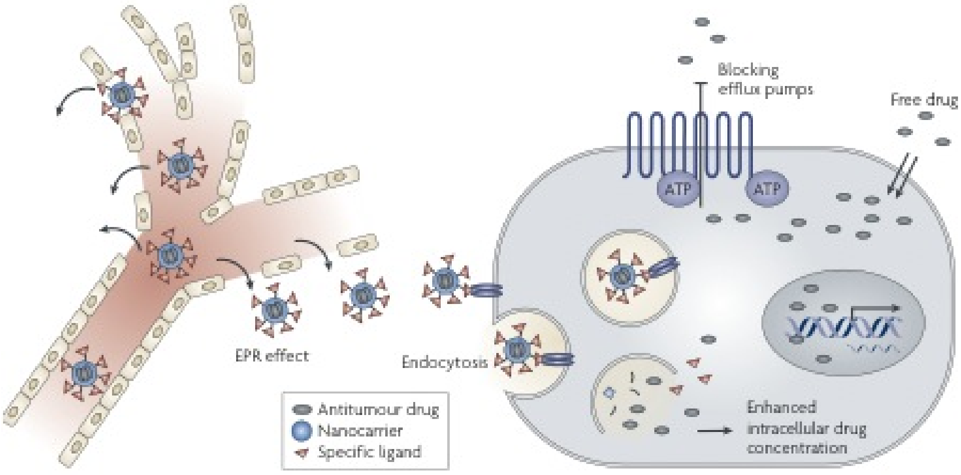

Figure 2.11: Illustration of how circulating NPs in plasma may extravasate into tumor tissue through leaky vasculature and further enter specific cells via ligand tags. By using NPs as carriers, the intracellular concentration of the drug may become high enough to overcome drug resistance by efflux pumps [26].

The general idea is that a combination of the EPR effect and the use of NP-conjugated ligands elevate the specificity and efficacy of NP systems, as schematically shown in figure 2.11. When NP-conjugated ligands bind to target cells, an increase in NP uptake can be induced, or at least an increase in the number of NPs surrounding the target cell surface [14, 71, 73]. Such NPs are *actively* binding to target cells due to specific interactions with receptors. This is an important aspect of NP systems, because it is indeed required that the NPs locate and/or enter the target cells when used for *therapeutic* purposes. It has been shown that the number of particles that enter the cell is higher for actively targeted NPs than for non-targeted NPs in numerous experimental setups *in vitro* and *in vivo* [14, 71, 26]. In that matter, active targeting offers advantages not only because of specificity, but also because the amount of drug potentially released inside the cell may overcome drug resistance caused by cythochrome efflux pumps [26]. For other applications, such as imaging and diagnostics, it may not be needed that NPs enter target cells, but it is advantageous that they locate target cells to a larger degree than that exerted by passive targeting alone [12, 73].

2.3.5 The ECM Diffusion Problem

A common problem associated with the treatment of solid tumors, is physiological resistance exerted by the extracellular matrix. Tumor cells produce and assemble a support matrix of organic substances, such as collagens and proteoglycans, and these substantially hamper the penetration of macromolecules conventionally used for cancer therapies. Resistance against treatments increases as the tumors grow and develop larger volumes of connective tissue [74]. The problem is especially serious for the use of NPs, because they may possess a larger size than the pores present in the ECM [75]. Furthermore, the ECM of tumors has a different composition of organic substances than that of the ECM in normal tissue [74, 76, 77]. These differences, such as the increased interstitial pressure previously explained, involve a larger penetration barrier in solid tumors, and accumulation of NPs due to the EPR effect may not suffice to obtain effective cancer treatments [75].

There are basically two transport mechanisms for the penetration of NPs in tumors. The first is convection and the second is diffusion. Convection mainly participates in particle transport at the tumor periphery, but is poor throughout tumors due to the increased interstitial pressure. This leaves diffusion as the major transport mechanisms for NPs. As diffusion is dependent on size, small NPs have advantages regarding tumor penetration compared to larger NPs [78].

The problem of limited penetration in tumor ECM is recognized as a flaw that needs to be overcome for developing new types of therapeutics. For example, methods to manipulate the ECM to enhance NP penetration are being explored. Neeves et al. showed that by administrating NPs and ECM-modifying agents sequentially or simultaneously in rat brains, the NP distribution volume increased with 50% or more [75].

2.4 Uptake Mechanisms and Intracellular Trafficking Pathways

The nature of how substances are taken up and processed by cells is still only partially revealed. However, there are two main categories for such mechanisms, namely phagocytosis and pinocytosis. Phagocytosis only occurs in certain specialized cells, such as macrophage immune cells, and involves uptake of large particles visible by light microscopy. Pinocytosis, on the other hand, happens in all cell types and involves uptake of fluids, solutes or small particles, such as NPs. The pinocytosis category has several subgroups. Of these, the clathrin-mediated endocytosis mechanism is the most well characterized one. Other, clathrin-independent subgroups, such as endocytosis via caveolae, macropinocytosis and clathrin/caveolae independent endocytosis, still remain to be fully understood [57, 79, 80, 81, 82]. An illustration of general uptake mechanisms can be seen in figure 2.12, and mechanisms of pinocytosis relevant for uptake of NPs are explained below.

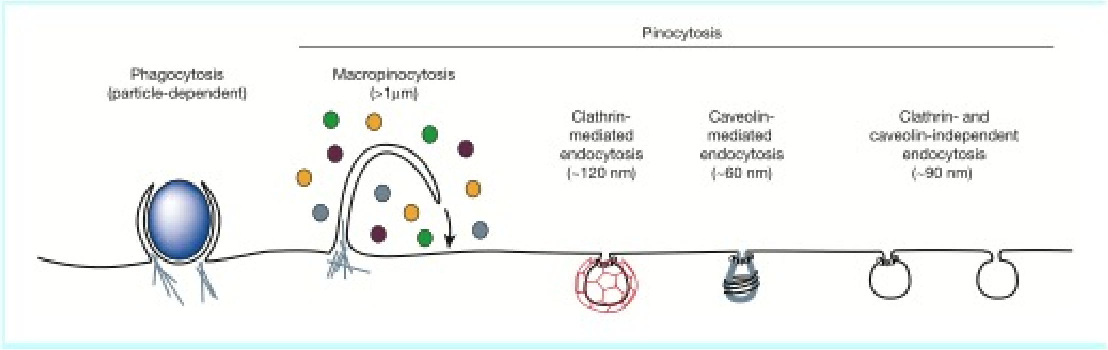
Pinocytosis
Phagocytosis (particle-dependent)
Macropinocytosis (>1μm)
Clathrin-mediated endocytosis (~120 nm)
Caveolin-mediated endocytosis (~60 nm)
Clathrin- and caveolin-independent endocytosis (~90 nm)

Figure 2.12: Illustration of the different types of known entry portals into mammalian cells. Essentially, the endocytic pathways differ for vesicles with different formation mechanisms and sizes, and with different types of content [80].

2.4.1 Clathrin-mediated Endocytosis

Details of clathrin-mediated endocytosis are thoroughly discussed in many articles and textbooks [57, 80, 81, 82]. This mechanism of endocytosis ensures continuous uptake of essential nutrients, antigens and growth factors in all cell types. Binding of a ligand to specific cell surface receptor normally onsets the endocytosis process, by initiating clustering of other receptor-ligand complexes in pits of the plasma membrane. Additionally, proteins on the cytosolic side of the plasma membrane, clathrins, assemble by the help of adaptor proteins to facilitate stability and curvature of the pit. When clathrin covered pits are sufficiently invaginated, a protein called dynamin is responsible for pinching them off. In this way, they form vesicles on the cytosolic side of the plasma membrane. Next, the clathrin coat depolymerizes, and the vesicles are defined as early endosomes. The early endosomes mature into endosomes, which can fuse with other endosomes. Finally, they become late endosomes, which fuse with lysosomes. During this development, the pH drops drastically from neutral and stepwise down to the lysosomal pH of 5, due to the action of ATP proton pumps. Within the endosomes, substances such as ligands and receptors are sorted to go to their final destination. These destinations can for example be the Golgi, endoplasmatic reticulum (ER), or back to the plasma membrane. However, the substances that are not sorted follows the maturation pathway of the endosomes, and are finally degraded by the acidic environment in the lysosomes [57, 80, 81, 82]. A schematic cartoon can be seen in figure 2.13.

2.4.2 Caveolae-mediated Endocytosis

Caveolae are flask-shaped, flat or tubular invaginations (50-80 nm) of the plasma membrane, and have been known since the 1950s [83, 84, 85]. However, knowledge about the types of substances taken up and their destination in the cell is still ambiguous [83].

Similar to clathrin- coated pits, the caveolae invaginations are coated with a protein on the cytosolic side, namely caveolin. This protein is essential for the formation and stability of caveolae, and no caveolae are seen in caveolin deficient cells [86]. Another similar feature is the presence of dynamin to pinch off the caveolar vesicle. Once pinched off, the caveolar vesicle either fuses early endosomes, or with a membrane sorting organelle called the caveosome. The caveosome has neutral pH (in contrast to the acidic endosome) and is rich in caveolin, cholesterol and glycosphingolipids. The destination of the caveosome seems to be dependent on the internalized substance, but a clear picture of the trafficking remains to be obtained. For example, it has been shown that the caveosomes end up in the ER when the SV40 virus is internalized, but in the cis-Golgi when lactosylceramide is the subject of transportation. Further, ligands and other membrane constituents may reside in the caveosome for some time. There is also a probability that substances may be transported from caveosomes to endosomes or other, unknown targets, as seen in figure 2.13 [83].

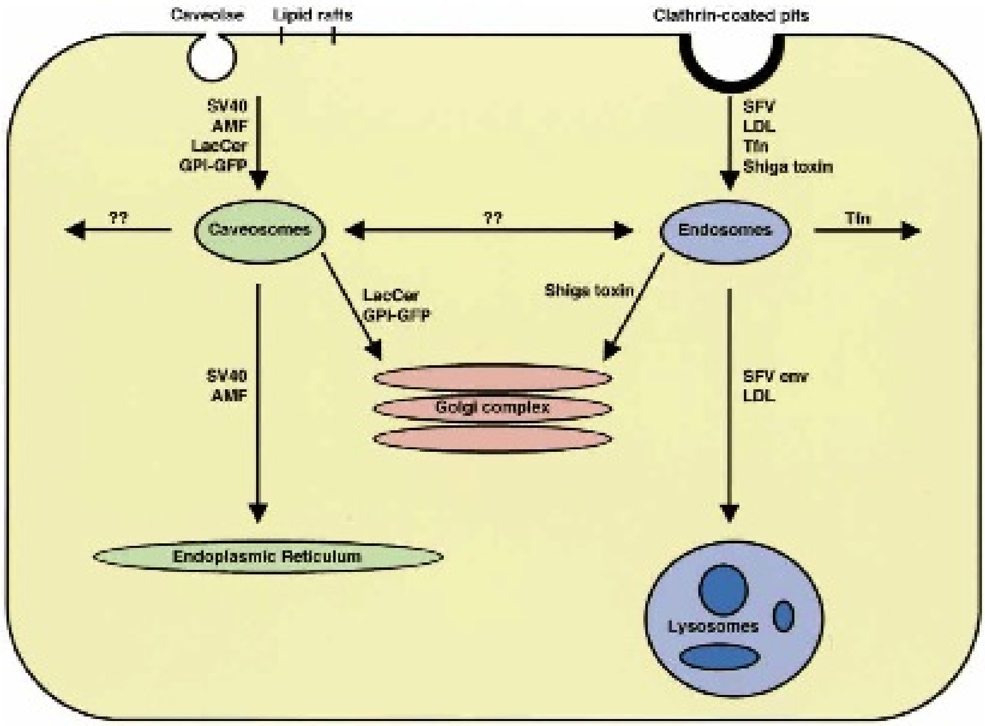
Caveolae
Lipid rafts
Clathrin-coated pits
SV40
AMF
LacCer
GPI-GFP
SFV
LDL
Tfn
Shiga toxin
??
Caveosomes
??
Endosomes
Tfn
LacCer
GPI-GFP
Shiga toxin
SV40
AMF
Golgi complex
SFV env
LDL
Endoplasmic Reticulum
Lysosomes

Figure 2.13: Intracellular pathways of various substances after uptake in caveolae and clathrin-coated pits. The trafficking depends on the substance internalized, and question marks indicate that there is a large uncertainty concerning other possible pathways for caveosome sorting.

2.4.3 Macropinocytosis

Macropinocytosis is an endocytic mechanism that involves the formation of large, irregularly sized endocytic vesicles. Such vesicles do not rely on protein coats, and do not concentrate receptors in their lumen. However, stimulation by growth factors or other signals may indirectly induce macropinocytosis. What happens is that ruffles in the plasma membrane form, due to actin movements. These ruffles are normally always present, but upon stimulation by mitogenic factors, they elongate and close into macropinosomes as seen in figure 2.12. In some cases, macropinosomes can be as large as 5-10 μm, and this is therefore and efficient way for the cell to non-specifically take up solute macromolecules [80, 81, 82]. The destination of the macropinosomes varies significantly from cell type to cell type. For example, the macropinosomes can in some cases shrink and fuse with lysosomes to degrade the content, while in other cases most of the content is recycled back to the plasma membrane. Compared to the other internalizing vesicles, the macropinosome is leaky. This means that some substances taken up by this mechanism may diffuse out in the cytosol [81].

2.4.4 Clathrin and Caveolae Independent Endocytosis

It has been shown that several substances taken up by the above-mentioned mechanism, also are taken up in cells devoid of clathrin and caveolin. For example, it has been found that the simian SV40 virus and sphingomyelin, which are known to exploit the caveolar and clathrin mediated pathway respectively, also were taken up in cells by other, unknown mechanisms [87, 88]. These mechanisms are called clathrin and caveolae independent endocytosis, and appear to give rise to multiple trafficking pathways that are further classified into several subgroups. They remain to be properly characterized, but seem to be dependent on cholestrol and specific lipid compositions. One important property of these uptake mechanisms is that substances taken up bypass the early endosomes [82].

2.4.5 Uptake and Trafficking of Nanoparticles

Uptake and trafficking of different types of NPs have been investigated in a number of studies. In general, it has been found that NPs can employ multiple pathways for cellular entry, and these are currently poorly understood. Properties such as size, shape, material composition, surface chemistry and/or charge can affect the uptake and trafficking significantly. Moreover, the uptake and trafficking is also dependent on the cell type utilized [82].

Uptake studies with fluorescent latex beads of 50 to 1000 nm have been done to elucidate the effect of size differences alone. The cell type used was non-phagocytic B16 cells, and it was found that beads with diameters of 200 nm or below were all internalized by clathrin-mediated mechanisms, while beads of diameters around 500 nm and up were mainly internalized by caveolae-mediated mechanisms. Furthermore, the beads taken up by caveolae avoided lysosomes [89].

However, uptake mechanisms are not dependent on NP size alone. For example, PLGA NPs of approximately 300 nm in size and with a negative surface charge were taken up by clathrin-mediated mechanisms in vascular smooth muscle cells, but by clathrin and caveolae independent mechanisms in rat corneal epithelial cells. Modifications of surface charge with cationic poly(L-lysine) polymers lead to more rapid clathrin-mediated uptake in vascular smooth muscle cells, possibly due to larger interaction with the cell membrane by charge effects (negative charge of cell membrane and positive charge of particles). Furthermore, cationic chitosans with high polydispersity and an average size of 430 nm were also taken up by clathrin-mediated endocytosis, in Caco-2 and A549 cells. Several similar findings indicate that positive charge may be one of the parameters that induce clathrin-mediated endocytosis. However, other properties do also affect the uptake, for example seen for hydrophobically modified cationic chitosans of 360 nm size. These chitosans were taken up by multiple pathways, including clathrin-mediated endocytosis, caveolae-mediated endocytosis and macropinocytosis [82].

Many negatively charged NPs seem to be taken up by caveolae-mediated mechanisms, although not without exceptions. For example, Doxil, polysiloxane NPs, and polymeric micelles of around 100 nm in size and with negative charge were taken up primarily by caveolae-mediated endocytosis [82]. Even though their uptake mechanism was the same as that for latex beads above 500 nm in size, their trafficking route was not. Doxil and polymeric micelles were shown to reach the lysosomes while the latex beads were not [82, 89].

A special case for uptake and trafficking concerns NPs with targeting ligands. The use of targeting ligands can affect the uptake mechanism of the NP substantially compared to its non-conjugated version. For example, RGD-targeted micelles were shown to be mainly taken up by caveolae-mediated mechanisms while its non-targeted version was taken up by clathrin-mediated mechanisms [90]. Another effect is that such NPs may be more quickly internalized than its non-conjugated version, due to specific receptor mediated endocytosis [71]. However, subsequent trafficking might be more complicated than that of the ligand alone, and can be affected by NP properties [82].

2.5 Tools for Studying Nanoparticle Cellular Uptake and Trafficking

To study NP uptake and trafficking, certain tools are required. Such tools may have certain limitations, but when analyzed in context of each other they can provide invaluable information.

2.5.1 The use of Fluorophore Markers

One way to study NP uptake and trafficking, is to fluorescently mark specific endocytosis vesicles or intracellular organelles, as well as the NPs. Provided that the probes on the NPs have fluorescence at a wavelength other than that of the marked cellular compartment, NP locations can be analyzed and compared in a confocal laser scanning microscope (CLSM, section 2.6.2). The most important point is to see if the dyes are *colocalized* (at the same place) or not. Colocalized fluorescence means that the NPs are in the marked vesicle or organelle, while non-colocalized fluorescence means that they are not. This can reveal the NP uptake and trafficking route in the cell by methods of elimination or confirmation.

Fluorophore markers used for marking cellular compartments are many, but they may be divided into two groups. The first group represents the type of fluorophores that are expressed by the cell due to the use of various transfection agents (plasmids or viruses). This means that the cells are modified to express protein or peptide fused fluorophores that end up in specific compartments. The other group represents the fluorophores that are added directly to the system, taken up by the cell and that arrive at a certain destination. This can be small molecular mass probes that selectively end up in target compartments, or probes that are fused with facilitator proteins that follows a specific endocytic route.

Some examples of fluorophore markers are LysoTracker®, transferrin-Alexa Fluor and CellLight™. The advantage of these markers is that they enable imaging of live cells. Live cell imaging is the method that causes the least artifacts, and is therefore preferable. The LysoTracker® probe is a specific marker for late endosomes and lysosomes, and consists of a fluorophore linked to a weak base. The exact mechanism of action is not elucidated, but seems to involve protonation of the base and subsequent retention in acidic organelles [91]. Transferrin is a monomeric serum glycoprotein that binds and delivers iron atoms to cells through clathrin-mediated endocytosis. More specifically, it enters the early endosomes and is subsequently recycled back to the plasma membrane. It can be conjugated with fluorescent probes, such as Alexa Fluor, and is therefore used for visualizing early endosome vesicles in uptake and trafficking studies [92, 93]. CellLight™ falls within the group of markers that modify the cells to express fluorescent proteins. It utilizes the BacMam system, which consists of an insect virus (baculovirus) that efficiently delivers and expresses genes in mammalian cells. Furthermore, the virus can be modified to give expression of different types of GFP (green fluorescent protein)-linked peptides or proteins, such as GFP-Rab5 that specifically mark early endosomes

[94].

Even though the use of fluorophore markers of endocytosis vesicles or intracellular organelles is valuable to give qualitative information concerning uptake mechanisms and trafficking routes of NPs, the fluorescence of NPs alone can also be useful. This is because the *amount* of fluorescent NPs taken up by cells can be measured by flow cytometry (section 2.6.3). The data of such experiments can be analyzed, and quantitative results from cell uptake can be obtained.

2.5.2 Colocalization Coefficients

To obtain quantitative values for colocalization of two different fluorophores in CLSM images, special data analysis programs that calculate colocalization coefficients can be utilized. The calculated coefficients describe to which degree fluorescently marked components from two different channels overlap [95].

Two commonly employed coefficients for colocalization analysis are the Mander's coefficients and the Pearson coefficient. These two types of coefficients differ in the way they calculate the degree of overlap based on intensity. The Mander's coefficients describe what proportion of one channel signal that is coincident with signal from another channel, while the Pearson coefficient describes the correlation of intensity distributions between channels. The equations for calculating Mander's and Pearson coefficients are shown in 2.1 and 2.2 respectively [95].

$$M1 = \frac{\sum_i R_{i,coloc}}{\sum_i R_i}, M2 = \frac{\sum_i G_{i,coloc}}{\sum_i G_i} \tag{2.1}$$

$$R_r = \frac{\sum((R_i - R_{av})(G_i - G_{av}))}{\sqrt{\sum(R_i - R_{av})^2 \sum(G_i - G_{av})^2}} \tag{2.2}$$

R_i is the intensity of the first (red) fluorophore in individual pixels, G_i the intensity of the second (green) fluorophore in individual pixels, $R_{i,coloc}$ is the intensity of red fluorophore colocalized with green fluorophore, $G_{i,coloc}$ is the intensity of green fluorophore colocalized with red fluorophore, whereas R_{av} and G_{av} are the arithmetic means for red and green fluorophores respectively [95].

The values for Mander's coefficients span from 0 to 1, where 0 corresponds to no colocalization while 1 corresponds to perfect colocalization. M1 describe the total overlap of red fluorophores in green fluorophores, whereas M2 refers to the total overlap of green fluorophores in red fluorophores. For M1, $R_{i,coloc} = R_i$ if $G_i > 0$ and $R_{i,coloc} = 0$ if $G_i = 0$, and vice versa for M2 [95].

For the Pearson coefficient, the values span from -1 to 1, where -1 corresponds to perfect exclusion, 0 corresponds to random localization, and 1 corresponds to perfect colocalization. The inclusion of averages makes the Pearson coefficient independent of background signal disturbance [95].

There are advantages and disadvantages for the use of both approaches. First of all, they are both independent on the brightness of the images. Furthermore, the Mander's coefficients are sensitive to background fluorescence while the Pearson coefficient is not.

This means that a threshold needs to be set for the background in order to employ the Mander's coefficients. Although this is a disadvantage for Mander's coefficients, the Pearson coefficient is not always easy to interpret, and moreover it is only reliable for high correlation because non-colocalized signals are added to the calculations. The Mander's coefficients give a good indication of the contribution of each channel to the colocalization, and can be used even when only low colocalization is present [95].

2.5.3 The use of Endocytic Inhibitors

Another way to study the uptake pathways of NPs in cells is to block alternative uptake routes. If the major uptake route for the particle in question is blocked, a substantial decrease in uptake can be monitored by the use of flow cytometry (quantitatively) or CLSM (qualitatively). The most common way to do this is to use inhibitors with well-characterized blocking actions.

Two common inhibitors are chlorpromazine and genistein. Chlorpromazine is a cationic amphiphilic drug that prevents assembly of adaptor proteins and clathrin, by relocating these proteins into intracellular vesicles. In that matter, it specifically inhibits clathrin-mediated endocytosis [96]. Genistein is a tyrosine kinase inhibitor, and inhibits the formation of caveolae by inhibiting dynamin II and interfering with the actin network at endocytic sites [98, 99]. As clathrin-mediated and caveolae-mediated endocytosis are two major uptake mechanisms for NPs, their effect can be evaluated in light of each other to confirm or disclaim theoretical uptake routes.

It should be mentioned that the use of inhibitors might give results that are not consistent with reality. This is because they may show varying effect in different cell types, show toxicity towards cells, and additionally interfere with other uptake mechanisms [81, 96, 97]. For example, it has been shown that certain uptake mechanisms get upregulated in response to chlorpromazine treatment [96, 97].

2.6 Experimental Techniques

The theory behind techniques used for characterizing LNP sizes, and further uptake and trafficking in cells, are described below. Section 2.6.1 was taken from previously elaborated project work [40].

2.6.1 Dynamic Light Scattering

Dynamic Light Scattering (DLS) is based on the fact that small particles in suspension move faster than larger particles in suspension. The constant movement of particles is due to Brownian motion, which means that the particles are forced to move because of constant bombardment by surrounding molecules. However, their speed of movement is related to their size, and DLS is a method of determining size by interpreting their speed [100].
This is done by sending a laser beam through a small volume of diluted particles. The photons in the laser beam are scattered by the particles, and captured by a detector. Constructive and destructive interference by scattered photons will generate an interference pattern at the detector at time t. However, the particles are constantly moving, so at time $t + \delta t$ the signal from the particles will generate an interference pattern that looks a little bit different than the interference pattern from time t. Further, the signal is recorded at different times $t + \delta t_2, t + \delta t_3$ etc., and compared to the initial signal from time t. This means that after ended processing time the measurement system has recorded a series of correlations between the initial signal and other signals during that specific period of time. The software of the DLS plots all the correlations as a graph of a function called the correlation function. A constant correlation of 1 means perfect correlation between the initial signal and the other measured signals, and the particles have not moved at all. This is not realistic because of Brownian motion, so a correlation function will always decrease with time. The faster the correlation function decreases, the faster the particles move and the smaller they are in size. The speed-size relationship is shown by the Stokes- Einstein equation (2.3), and this is the basic of how a size distribution of the particles can be generated by using the method of DLS. In (2.3)

$$D = \frac{K_B T}{3\pi\eta d} \tag{2.3}$$

D is the diffusion coefficient of the particles, K_B is the Boltzmann's constant, T is the temperature, η the solvent viscosity and d the mean hydrodynamic diameter [100, 101].

Results from DLS experiments usually estimate two different values for the particles diameter, one is the mean peak value and the other is the Z-average. The mean peak value represents the mean particle size when differences in refractive index are taken into account. The calculation of Z-average is only based on the mean intensity. As large particles scatter more light than small particles (the intensity is proportional to r^6, where r is the radius of the particle), the mean peak value is usually considered to be more correct than the Z-average [100].

A value called the polydispersity index (PDI) is also obtained with DLS measurements. The PDI is defined as the standard deviation divided by the mean size, and thus describes the distribution of individual sizes. If there is a wide range of individual sizes, the emulsion is polydisperse [100].

2.6.2 Confocal Laser Scanning Microscopy

Confocal Laser Scanning Microscopy (CLSM) is an optical imaging technique that provides high-resolution images of specified focal planes. CLSM is commonly used for the study of biological samples, and allows investigation of thin sections *within* the sample. Additionally, *several* thin sections at different depths in the sample can be scanned and collected to generate a 3-dimensional image [102, 103].

The setup of a CLSM is shown in figure 2.14. Firstly, coherent rays from the light source go through a pinhole aperture and are reflected by a dichromatic mirror. The reflected rays are focused onto a small focal volume of the sample by an objective lens. Light reflected by the sample is able to pass the dichromatic mirror on its way back, while light of original laser beam wavelength is stopped. Next, only rays from one defined, specific confocal point are focused onto the photomultiplier detector by a second pinhole aperture in front of the detector. This pinhole eliminates all background noise from planes situated below or above the exact plane of interest, and a remarkably sharp image is created. The difference in background noise compared to conventional light microscopy can be seen in figure 2.15. When data is collected from one confocal point, the laser beam moves in the x-y plane until data from all points of the defined horizontal plane of the sample is collected. The resolution and the contrast of the resulting image can be adjusted by changing the scan speed of the laser. Slower scan speeds gives higher image quality, but requires longer acquisition time [102, 103].

When using CLSM, it is desired to look at specific components of the sample within the specified plane. These components can be marked with fluorescent molecules, as explained in section 2.5.1, so that only the fluorescence emission is collected by the detector. Various filters and lasers can be used to allow imaging of different fluorescent labels within the same plane of the sample. An additional advantage of this is that fluorescent molecules can be detected even if their size is below the spatial resolution of the microscope [102].

CLSM can be used in differential interference contrast (DIC) mode for obtaining images of cells without excitation of fluorescent labels. What happens is that light is sent *through* the sample, and the refractive indexes of objects in the sample causes phase shifts of the light. The phase shifts are further transformed into detectable amplitude differences. In that matter, DIC is used to obtain information about the optical density of a sample, to see features that are otherwise invisible. Dense features will appear black while light features appear white on a grey background [104].

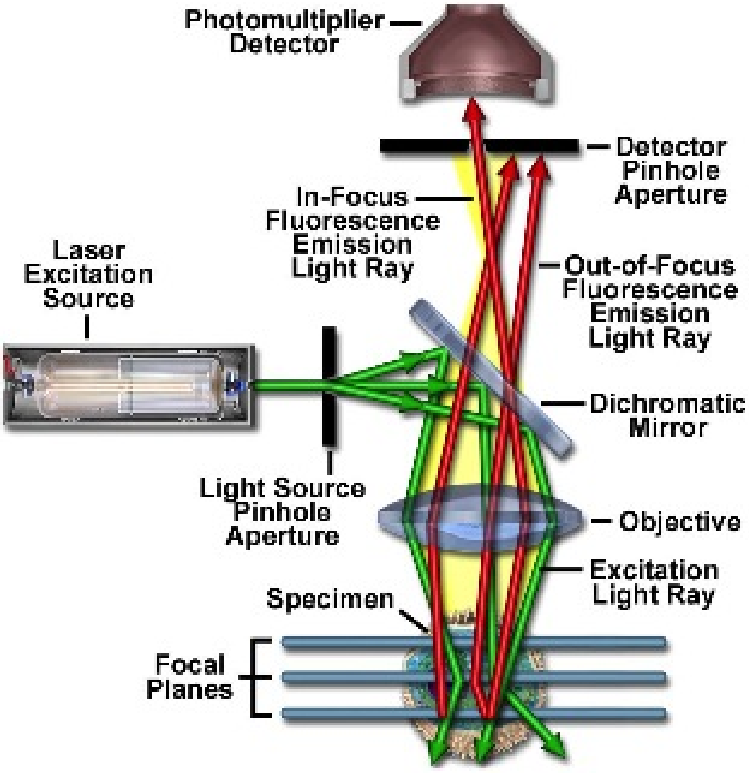
Photomultiplier Detector
Detector Pinhole Aperture
In-Focus Fluorescence Emission Light Ray
Laser Excitation Source
Out-of-Focus Fluorescence Emission Light Ray
Dichromatic Mirror
Light Source Pinhole Aperture
Objective
Excitation Light Ray
Specimen
Focal Planes

Figure 2.14: Schematic diagram of the optical pathway and principal components in a confocal laser scanning microscope [102].

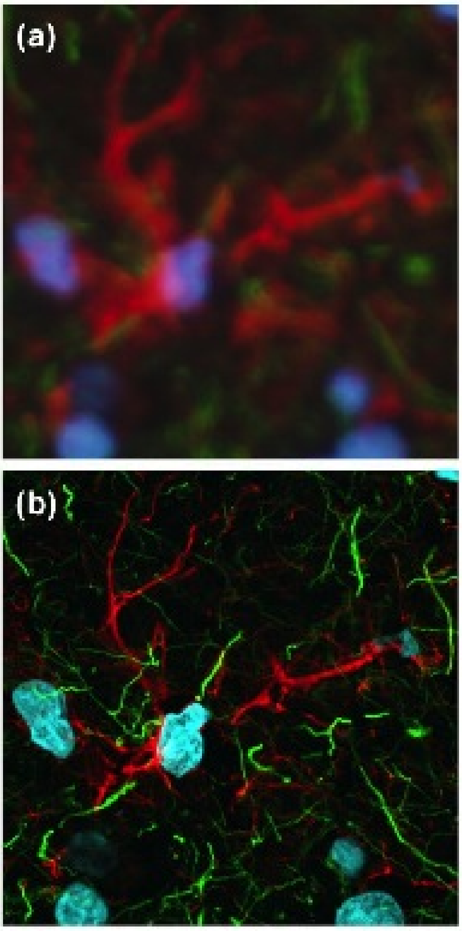

Figure 2.15: Image aquired by a conventional optical microscope (a) versus a confocal laser scanning microscope (b) [102].

2.6.3 Flow Cytometry

Flow cytometry is a technique used for counting and analyzing micrometer sized objects, such as living cells. Compared to CLSM, it is a *quantitative* technique. This means that no images are created, but data values that describe numbers, contents and sizes of objects can be extracted. In practice, flow cytometry measures the fluorescence emittance and light scattering of objects in the sample. As there will be a stoechiometric relationship between the amount of fluorescent labels and the number of labeled features, objects can be sorted according to fluorescence intensity. Examples of applications for flow cytometry can be to measure the number of cells in a cell population that are in mitosis, or to measure the uptake amount of fluorescently labeled NPs in single cells [105].

A schematic setup of flow cytometry can be seen in figure 2.16. Firstly, the objects that are to be analyzed are taken up by a thin syringe and hydrodynamically focused into a fine stream by the help of a sheath fluid. The goal is to make only one object pass the cross section of the stream at a time. Once inside the fluidic system, the stream reaches a point where it is intersected by a light beam, usually from a laser source. The objects in the stream causes optical scattering of the light, and additionally emit fluorescent light if fluorophores are included. To record the interaction between the stream and the light, detectors are situated both in line with, and perpendicular to the light source. In that matter, both forward scattering (FSC) and side scattering (SSC) is recorded. Additionally, there are separate detectors to record the fluorescence intensity. The detectors translate the intensity pulse (amount of photons per area) from each object into a voltage pulse. Further, the voltage is amplified by a series of linear or logarithmic amplifiers, and converted into a digital signal that is collected by a computer system [105, 106].

Concerning the different scattering directions, the FSC is roughly proportional to the sizes of the objects. This is because small objects only produce a small amount of forward scattered light, while large objects produce a large amount of forward scattered light. SSC, on the other hand, is created by the complexity of the object. For example, structures that are inside the object may scatter light in larger angles than that of the FSC. The more side scattered light, the larger complexity of the object. In that matter, side scattering can sort the objects based on qualities of structures in their inside or on their surface [105, 106].

FSC and SSC can be plotted as one- dimensional histograms. For FSC, small objects will be placed far to the left, while large objects are placed to the right. For each object recorded of a certain size, the vertical part of the histogram grows. The same is true for the SSC, except that the histogram populations are divided into complexity and not size. This means that one size-population may have several complexity-populations and vice versa. The one- dimensional histograms from FSC and SSC can be combined to yield a 2-dimensional scatter plot, where both the complexity and sizes of objects are represented [105, 106].

For the fluorescent light, various filters and mirrors make sure that each wavelength arrives at its appropriate detector, as seen in figure 2.16. Other than that, the signal is

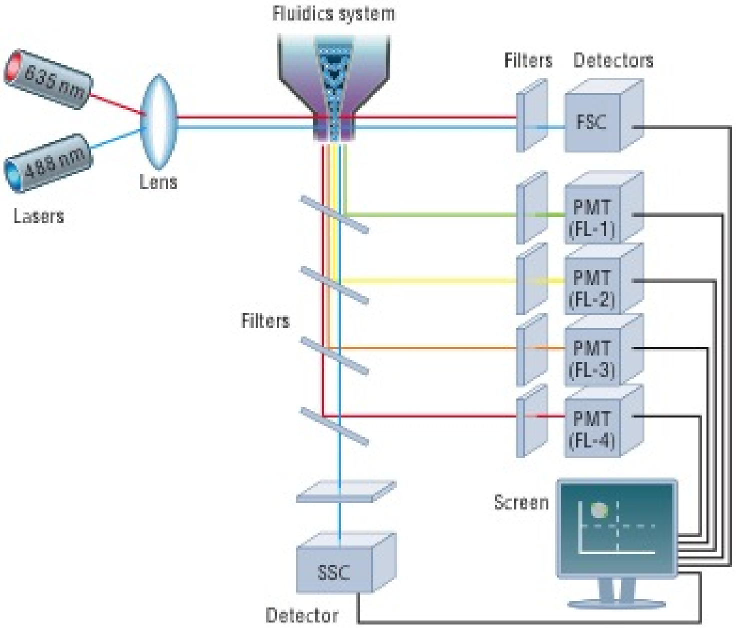
Fluidics system
635 nm
488 nm
Lasers
Lens
Filters
Detectors
FSC
PMT (FL-1)
PMT (FL-2)
PMT (FL-3)
PMT (FL-4)
Filters
Screen
SSC
Detector

Figure 2.16: Schematic diagram of the optical pathway and principal components in a flow cytometer [106].

recorded and presented the same way as for FSC and SSC. This means that each object is sorted based fluorescence intensity. One- dimensional plots show objects with small fluorescence intensities to the left, and large fluorescence intensities to the right, as seen in figure 2.17 [105, 106].

It should also be mentioned that data from flow cytometry can be *gated* to selectively visualize the objects of interest, while eliminating data from unwanted objects such as dead cells or debris [106].

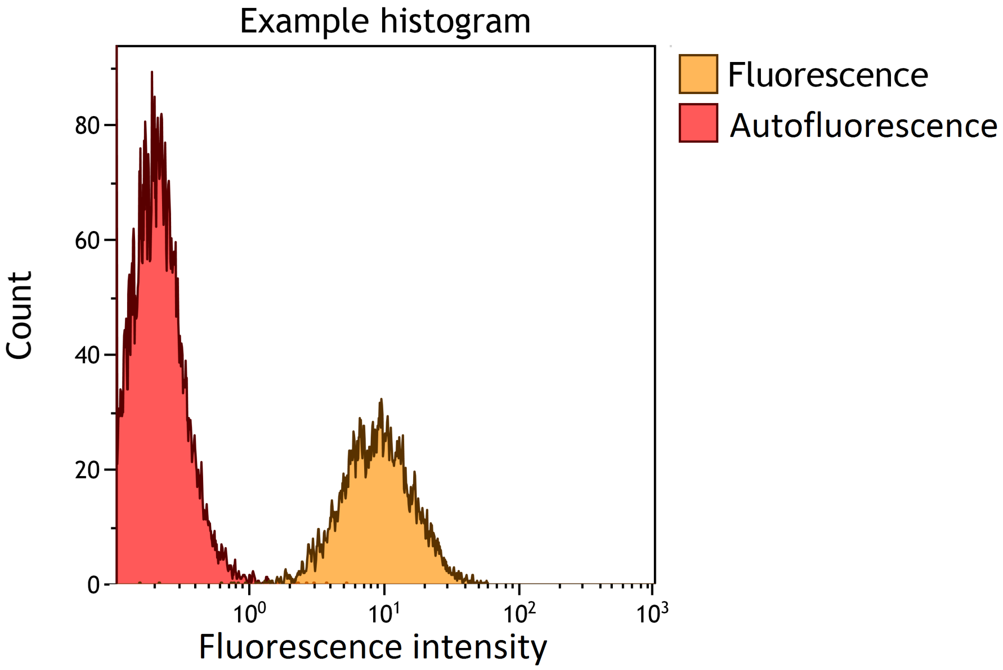

Figure 2.17: A typical histogram for the logarithmic fluorescence intensity in a population, compared autofluorescence of the control population. The y-axis represents the number of objects (counts), while the x-axis represents the fluorescence intensity.

Chapter 3

Materials and Methods

3.1 Materials

3.1.1 Nanoemulsions

Cholesterol, distearoyl-sn-glycero-3-phosphocholine (DSPC), distearoyl-sn-glycero-3 phosphoethanolamine- N-[methoxy(polyethylene glycol)-2000] (PEG-DSPE), distearoyl-sn-glycero-3 phosphoetanolamine-N-[maleimide-(polyethylene glycol)-2000] (MAL-PEG-DSPE) and gadolinium-diethylene triamine pentaacetic acid-di-stearylamide (Gd-DTPA-DSA) were purchased from Avanti® Polar Lipids, Inc. Phospholipids with fluorescent probes, 1,2-dipalmitoyl-sn-glycero-3-phosphoethanolamine-N-(lissamine rhodamine B sulfonyl) (Rhodamine-PE) and distearoyl-sn-glycero-3 phosphoetanolamine-N-[NIR664-(polyethylene glycol)-2000] (NIR664-PEG2000-DSPE) were purchased from Avanti® Polar Lipids and SyMO-Chem BV respectively. Soybean oil was purchased from Sigma Aldrich® .

3.1.2 Fluorescent Cell Markers

CellMask™ Orange, LysoTracker® Red, CellLight™ Early Endosomes-GFP ∗BacMam 2.0∗ and transferrin from human serum-Alexa Fluor® 488 conjugate were purchased from Invitrogen™. Hoechst 33452 was purchased from Sigma Aldrich®.

3.1.3 Endocytic Inhibitors

Chlorpromazine and genistein were purchased from Sigma Aldrich®.

3.1.4 Cell Culture

Human umbilical vein endothelial cells (HUVECs) were purchased from Lonza, and cultured in Dulbecco's modified eagle medium (DMEM) from Gibco®/Invitrogen™. The medium was supplemented with an EGM BulletKit ® from Lonza, containing fetal bovine serum, hydrocortisone, hFGF-B,VEGF, R3-IGF-1, ascorbic acid, hEGF, GA-1000 and heparine.

3.2 Cell Cultivation

HUVECs were cultivated in gelatine coated 75 cm^2 plastic flasks (nunc™), and incubated at 37 C° and 5% CO^2 water saturation. The cells were grown until 80 % confluency before passaged to a new flask. To perform passaging, the growth medium was removed and the cells were washed with 5 ml phosphate buffer saline (PBS, Sigma Aldrich®). Next, 3 ml of trypsin/EDTA (0.25 %/ 0.22%, Sigma Aldrich®) was added and the cells were incubated for 3-5 minutes to allow cell detachment. 7 ml of medium was added to stop the trypsination process, and the cell suspension centrifuged for 5 minutes at 1500 rpm to sediment cells. Finally, the supernatant was removed and the cells diluted in medium to a concentration of 300.000 cells/ml. 1 ml of the cell suspension was subsequently added to a new flask and incubated.

3.3 Gelatin Coating

Plastic flasks from nunc™, Ibidi®8-well μ-slides and Costar®12/24-well slides were coated with gelatin to improve cell attachment and growth.

For the plastic flasks, 0.2 g of gelatin was weighed out and dissolved in warm PBS (57 C°) to obtain a 0.2% gelatin solution. The solution was filtered under sterile conditions. Subsequently, 5 ml of the solution was added to each flask, and the flasks incubated for 20 minutes. Finally, the excess gelatin solution was removed and the flasks washed three times with 5 ml of PBS.

For the slides, the procedure was repeated. However, the gelatin content used was 1 % and the incubation time 30 minutes. 300 μl of gelatin solution was added to the ibidi 8-well μ-slides, whereas 900 μl and 1.5 ml was added to the 24 and 12-well slides respectively.

3.4 Preparation and Characterization of Nanoemulsions

Nanoemulsions with approximate sizes of 100 nm were made. All batches consisted of soybean oil droplets stabilized by a lipid monolayer comprised of DSPC, PEGylated DSPE, cholesterol and Gd-DTPA-DSA at a molar ratio of 1.1/0.15/1/0.75. To enable CLSM and flow cytometry, 0.1 mol% of fluorescent NIR664-PEG2000-DSPE or rhodamine-PE were added to the lipid mixture. Finally, the batches were split in two. One half was conjugated with RGD peptides to target $\alpha_v\beta_3$ integrins on activated endothelial cells, while the other half served as control emulsion. To make sure the emulsions were of expected quality, they were characterized in DLS for size and polydispersity determination. Table 3.1 shows the amount of each type of material used for making 100 nm emulsions.

Table 3.1: *Amounts used of the different compounds for making 100 nm sized nanoemulsions.*

Compound	**Molar ratio/3**	**Mw [g/mol]**	**Amount [mg]**
DSPC	1.1	790	2.90
PEG-DSPE	0.075	2806	0.70
Gd-DTPA-DSA	0.75	1050	2.63
Mal-PEG-DSPE	0.075	2941	0.74
Cholesterol	1	387	1.29
Soybean Oil	240 μl [125 mg/ml]		
NIR664-PEG2000-DSPE	87.825 μl [0.4 mg/ml]		
Rhodamine-PE	32.525 μl [0.4 mg/ml]		
Total amount of lipids = 10 μmol			

3.4.1 Synthesis

Firstly, the correct amounts of DSPC, PEG-DSPE, Gd-DTPA-DSA, Mal-PEG-DSPE and cholesterol (seen in table 3.1) were weighed out and dissolved in chloroform. The dissolved lipids were subsequently added to a roundbottom flask, along with soybean oil and fluorescent probe lipids. Next, the chloroform was evaporated in a rotary evaporator (with water bath of 35 C°) to form a thin lipid film. The lipid film was dried by decreasing the pressure and allowing the roundbottom flask to spin in room temperature (without water bath) for approximately 1 hour. To form the crude emulsion, the lipid film was hydrated with 1ml preheated HEPES-buffer (pH of 6.7) containing small glass beads at a water bath- temperature of 40C° and no vacuum. The emulsion was allowed to spin at maximum speed for 5-10 minutes before taken out of the rotary evaporator. To make the emulsion smaller and more uniformly sized, it was put in a tip sonicator (Heat Systems- Ultrasonics, Inc, W-225R) for 20 minutes at duty cycle=35% and frequency of 20kHz. Finally, the emulsion was spun in an ultracentrifuge for 6 minutes at 4000 rpm to sediment impurities from the tip sonicator. The purified emulsion was split in two and transferred to two eppendorf tubes, where one would be conjugated to RGD (section 3.4.2).

3.4.2 RGD-conjugation

The purpose of including Mal-PEG-DSPE into the lipid composition of the emulsions was to enable conjugation of the maleimide groups to cyclic RGD peptides. However, the linkage process requires that free thiols of the RGD peptides are accessible to maleimide. Commercially available cyclic RGD has an ”acetyl cage” around its thiol groups to prevent unwanted reactions. This means that the acetyl groups must be cleaved in order to perform conjugation, and this can be done by adding a de-acetylation buffer.

The de-acetylation buffer used consisted of 5.95 g/l HEPES, 1.74 g/l hydroxylamine, 0.37 g/l EDTA and of 5 tablets/l NaOH (Sigma Aldrich®). The buffer was adjusted to a pH of 7, and added to a eppendorf tube of RGD solution (2.5 mg/ml RGD) in a 1:10 volume ratio. Next, the RGD-buffer solution was vortexed for 1 hour, and added to the nanoemulsion. 6 μl of the RGD-buffer solution was added per μmol of lipid in the emulsion, and the emulsion was subsequently vortexed and left over night at 4 C°.

To remove unconjugated RGD and salts from the de-acetylation buffer, the RGD-emulsions were dialyzed for 24 hours in 1 ml Float-A-lyzers (Spectrum Laboratories, Inc). The molecular weight cutoff was 100 kDa, which means that free RGD-peptides of 719.82 Da were efficiently removed while the nanoemulsion was not. The buffer (HEPES, pH 6.7) was changed 2-4 times. After dialysis, the emulsion was stored in an eppendorf tube at 4 C°. RGD-emulsions were used for experiments not until three days after synthesis to make sure that unconjugated maleimide was hydrolyzed, such that the reactive maleimide would not interfere in experiments. The nanoemulsions were used within three weeks after preparation to assure reproducibility.

3.4.3 Characterization by DLS

To determine the mean sizes and polydispersity of nanoemulsions, a Zeta Sizer Nano Zs from Malvern Instruments with a laser beam of 633nm was used. Approximately 8 μl of emulsion was dispersed in a plastic cuvette containing 800 μl of filtered HEPES (pH 6.7). The solution was subsequently put into the Zeta Sizer instrument. Information related to the diffusion of emulsion particles was obtained according to the theory explained in section 2.6.1.

3.4.4 Calculating Concentrations

To determine the *approximate* concentration of lipids in the resulting emulsions, simple calculations were done. As the initial amount of lipids added is known, this amount can be used to determine the concentration in the end volume. However, it was needed to take some factors of the synthesis process into consideration. For example, the emulsion is pipetted from the roundbottom flask and into a new tube for sonication. Even though the flask is rinsed with buffer that is added to the solution, some percentage of lipids is assumed to be lost in this step. For the RGD-emulsion, even greater loss can be expected, as it is pipetted into and out of the float-A-lyzer tube. As a rule, 10 % lipid loss was accounted for in case of control emulsions, while 15 - 20 % were taken into consideration for RGD-emulsions. This approximate way of calculating lipid concentrations was validated by coworkers as sufficient for performing the experiments in this thesis. An example of the calculations performed can be shown in (3.1) for an emulsion with 5 μmol initial lipids, 10 % lipid loss, and resulting end volume of 500 μl:

$$\frac{5\mu mol \cdot 0.9}{500\mu l} = 0.009M = 9mM \tag{3.1}$$

3.5 Experimental Assays and Setup for CLSM

For experiments using CLSM, cells were seeded in Ibidi®8-well μ-slides with gelatin-coated glass bottom (1 cm^2 per well). The concentration of cells in each well was dependent on the timing of the experiments. As a rule, 10.000 cells/300 μl medium were seeded 48 hours in advance of experiment, or 20.000 cells/300 μl medium were seeded 24 hours in advance of experiment.

The CLSM used for studying nanoemulsion uptake and trafficking, was a Carl Zeiss LSM 510 Meta with a C-Apochromat 40x/1.2 water corrective objective. Four different lasers were utilized to excite the different fluorophores: argon (BP 500-530 IR filter), HeNe1 (590-612 filter), HeNe2 (655-697 filter) and Titanium:Sapphire (BP 435-485 IR filter).

The argon laser was used to excite the transferrin-Alexa Fluor 488 early endosome marker at a wavelength of 488, and also to produce differential interference contrast (DIC) images of the cells at 514 nm. The HeNe1 (Helium Neon 1) laser at 543 nm was used to excite the Rhodamine-PE probes, the CellMask Orange membrane staining and the LysoTracker lysosome staining. The HeNe2 (Helium Neon 2) at 633 nm was used to excite the NIR664-PEG2000-DSPE fluorescent probes. The Titanium:Sapphire two-photon laser (780 nm) was used to excite the Hoechst 33452. For colocalization studies and Z-stacking, the frame size was set to 1024 x 1024, 8 bit, with a zoom of 3.2 and minimal scan pixel time of 1.25 μsec to achieve proper image quality. The confocal pinhole size/Airy size was set to 1. The laser intensity, gain and offset was adjusted to achieve maximum signal with minimal saturation and background disturbance.

3.5.1 Test Experiment for Studying Emulsion Uptake in Cells

As a first experiment, HUVECs were incubated with RGD and control-emulsion separately, and their cell membrane and nucleus stained with Cellmask Orange and Hoechst. Cellmask Orange probes are amphipathic molecules with a negatively charged hydrophilic dye that incorporates into the cell membranes, while Hoechst bind to nuclear chromatin.

Firstly, the respective emulsion types (both containing NIR664-PEG-2000-DSPE) were diluted in medium to a lipid concentration of 1 mM. The growth medium of the cells was removed, and 150 μl of emulsion-medium solution was added to each well. Two wells were incubated with RGD-emulsion, and two wells with control-emulsion for 2.5 - 3 hours. After the incubation, the emulsions were removed and the cells washed with 200 μl of growth medium. To perform staining of the cell nucleuses, 150 μl of Hoechst-medium solution (with a concentration of 5 ug/ml) was added to each well, and the cells were further incubated for 25 minutes. The Hoechst solution was removed, and the cells were washed with 200 μl of growth medium, before 150 μl of Cellmask Orange-medium solution (concentration of 2.5 μg/ml) was added. This was allowed to incubate for 5 minutes. Finally, the cells were washed three times with growth medium and imaged with CLSM.

3.5.2 Investigating Optimal Incubation Times for RGD versus Control Emulsions

To better compare and investigate uptake mechanisms and trafficking pathways for targeted and non-targeted emulsions, it was desired to achieve a similar uptake for both types of emulsions. From previous experiments conducted by coworkers, it was seen that 3 hours of incubation with emulsion was sufficient for a substantial uptake of both RGD and control emulsions. However, the uptake of RGD-emulsion was larger than for control-emulsion, to the point where the cells were practically loaded with particles. As this is not something that would occur *in vivo*, it was desired to reduce the uptake to avoid incorrect observations in further uptake and trafficking studies. Thus, the uptake of targeted and non-targeted emulsions was studied after different time points to evaluate the optimal incubation times for the respective emulsion types.

The procedure for emulsion incubation was as follows: Firstly, the existing growth medium was removed from the wells, and the two types of emulsions (both containing NIR664-PEG2000-DSPE) were diluted in medium to a lipid concentration of 1 mM. Further, 150 μl of the medium-emulsion solution was added to each well. The RGD-emulsion was incubated with cells for 10, 20, 40 minutes and 1 hour in respective wells, whereas the control-emulsion was incubated for 10, 20, and 40 minutes, and 1, 2, 2.5, 3 and 3.5 hours. After incubation, the cells were washed three times with 200 μl of growth medium per well, and subsequently imaged with CLSM.

3.5.3 Lysosome Staining Using LysoTracker

Lysosomes were stained by LysoTracker to investigate if targeted and non-targeted emulsion particles were colocalized with these acidic compartments. The cells were imaged at different time points after ending the incubation, to assess changes in emulsion colocalization with time.

The medium in each well was removed and 150 μl of LysoTracker-medium solution with a LysoTracker concentration of 50-75 nM was added. The cells were incubated for 45 minutes before the LysoTracker was removed and washed with 200 μl of growth medium. 150 μl of emulsion-medium solution with lipid concentration of 1 mM was subsequently added. In case of the control emulsion, the cells were incubated for approximately 3 hours, whereas for the RGD-emulsion the cells were incubated for only 20 minutes. These incubation times were based on information obtained from the previous experiment (section 3.5.2). After incubation, the wells were washed three times with 200 μl of growth medium. In addition, one plate was prepared in order to investigate emulsion localization 24 hours after incubation. These cells were incubated with emulsion as explained above, then washed with medium and left overnight. 45 minutes before imaging the cells were stained with LysoTracker.

3.5.4 Early Endosome Staining Using CellLight Rab5-GFP

The CellLight viral system was utilized to obtain expression of GFP labeled Rab5, which is associated with early endosomes, and subsequently investigate nanoemulsion colocalization with these cellular compartments. The cells were incubated with virus particles at a concentration of ca. 40 particles per cell in 200 μl of medium 20 hours prior to CLSM experiments. 3 hours before the experiment, 100 μl of 3mM control-emulsion medium was added to two wells, so that the lipid concentration in the wells was 1 mM. 20 minutes prior to experiment, the same was done with RGD-emulsion to two new wells. All wells were washed three times with 200 μl of growth medium, before the samples were imaged with CLSM. Both emulsions contained the NIR664-PEG-2000-DSPE probe.

3.5.5 Early Endosome Staining Using Transferrin-Alexa Fluor 488

Transferrin-Alexa Fluor 488 staining was done to stain early endosomes, as an alternative to the previous experiment with CellLight. Firstly, targeted and non-targeted emulsions (NIR664-conjugated) were incubated with cells in the same manner as in previous experiments (3 hours incubation for control and 20 minutes for RGD). The last 10 minutes of the incubation time, the transferrin conjugates were added to the wells so that the final concentration of transferrin was 10 μg/ml in each well. Additionally, two separate wells were prepared in which *both* control-emulsion and transferrin were added simultaneously and incubated for 45 minutes. To achieve satisfactory emulsion uptake, the concentration of control-emulsion was 2 mM. As the incubation time was longer than that required for sufficient transferrin uptake, the concentration of transferrin was decreased to 2.5 and 5 μg/ml in the two wells respectively. The cells were washed three times with 200 μl of growth medium. Because the transferrin receptor is quickly recycled back to the cell membrane after internalization, the cells were put on ice before visualization.

3.5.6 Cells Incubated with Both Emulsion Types Simultaneously

To investigate if the control-emulsions and RGD-emulsions were taken up by different mechanisms and further trafficked in distinct pathways, cells were incubated with *both* emulsion types simultaneously. To distinguish the different emulsion particles, the control-emulsion was labeled with rhodamine-PE fluorescent probes, whereas the RGD-emulsion was labeled with NIR664-PEG-2000-DSPE. Two wells were prepared in which 1 mM of control-emulsion plus 0.15 mM of RGD-emulsion was added, before an incubation time of approximately 3 hours. Cells were washed three times with 200 μl of growth medium before imaging.

3.6 Experimental Assays and Setup for Flow Cytometry

For flow cytometry experiments, cells were seeded in plates containing either 12 wells of 5 cm^2 each, or 24 wells of 2 cm^2 each (Costar®). For the 24 well plates, 12.000 cells/600 μl were seeded 48 hours in advance of the experiment or 20.000 cells/600 μl were seeded 24 hours before the experiment. For the 12 well plates, 25.000 cells/1.5 ml were seeded 48 hours in advance of experiment, or approximately 40.000 cells/1.5 ml 24 hours before the experiment.

The flow cytometer used was a Gallios Beckman Coulter, and the NIR664-PEG2000-DSPE probe was excited with a 633 nm laser. By using a bandpass filter of 650-670 nm, background noise from the original laser wavelength was stopped, while the emission was allowed to reach the detector. Approximately 90 % of the cells were gated in the FSC/SS scatter plot to eliminate dead cells, debris and cell clusters (the percentage varied somewhat because of different quality of the samples). An example of selection of cells for gating can be seen in the appendix. Furthermore, the fluorescence intensity boundary line for excluding autofluorescence from measurements was set to 6-7 (seen in the appendix). Measurements were allowed to run for maximum 5 minutes, or to a maximum cell count number of 50.000. The median of fluorescence intensities was acquired for both positive cells (cells with emulsion uptake, defined by the boundary line), and for all cells in each sample.

3.6.1 Investigating the Effect of RGD-dialysis

To investigate if the dialysis of RGD-emulsions had effect on the cell-uptake of emulsion particles, flow cytometry was done of cells incubated with dialyzed RGD-emulsion and with cells incubated with non-dialyzed RGD-emulsion. The wells were prepared in duplo and incubated in the same manner as for the previous experiment.

3.6.2 Chlorpromazine and Genistein Endocytic Inhibition

Flow cytometry of cells incubated with NIR664-emulsion particles and endocytic inhibitors was performed in order to assess quantitative information about uptake mechanisms by methods of elimination. Chlorpromazine and genistein endocytic inhibitors were used, blockers of clathrin-mediated uptake and caveolae-mediated uptake respectively.

Firstly, the cells were washed with PBS, before they were pre-incubated with medium containing inhibitors for 30 minutes. The concentration of inhibitors was 10 μg/ml for chlorpromazine, and 70 μg/ml for genistein. This was based on endocytic inhibition work conducted by coworkers for HeLa cells, as it was shown that these concentrations gave satisfactory inhibition without severe toxicities. Next, the inhibitor medium was removed, and new medium containing both emulsion and inhibitors were added (1 mM of emulsion). The cells were subsequently incubated for 3 hours. After this incubation, the cells were washed two times with PBS, and detached with trypsin. Finally, the cells were resuspended in ice cold PBS containing 5 % fetal bovine serum, and pipetted through 40 μm nylon meshes into flow cytometer plastic tubes. The cells were kept on ice until the time of flow cytometry analysis.

As for the organization of samples, all samples were prepared in duplo and all combinations were tested together. This means that the following combinations were analyzed: cells/RGD/genistein, cells/RGD/chlorpromazine, cells/RGD/genistein/chlorpromazine, cells/RGD, cells/contr./genistein, cells/contr./chlorpromazine, cells/contr./genistein/chlorpromazine, cells/contr.

3.7 Data Analysis and Image Handling

Four different programs were used to analyze the data obtained from CLSM and flow cytometry experiments, and their use is more thoroughly explained below.

3.7.1 ImageJ

All images from CLSM experiments were handled and processed in ImageJ (available online). To obtain improved contrast and minimal background disturbance, the background fluorescence was subtracted using the ImageJ plugin "ROI: Background Subtraction from ROI", with a number of standard deviation from mean of 3.0. Further, the channels of the lsm. files from CLSM were split and merged to obtain images with overlays (e.g. overlay of two different fluorescent signals).

To do quantitative analysis of CLSM images, the plugin "Colocalization Analysis" was used.

3.7.2 Amira

The Amira® software from Visage Imaging® was used to obtain 3-dimensional visualization of Z-stacks acquired in CLSM. The "Isosurface" tool produced contours of the emulsion vesicles, where colors and thresholds could be set for the uploaded data. The optimal threshold values were found by varying the threshold of the stacks in ImageJ.

3.7.3 Kaluza

The Kaluza® software from Beckman Coulter was used to acquire overlays of flow cytometry histograms from control cells and cells incubated with emulsion and endocytic inhibitors. This was done by firstly making a composite of all datasets, and then using the "overlay" tool to drag and drop desired histograms on top of each other. The histograms were customized with colors and legends using the radial menu.

3.7.4 Statistics

Student T-tests were performed for statistical evaluation of data from quantitative colocalization analysis and flow cytometry uptake studies. This was done in order to assess significant differences in means between datasets. It was assumed that the data are normally distributed and that standard deviations are known. The analyzing function "TTEST" in Excel (Microsoft Office) was used to conduct two tailed tests with the assumption of unequal variances, and with a level of significance of 0.05. Resulting p-values were considered to indicate significant differences between datasets only when below the level of significance.

Chapter 4

Results

Below, results are presented experiment by experiment. A short overview of experiments and results can be found in table 4.2.

4.1 Characterization by DLS

DLS was used to investigate size distributions and polydispersity of the nanoemulsions. Figure 4.1 shows a typical size distribution curve of a nanoemulsion of an expected size of 100 nm, included Z-average value and PDI. Table 4.1 shows the values from nanoemulsions synthesized in this thesis. An acceptable PDI for nanoemulsions was set to 0.2. Some of the measurements showed PDIs that were slightly above 0.2. As it is assumed that large variations in size might affect trafficking pathways in cells, these emulsions were not used for CLSM studies.

The sizes of the RGD targeted-emulsions seem slightly elevated compared to that of control-emulsions. However, T-tests gave p-values of 0.262 and 0.292 for the mean peak diameters and Z-averages respectively, which is above the significance level of 0.05. Hence, the size differences between RGD and control-emulsions were not significant.

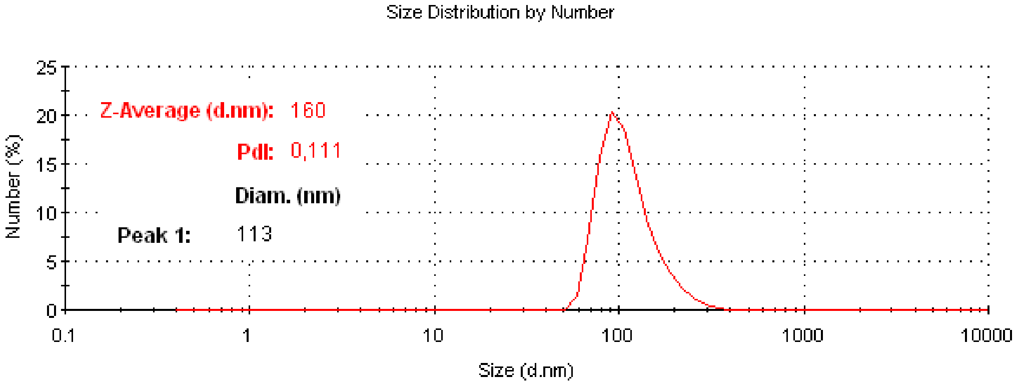

Figure 4.1: A typical size distribution curve for an emulsion of 100 nm expected size, aquired from the DLS software system.

Table 4.1: *Values from DLS analysis of the nanoemulsions used in this thesis.*

Fluorescent probe	**Mean peak diameter**	**PDI**	**Z-average**
Control-emulsions			
NIR664	109 nm	0.125	159 nm
NIR664	118 nm	0.183	187 nm
NIR664	121 nm	0.224	201 nm
Rhodamine	93 nm	0.071	124 nm
RGD-emulsions			
NIR664	113 nm	0.111	160 nm
NIR664	117 nm	0.216	205 nm
NIR664	118 nm	0.230	201 nm
NIR664	130 nm	0.175	199 nm

4.2 CLSM Experiments

4.2.1 Test Experiment for Studying Emulsion Uptake in Cells

In this experiment, HUVECs were incubated with RGD and control-emulsion for 3 hours. Further, the nucleuses and cell membranes were stained by Hoechst 33452 and CellMask Orange respectively.

From images acquired it seemed as both emulsion types were trafficked to the perinuclear region of the cells, e.g. close to the cell nucleus. However, the uptake amount of control-emulsion was lower than for RGD-emulsion. Representative images of RGD and control-emulsions with overlays of cell membrane and nucleus staining clearly show this (figure 4.2).

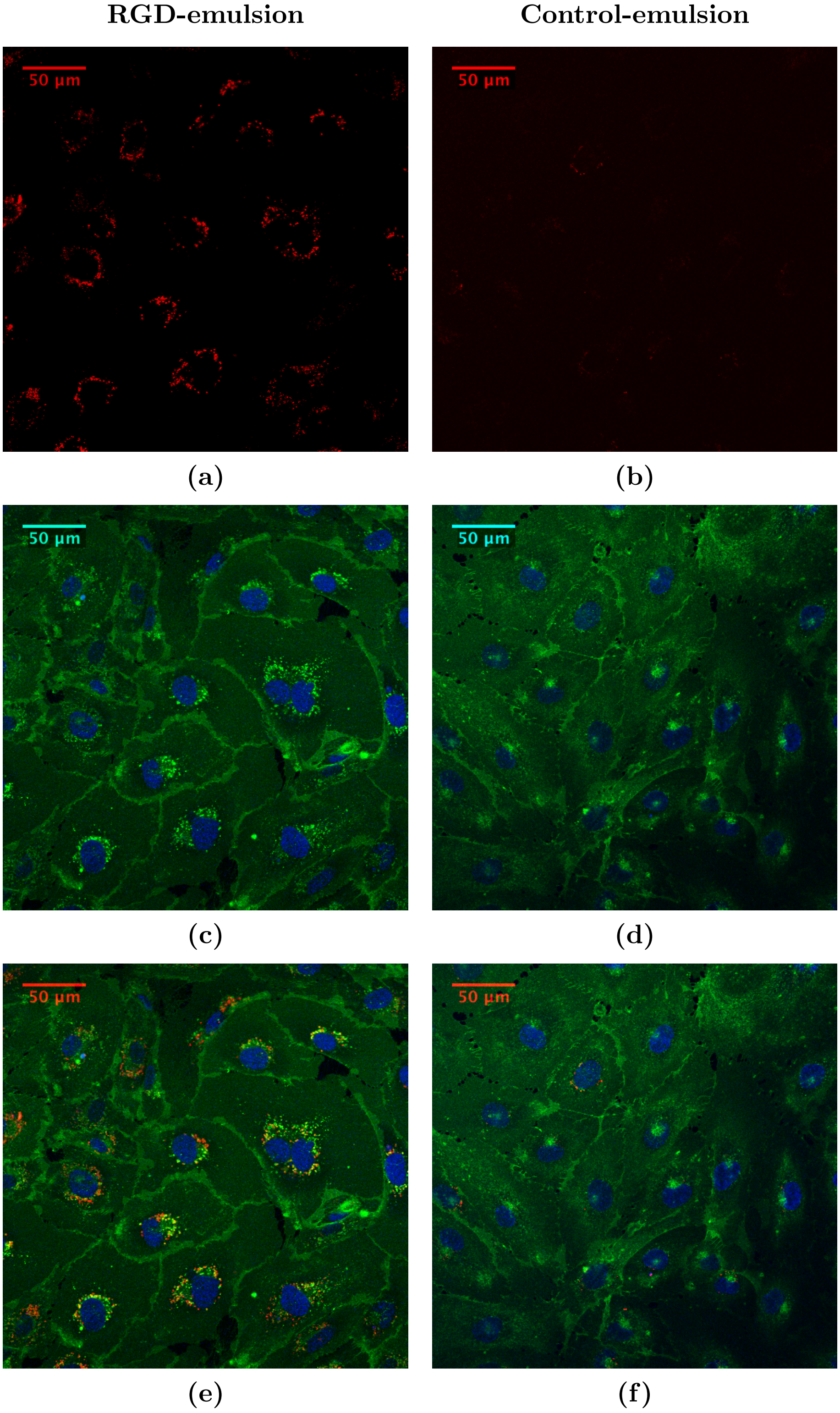

(a) (b) (c) (d) (e) (f)

Figure 4.2: CLSM images of HUVECs with cell membrane staining (green), nucleus staining (blue) and emulsion (red). (a): RGD-emulsion, (b): control-emulsion, (c) and (d): overlays of cell membrane and nucleus staining, (e) and (f): overlays of cell membrane staining, nucleus staining and emulsion for RGD and control-emulsions respectively. The green "vesicles" seen near the nucleus in (c) and (e) are parts of the cell membrane containing CellMask Orange that have been internalized after incubation. Both emulsions were incubated with cells for 3 hours, and it is clear that the uptake of RGD-emulsion is substantially larger than for control-emulsion.

4.2.2 Investigating Optimal Incubation Times for RGD versus Control Emulsions

From experiments with HUVECs incubated with control and RGD-emulsions for different times, it was confirmed that RGD-emulsions are taken up faster by the cells than control-emulsions and thus need a shorter incubation time. The different incubation times and resulting images are explained below.

When it comes to samples of cells incubated with control-emulsions for 10 and 20 minutes, there was no fluorescence to be seen. Only when using a very high laser power and high gain, some spots were seen. However, the background noise was too high to discern the actual emulsion signal. A representative image for 20 minutes incubation is seen in figure 4.3 with corresponding DIC image. The 10 minutes image was similar to that of 20 minutes, and is not included. For HUVECs incubated with control-emulsion for 1 hour, it was possible to acquire some images with the use of lower laser power and gain, and resulting minimal background disturbance. The uptake was very small and not seen in most cells. After 2 and 2.5 hours, the uptake had increased. Incubation times at 2 hours and above showed a substantial uptake. Representative images are shown in figure 4.3.

In contrast to the low uptake of control-emulsion at time points of 10 and 20 minutes, the uptake of RGD-emulsion was higher for the same incubation times. After 10 minutes, the uptake was not high but definitively present, as the laser power and gain could be reduced to a satisfactory level for obtaining images with low background noise. However, some locations on the samples had no uptake at all. After 20 minutes, the uptake was larger and almost all HUVECs had internalized emulsion. At 40 minutes and 1 hour, the uptake was even further elevated. Figure 4.4 shows representative images of HUVECs incubated with RGD-emulsion for 10, 20, 40 minutes and 1 hour. DIC images are included for time points of 10 and 20 minutes.

From this experiment it could be concluded that 2.5-3 hours incubation was needed for sufficient control-emulsion uptake, while 20 minutes of incubation was enough for satisfactory RGD-emulsion uptake.

Control – emulsion

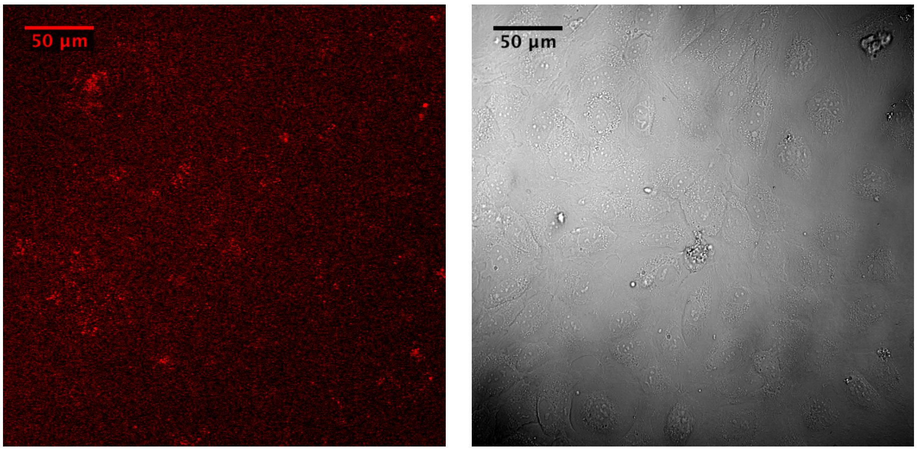

20 min **20 min DIC**

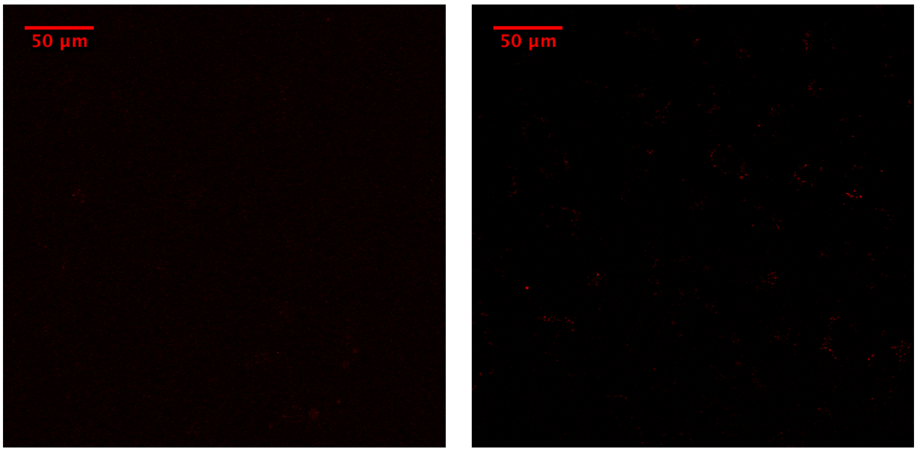

1 hour **2 hours**

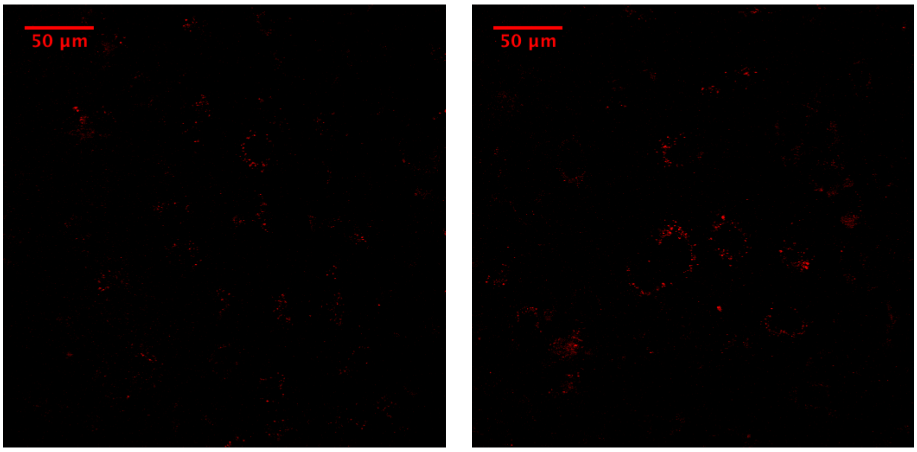

2.5 hours **3 hours**

Figure 4.3: Cells incubated with control-emulsion for 20 minutes, 1 hour, 2 hours, 2.5 hours and 3 hours. It can be seen that the uptake amount is substantial after approximately 2.5 - 3 hours.

RGD – emulsion

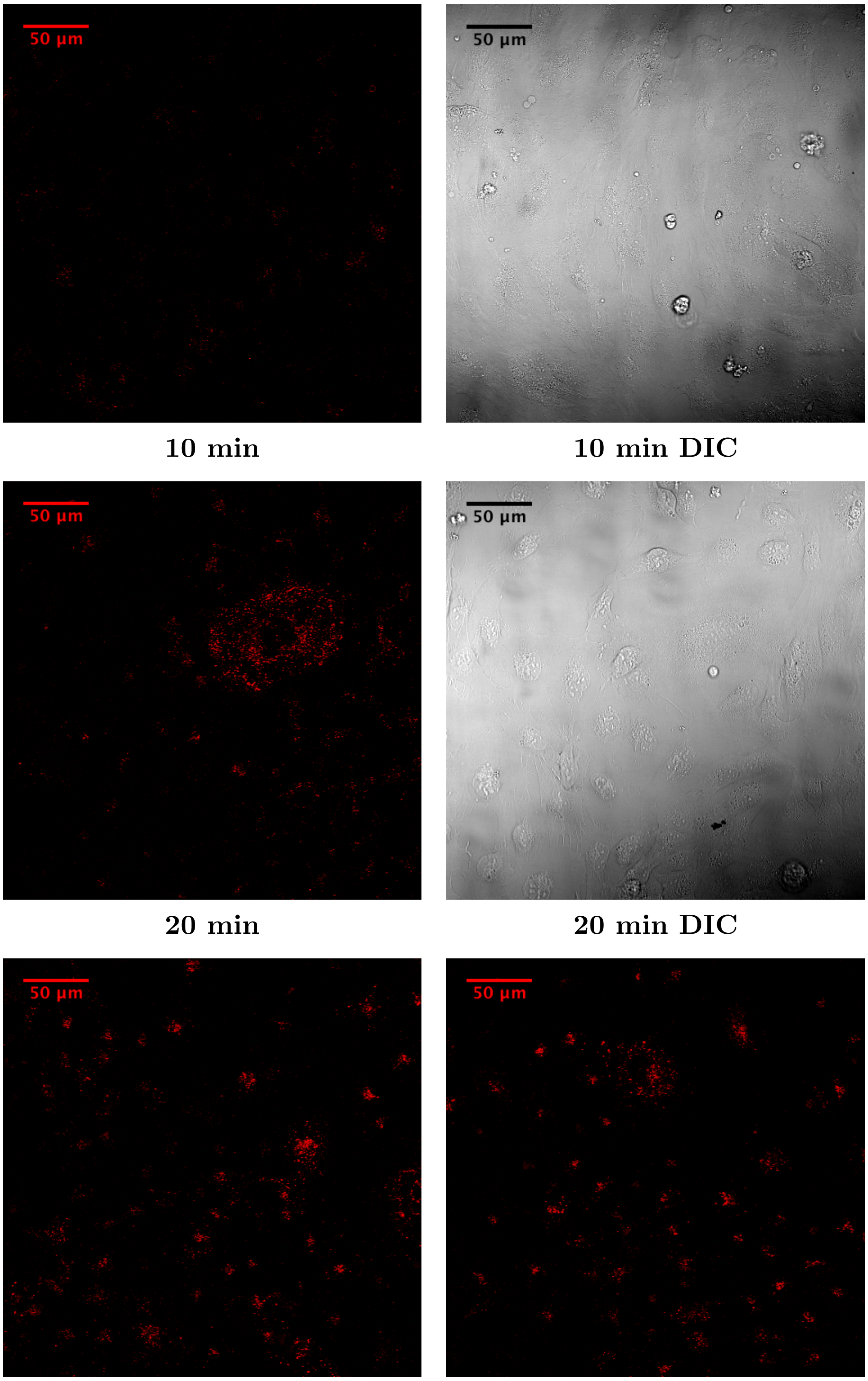
50 µm
50 µm
50 µm
50 µm
50 µm
50 µm

10 min **10 min DIC**

20 min **20 min DIC**

40 min **1 hour**

Figure 4.4: HUVECs incubated with RGD-emulsion for 10 minutes, 20 minutes, 40 minutes and 1 hour. The uptake was substantial already after 20 minutes.

4.2.3 Lysosome Staining Using LysoTracker

From experiments with LysoTracker staining of lysosomes, it was seen that the colocalization of control-emulsions in lysosomes was higher than for RGD-emulsions. Furthermore, the degree of colocalization changed with time, especially for the RGD-emulsion.

In figure 4.5 images of HUVECs incubated with emulsions and LysoTracker can be seen. The images were taken at different time points *after* completed incubation time of 20 minutes for RGD-emulsion and 3 hours for control-emulsion. Examples of images captured 5 min, 1 hour, 2 hours and 24 hours after incubation are shown. Additionally, an image of the RGD-emulsion captured 3 hours after incubation was included. This was done to compare the colocalization to that of control-emulsions imaged directly after incubation (at this point the RGD and control-emulsions have been trafficked for the same amount of time inside the cells). Qualitatively, the control-emulsion is localized in lysosomes to a larger degree than RGD-emulsion already 5 minutes after ended incubation. This is shown as yellow pixels, due to an overlap of red (emulsion) and green (lysosomes) spots. It can also be seen that the RGD-emulsion is not qualitatively colocalized with lysosomes after 3 hours. This gives a good indication that the different incubation times for RGD and control-emulsions do not affect the colocalization results substantially. After 24 hours both emulsions seem to be mainly localized in lysosomes.

3-dimensional images were generated in Amira from Z-stacks acquired from samples with RGD and control-emulsion directly after incubation. These are shown in figure 4.6. It can be seen that the control-emulsion is more closely associated with the lysosomes, compared to the RGD-emulsion. However, because colocalization, some of the control-emulsion cannot be seen as it resides in the lysosomes.

Quantitative analysis of colocalization was done by the aid of ImageJ to confirm these differences in lysosome colocalization for emulsions. Column charts that show the average Manders coefficients of colocalization analysis are shown in figure 4.7, where 1 represent perfect colocalization and 0 represent no colocalization. The values for these charts were calculated by finding the average of Manders coefficients from a selection of 18 images from two respective time periods (5 min-3 hours and 24 hours). These quantification studies indicate that a larger amount of control-emulsions than RGD-emulsions were in the lysosomes at all time points. They also showed that the amount of RGD-emulsion in lysosomes increased substantially after 24 hours. T-testing confirmed that the difference in RGD-emulsion colocalization in lysosomes was significant between the two time periods, with a p-value of $5.9 \cdot 10^{-6}$. The difference in control-emulsion colocalization of the time periods was also significant (p-value of $0.1 \cdot 10^{-3}$). Furthermore, the difference in lysosome colocalization between RGD and control-emulsions in the first time period was substantial, with a p-value of $3.6 \cdot 10^{-5}$. After 24 hours it can be concluded that the differences between RGD and control-emulsion colocalization in lysosomes were not significant, with a p-value of 0.154.

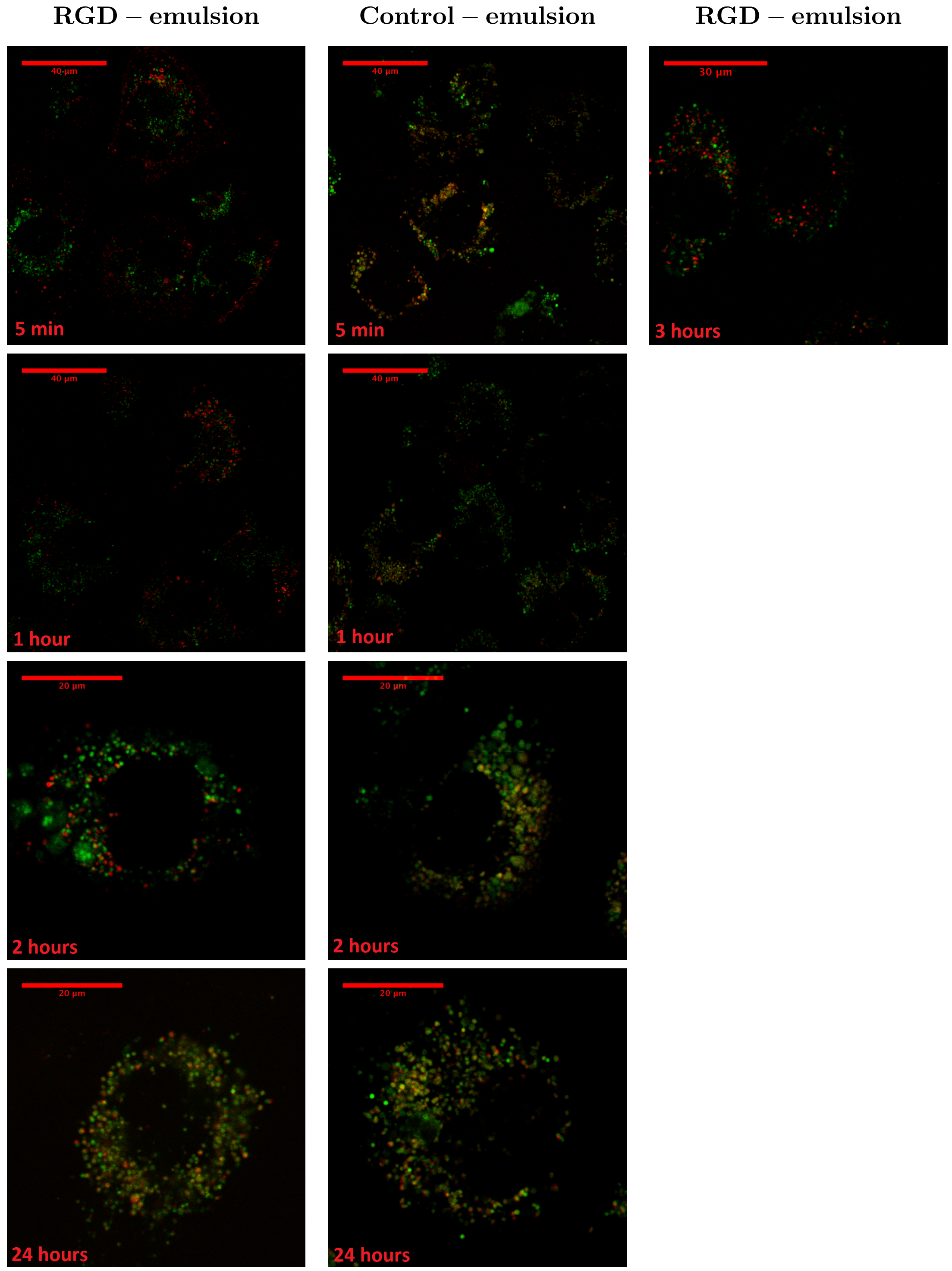
RGD – emulsion
Control – emulsion
RGD – emulsion
40 µm
5 min
40 µm
5 min
30 µm
3 hours
40 µm
1 hour
40 µm
1 hour
20 µm
2 hours
20 µm
2 hours
20 µm
24 hours
20 µm
24 hours

Figure 4.5: Representative images taken 5 minutes, 1 hour, 2 hours and 24 hours after incubation time with RGD and control-emulsions. The red spots represent the emulsions, whereas the green spots represent lysosomes stained by LysoTracker. A high degree of colocalization (yellow spots) can be seen for control-emulsions already 5 minutes after incubation. After 24 hours the colocalization of the RGD-emulsion in lysosomes is similar to that of control-emulsion. An image that show the RGD-emulsion 3 hours after incubation is also included, in order to compare it with that of control-emulsions imaged shortly after incubation (as the emulsions have been trafficked inside the cells for the same amount of time at this point).

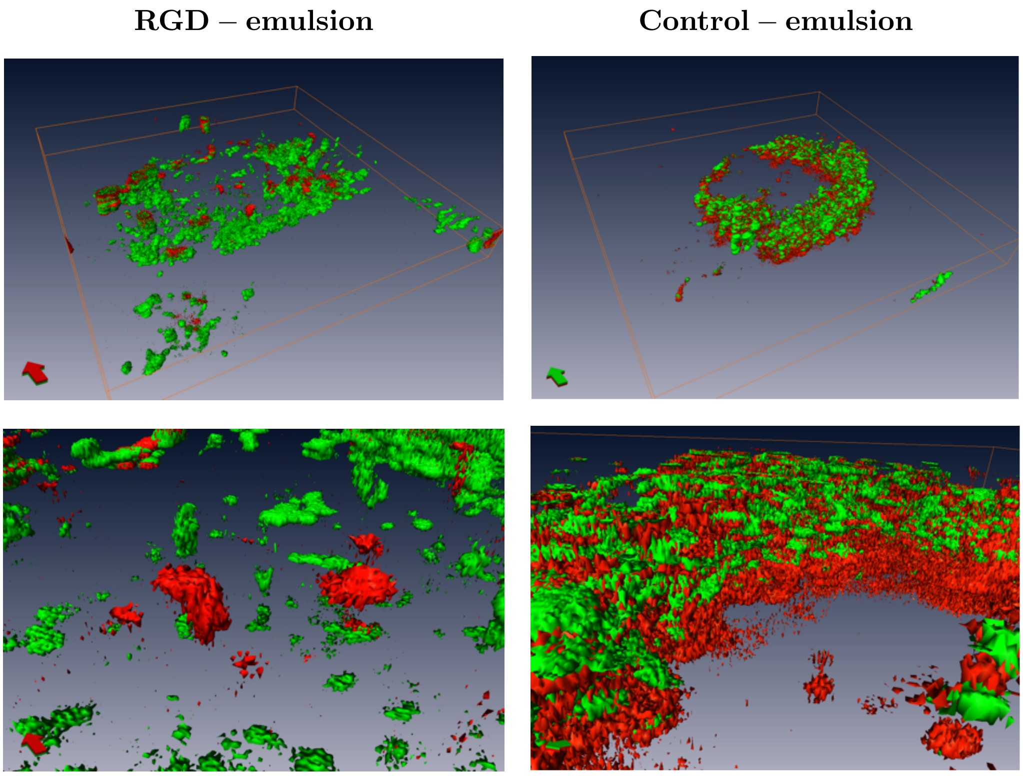
RGD – emulsion **Control – emulsion**

Figure 4.6: 3-dimensional images generated from Z-stacks of imaged cells incubated with LysoTracker plus RGD-emulsion and control-emulsion respectively. The images were taken directly after incubation. The emulsions can be seen in red, whereas lysosomes are marked as green. The control-emulsion seem to be more closely associated with the lysosomes. The bottom row shows images of the same cells as the first row, only zoomed in at areas near the nucleus.

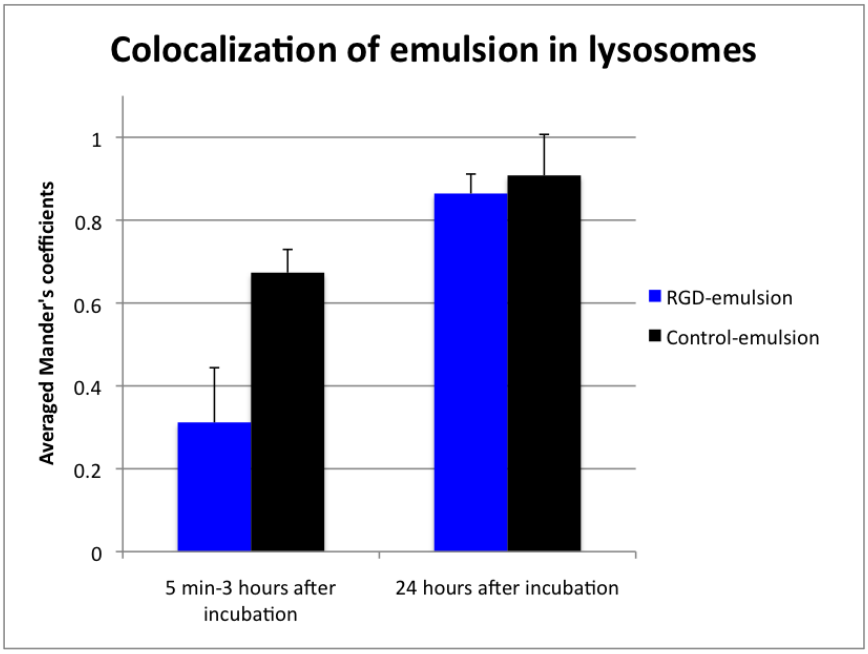

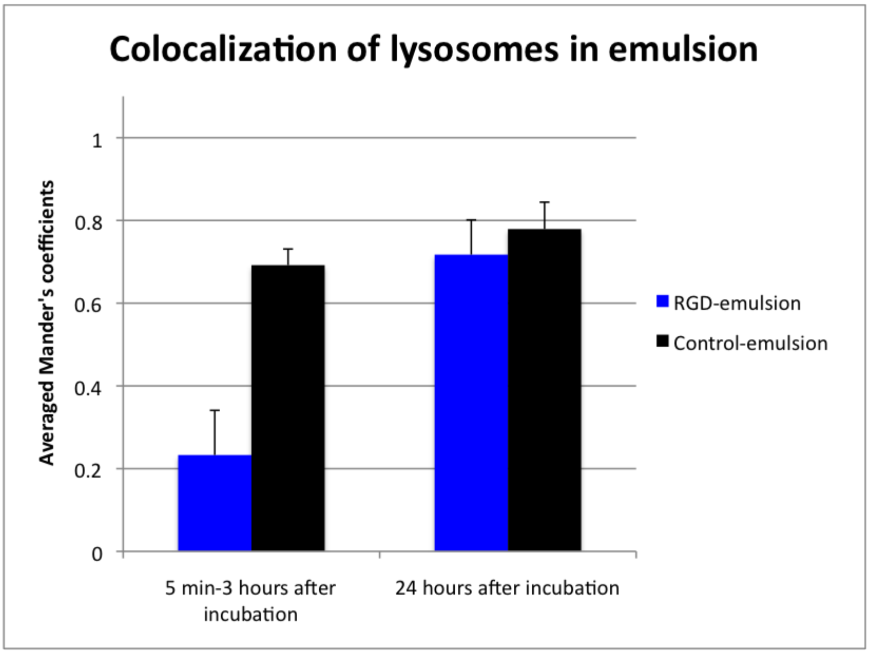

Figure 4.7: Quantitative analysis of colocalization of emulsion in lysosomes (M1), and lysosomes in emulsion (M2). Manders coefficient values were averaged over a selection of 18 images. 1 represent perfect colocalization overlap, whereas 0 represent no colocalization. The control-emulsion is colocalized with lysosomes (and vice versa) to a larger extent than the RGD-emulsion in the first 3 hours after incubation. After 24 hours the colocalization is more similar for both emulsion types. T-testing showed that the difference in RGD-emulsion colocalization between the two time periods was significant (p-value of 0.041), while the difference for control-emulsion was not (p-value of 0.273).

4.2.4 Early Endosome Staining Using CellLight Rab5-GFP

HUVECs were transfected with the CellLight Bacmam system in order to express Rab5-GFP of early endosomes and to do colocalization studies of emulsions in similar manner as for the LysoTracker experiment.

From this experiment, it was seen that the Rab5-GFP expression affected the uptake of emulsions. The cells were incubated with RGD and control-emulsions in the usual manner (20 minutes for RGD-emulsion and 3 hours for control-emulsion), but little or no uptake was observed for the RGD-emulsion. The uptake was also decreased substantially for the control-emulsion compared to previous experiments. Because of this, it was assumed that uptake mechanisms and trafficking pathways might be affected by the staining, and further colocalization experiments with Rab5-GFP were cancelled. Colocalization of emulsions and early endosomes was not observed visually for any samples, but due to the low emulsion uptake no quantitative colocalization studies were performed. Representative images can be seen in figure 4.8.

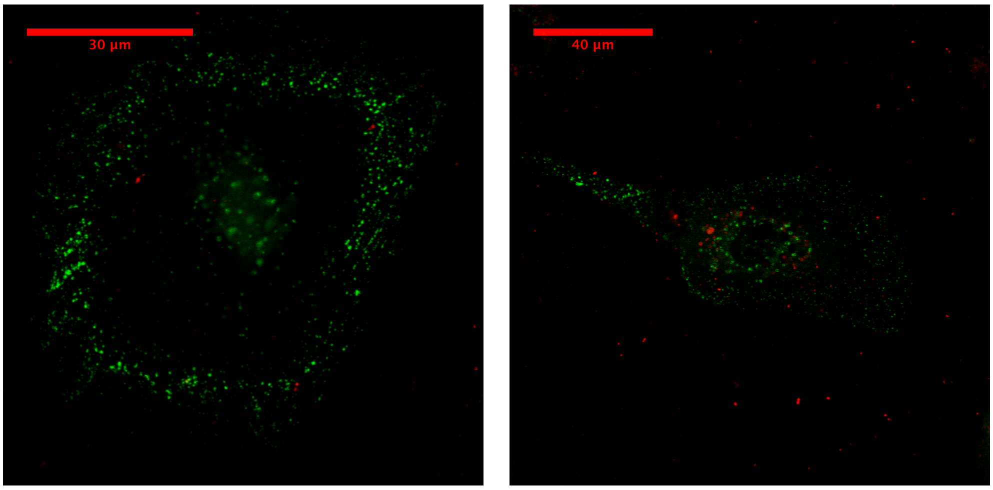

(a) (b)

Figure 4.8: CLSM images of HUVECs with Rab5-GFP staining of early endosomes (green) and emulsion (red). (a): cells incubated with RGD-emulsion (20 min), (b): cells incubated with control-emulsion (3 h). Almost no uptake of RGD-emulsion was observed.

4.2.5 Early Endosome Staining Using Transferrin-Alexa Fluor 488

As experiments with Rab5-GFP were not successful, alternative staining of early endosomes was performed with transferrin-Alexa Fluor 488. The samples were kept on ice and imaged in the CLSM directly after incubation.

The colocalization of emulsions in early endosomes was relatively low for both emulsion types, and could not be visualized qualitatively in images. Representative images for RGD an control-emulsions are included in figure 4.9. To allow for incubation of transferrin-Alexa Fluor and control-emulsion simultaneously, lower concentrations of transferrin were used for the samples seen in images 4.9 (e) and (f) (as explained in the materials and methods section).

Quantitative colocalization analysis was performed in same manner as for lysosome staining experiments with a selection of 14 images, and all show average colocalization values below 0.4 (figure 4.10). The t-test gave a p-value of 0.172 for comparison of RGD-emulsion and control-emulsion colocalization in early endosomes, which means that the difference in colocalization between the two types of emulsions was not significant.

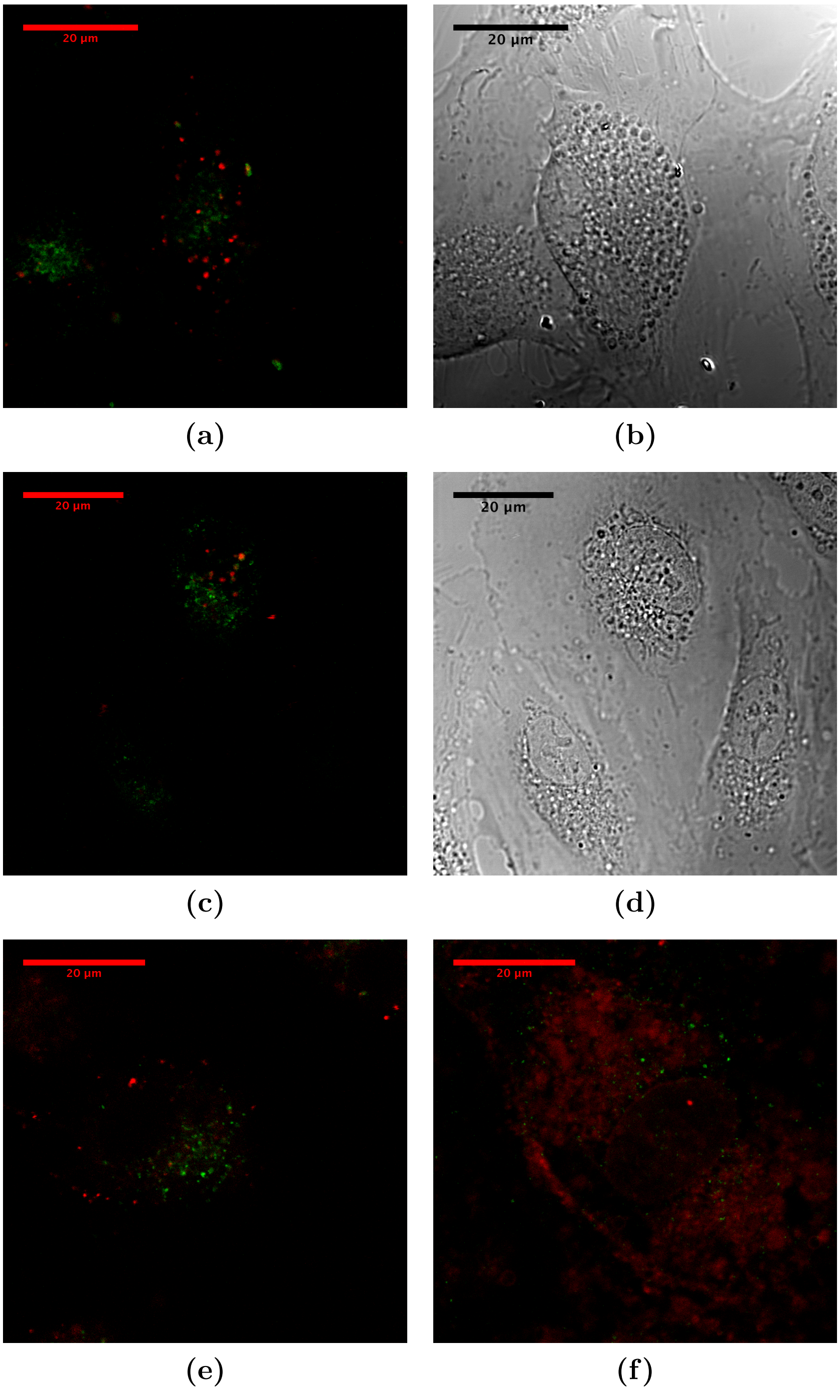

(a) (b)

(c) (d)

(e) (f)

Figure 4.9: CLSM images of HUVECs with transferrin-Alexa Fluor 488 staining of early endosomes (green) and emulsion (red). (a): RGD-emulsion and transferrin-Alexa Fluor (10 μg/ml) with corresponding DIC image (b), (c): control-emulsion and transferrin-Alexa Fluor (10 μg/ml) with corresponding DIC image (d). Two lower concentrations of transferrin-Alexa Fluor 488 were used along with a higher concentration of emulsion (2mM) for samples with control-emulsion, in order to incubate the cells with control-emulsion and staining for the same time period (45 minutes). (e): control-emulsion and transferrin-Alexa Fluor (2.5 μg/ml), (f):control-emulsion and transferrin-Alexa Fluor (5 μg/ml).

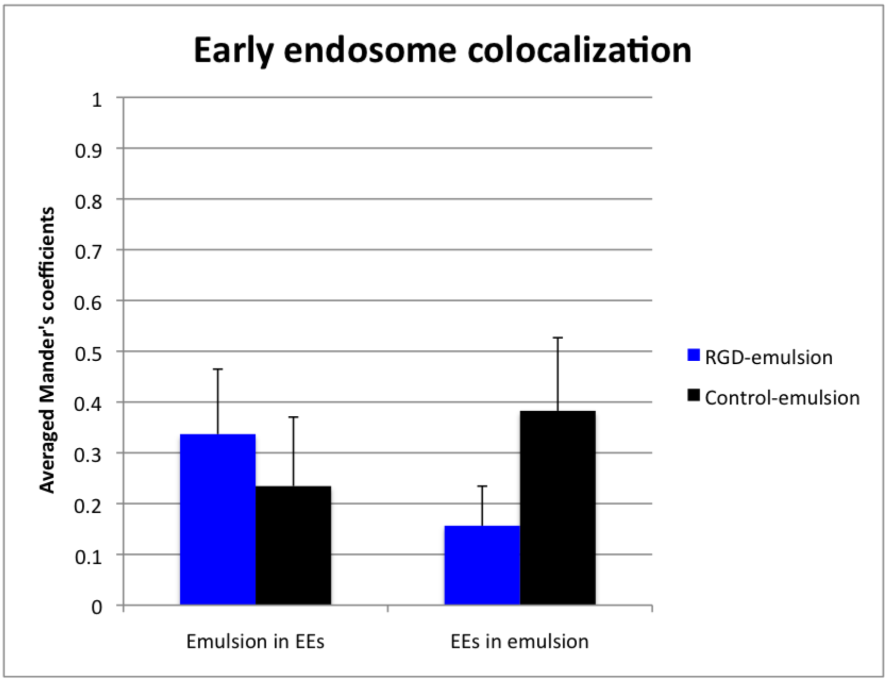

Figure 4.10: Quantitative analysis of colocalization of emulsion in early endosomes (M1), and early endosomes in emulsion (M2). Manders coefficient values were averaged over a selection of 14 images. 1 represent perfect colocalization overlap, whereas 0 represent no colocalization. The colocalization of both emulsions in early endosomes was low. T-testing showed that the difference in RGD and control-emulsion in early endosomes was not significant (p-value of 0.771).

4.2.6 Cells Incubated with Both Emulsion Types Simultaneously

To investigate if the two different emulsion types were taken up and trafficked by distinct mechanisms, cells were incubated with both RGD and control-emulsion simultaneously. Representative images are included in figure 4.11. In general, it could be seen that there was little colocalization of emulsions directly after incubation, and that the control-emulsion was localized towards the outer periphery of the cells to a larger degree than the RGD-emulsion. These vesicles containing control-emulsion also seemed smaller than those for the RGD-emulsion. After approximately 2 hours some vesicles of emulsion appeared to be fusing together, as seen in figure 4.11.

3-dimensional images were generated from Z-stacks, and these are included in figure 4.12. From these images, it is also seen that the control-emulsion is localized in more finely dispersed vesicles towards the periphery of the cell. Additionally, it seems as vesicles of RGD and control-emulsion are in fusion processes in the perinuclear area of the cell, in agreement with what was found in figure 4.11. This is more closely visualized in image (c) in figure 4.12.

Quantitative colocalization analysis was performed for a selection of 5 images from 0-45 minutes after incubation and 5 images from 2 hours after incubation. The averaged Mander's values are seen in figure 4.13. The values seem to increase with time, both for the colocalization of RGD-emulsion in control-emulsion and vice versa. T-testing showed that this increase with time was significant for the colocalization of RGD-emulsion in control-emulsion (p-value of 0.049), but not for control-emulsion in RGD-emulsion (p-value of 0.085). This means that the colocalization of RGD-emulsion in control-emulsion increases with time relative to the initial colocalization, but not the other way around. Furthermore, the difference in colocalization of RGD-emulsion in control-emulsion and control-emulsion in RGD-emulsion is significant for both time periods (p-value of 0.004 for both estimates). This means that there is always a larger fraction of the RGD-emulsion colocalized with control-emulsion than vice versa.

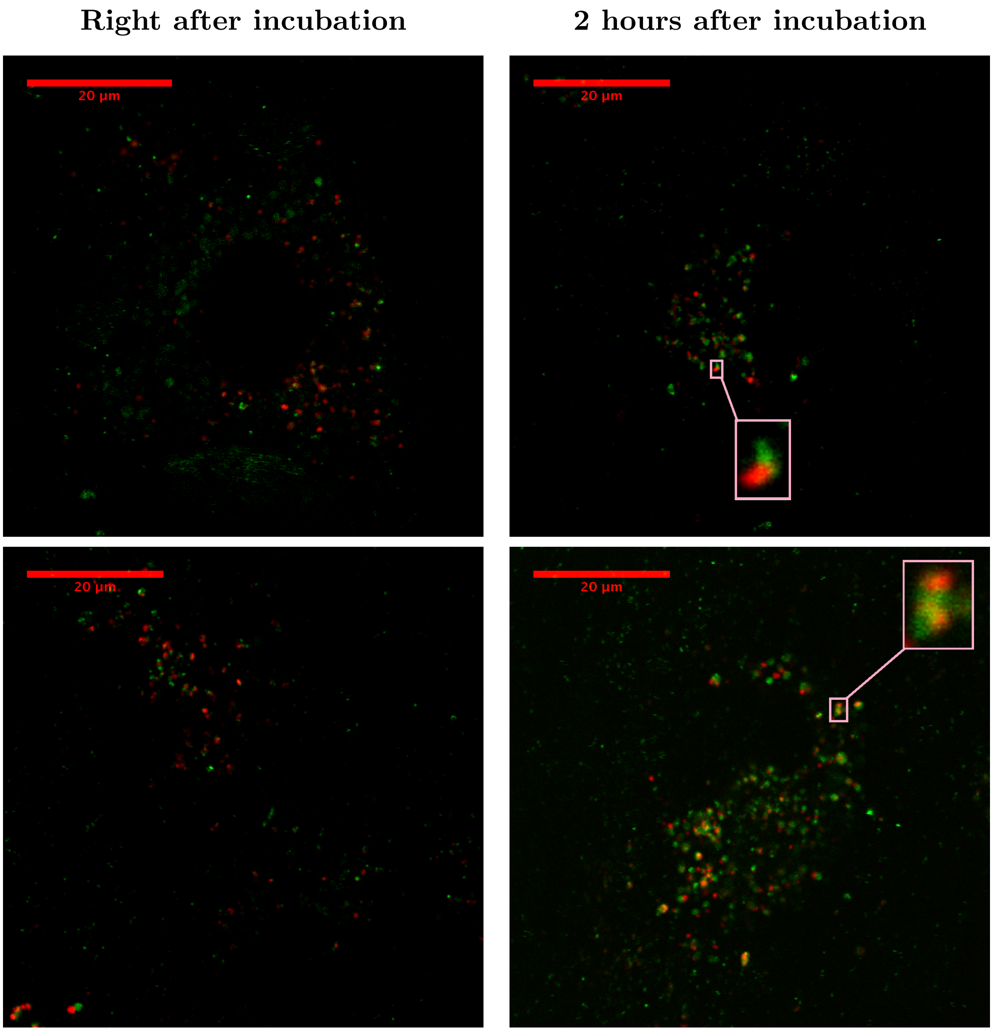
Right after incubation
2 hours after incubation
20 µm
20 µm
20 µm
20 µm

Figure 4.11: CLSM images of cells incubated with RGD (red) and control-emulsion (green) simultaneously. Little colocalization was seen visually directly after incubation, but increased with time. 2 hours after incubation, it was possible to see that vesicles of RGD and control-emulsion were fusing together, as highlighted by pink squares.

RGD-emulsion and Control-emulsion

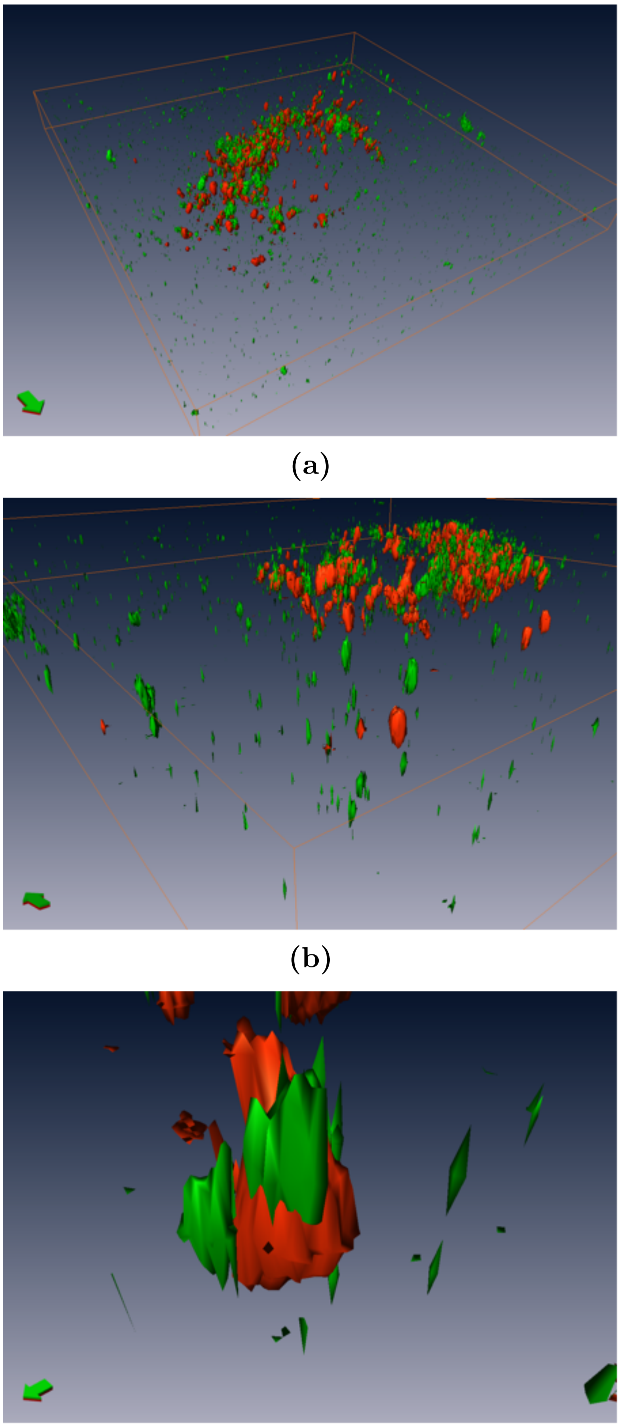

(a)

(b)

(c)

Figure 4.12: 3-dimensional images generated from Z-stacks of cells incubated with RGD (red) and control-emulsion (green) simultaneously. The control-emulsion is localized to the periphery of the cell to a larger degree than the RGD-emulsion. Image (a) shows an overview over the cell, while the periphery of the cell is zoomed in in image (b). In image (c), vesicles of RGD and control-emulsion near the perinuclear region are seen. They seem to be associated.

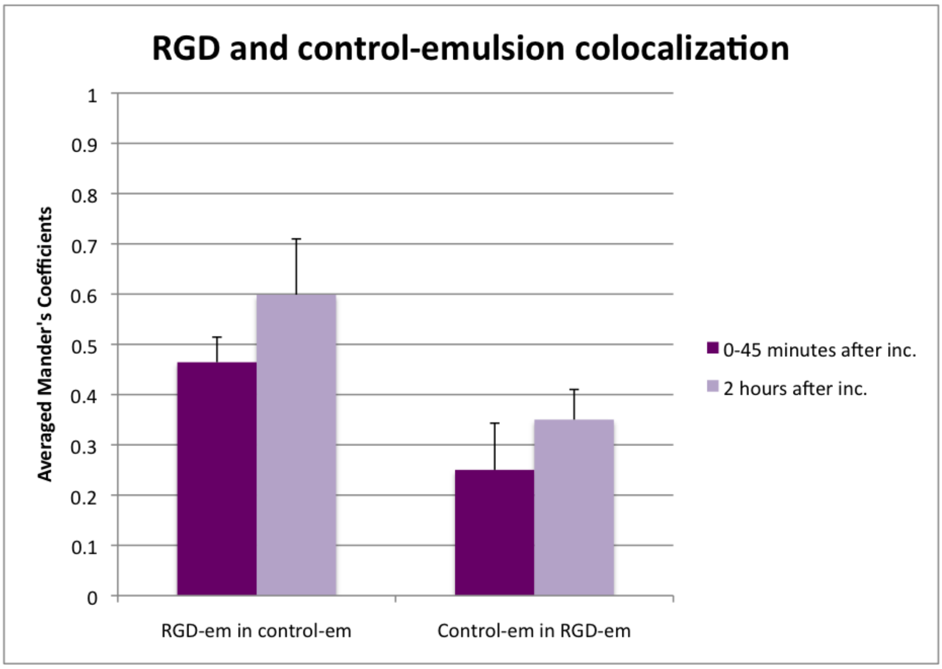

Figure 4.13: Quantitative analysis of colocalization of RGD-emulsion in control-emulsion (M1), and of control-emulsion in RGD-emulsion (M2). The analysis was done of images from two different time periods: 0-45 minutes after incubation and 2 hours after incubation. Manders coefficient values averaged over a selection of 5 images were used to generate the charts. 1 represent perfect colocalization, whereas 0 represent no colocalization. From t-tests it was found that the colocalization of RGD-emulsion in control-emulsion increased substantially with time.

4.3 Flow Cytometry Experiments

4.3.1 Investigating the Effect of RGD-Dialysis

Uptake studies of cells incubated with dialyzed and non-dialyzed RGD-emulsion respectively were done to assess the effect of the dialysis step. The resulting median of fluorescence intensities for all cells and for positive cells were averaged and normalized to the median of fluorescence intensity for untreated cells (autofluorescence). The values are presented in figure 4.14. It can be seen that the effect of dialysis was substantial, as the uptake amount of dialyzed RGD-emulsion was approximately 1.6 times larger than the non-dialyzed version. T-testing confirms this, with a p-value of 0.017 below the significance level of 0.05. Overlay histograms from two single samples of cells incubated with dialyzed and non-dialyzed RGD-emulsion can be seen in figure 4.15.

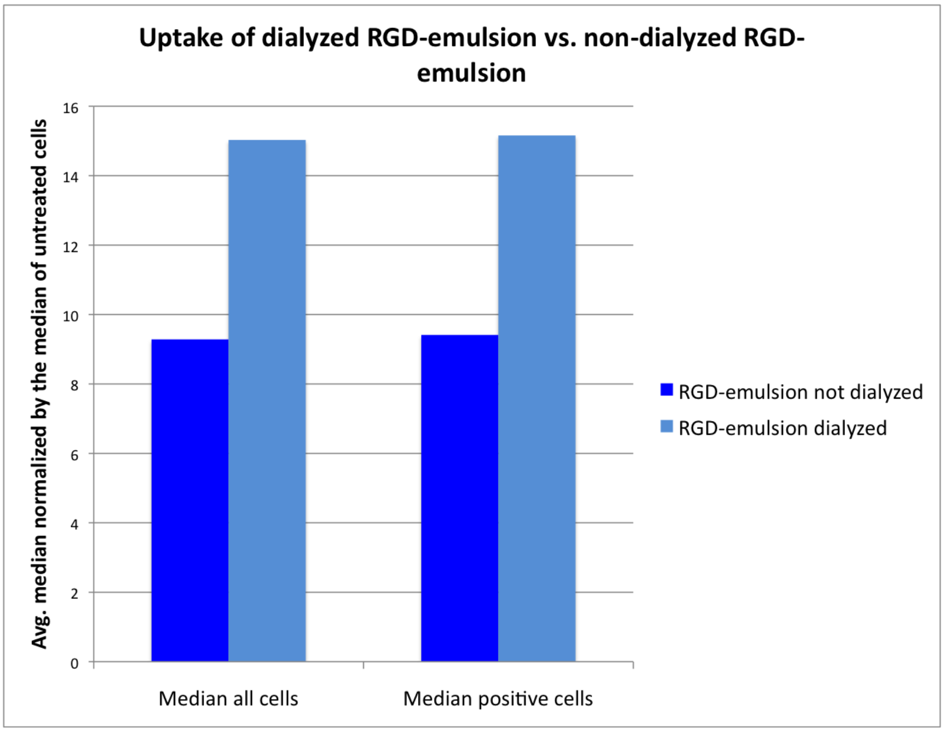

Figure 4.14: Uptake amount of dialyzed versus non-dialyzed RGD-emulsion. The values of the columns represent the average fluorescence intensity medians from flow cytometry experiments, normalized by the fluorescence intensity median of untreated cells (autofluorescence). Columns for uptake in all cells and in positive cells (cells with emulsion uptake) can be seen separately.

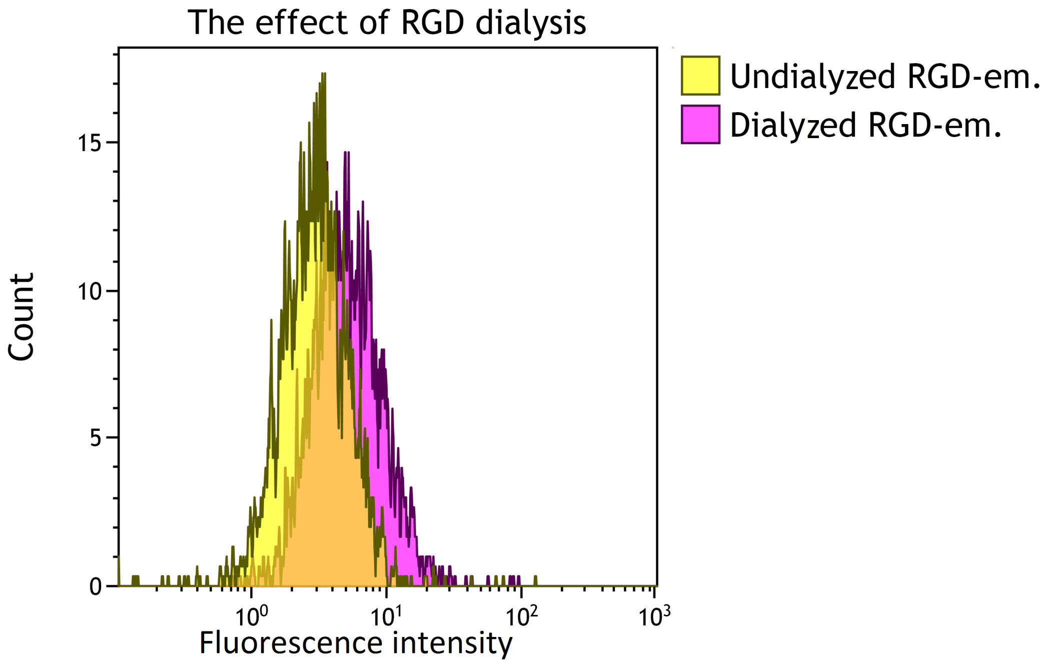

Figure 4.15: Representative logarithmic histograms obtained in flow cytometry from samples with dialyzed and non-dialyzed RGD-emulsion. The cellular uptake of dialyzed RGD-emulsion is approximately 1.6 times higher than the non-dialyzed RGD-emulsion.

4.3.2 Chlorpromazine and Genistein Endocytic Inhibition

Uptake studies of cells incubated with emulsions and different endocytic inhibitors was done to elucidate the uptake mechanism for the respective emulsion types. Column charts that show the uptake amount as averaged medians (of fluorescence intensity) normalized to the median (of fluorescence intensity) of untreated cells (autofluorescence) can be seen in figure 4.16. Representative overlay histograms can be seen in figure 4.17, and the number of positive cells in each sample (in %) can be seen in figure 4.18.

First of all the difference in uptake of RGD-emulsion and control-emulsion from samples with no inhibitors should be mentioned, as RGD-emulsion uptake is approximately 4.5 times larger than control-emulsion uptake (figure 4.16). In agreement with this, t-testing shows a p-value of 0.008, which means that the difference in uptake of RGD and control-emulsions is definitively significant.

For inhibition studies, genistein (inhibiting caveolae-mediated uptake) shows a large inhibiting effect on uptake amount of both emulsion types, but compared to the original uptake amount the effect is only significant for the RGD-emulsion (figure 4.16). This was shown by t-tests, as the p-value for difference between original RGD uptake and RGD uptake in response to genistein was 0.003, while the same t-test for control-emulsion gave a p-value of 0.053 (not significant).

Chlorpromazine (inhibiting clathrin-mediated uptake) also shows some inhibitory effect on the uptake of both emulsion types, but to a smaller extent than genistein. The difference was not significant for neither RGD-emulsions nor control-emulsions (p-values of 0.056 and 0.146 respectively). Furthermore, some percentage of the uptake was not inhibited by neither chlorpromazine nor genistein.

In figure 4.17 representative overlay histograms for endocytic inhibition studies are included, as well as histograms that show the difference in uptake for RGD and control-emulsions. It should be noted that the number of cells in certain samples was low, due to toxicity of the inhibitors. The number of cells was lowest in the genistein and genistein/chlorpromazine samples, which indicates highest toxicity for genistein.

As for the percentage of positive cells in each sample type (figure 4.18), it can be seen that samples with RGD-emulsion and no inhibitors has a slightly higher percentage of positive cells compared to that of the control-emulsion with no inhibitors. T-tests evaluated this to be a significant difference (p-value of 0.028). Furthermore, inhibitors seem to have the greatest effect on the number of positive cells for samples with control-emulsion, as the percentage was reduced to 92.8 for control-emulsion/chlorpromazine, and to 70.9 for control-emulsion/genistein. 70.9 % positive cells indicates that approximately 28 % of the cells do not take up control-emulsion due to inhibition by genistein. The greatest reduction in positive cells for samples with RGD-emulsion can be seen for RGD-emulsion/genistein (91.9 %) and RGD-emulsion/genisten/chlorpromazine (91.4 %).

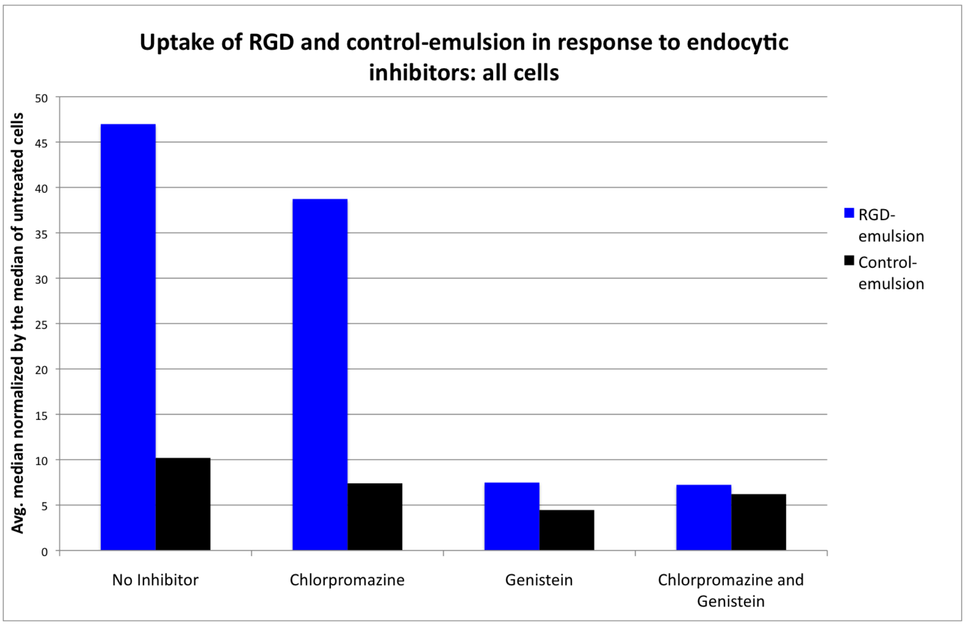

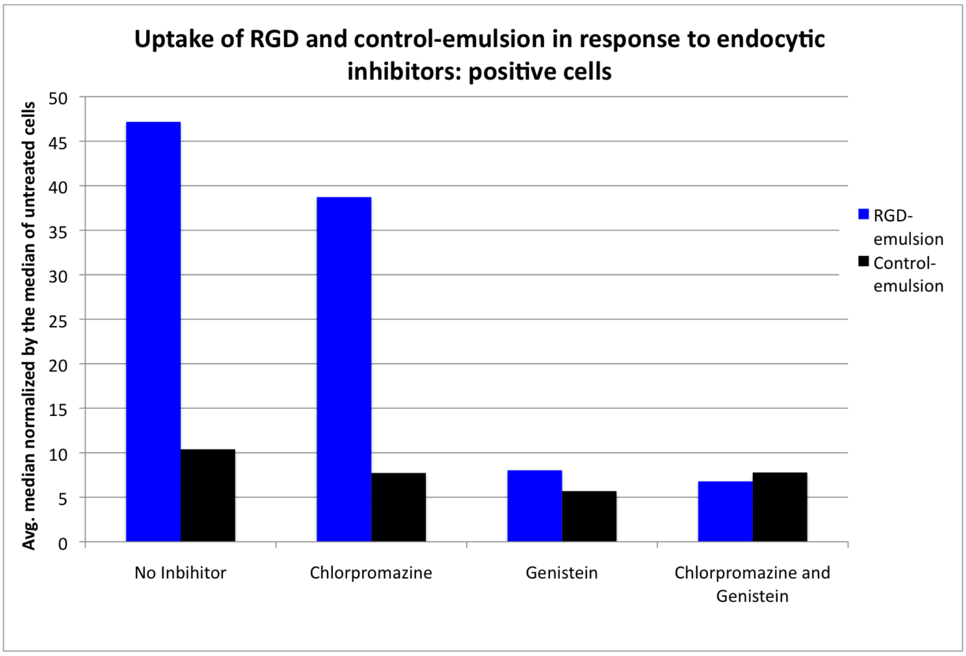

Figure 4.16: Uptake studies of cells incubated with emulsions and endocytic inhibitors. The values of the columns represent the average fluorescence intensity medians from flow cytometry experiments, normalized to the fluorescence intensity median of untreated cells (autofluorescence). Chlorpromazine is an inhibitor of clathrin-mediated uptake, whereas genistein is an inhibitor of caveolae-mediated uptake. Charts were generated for uptake in all cells (top) and in uptake positive cells (bottom)separately.

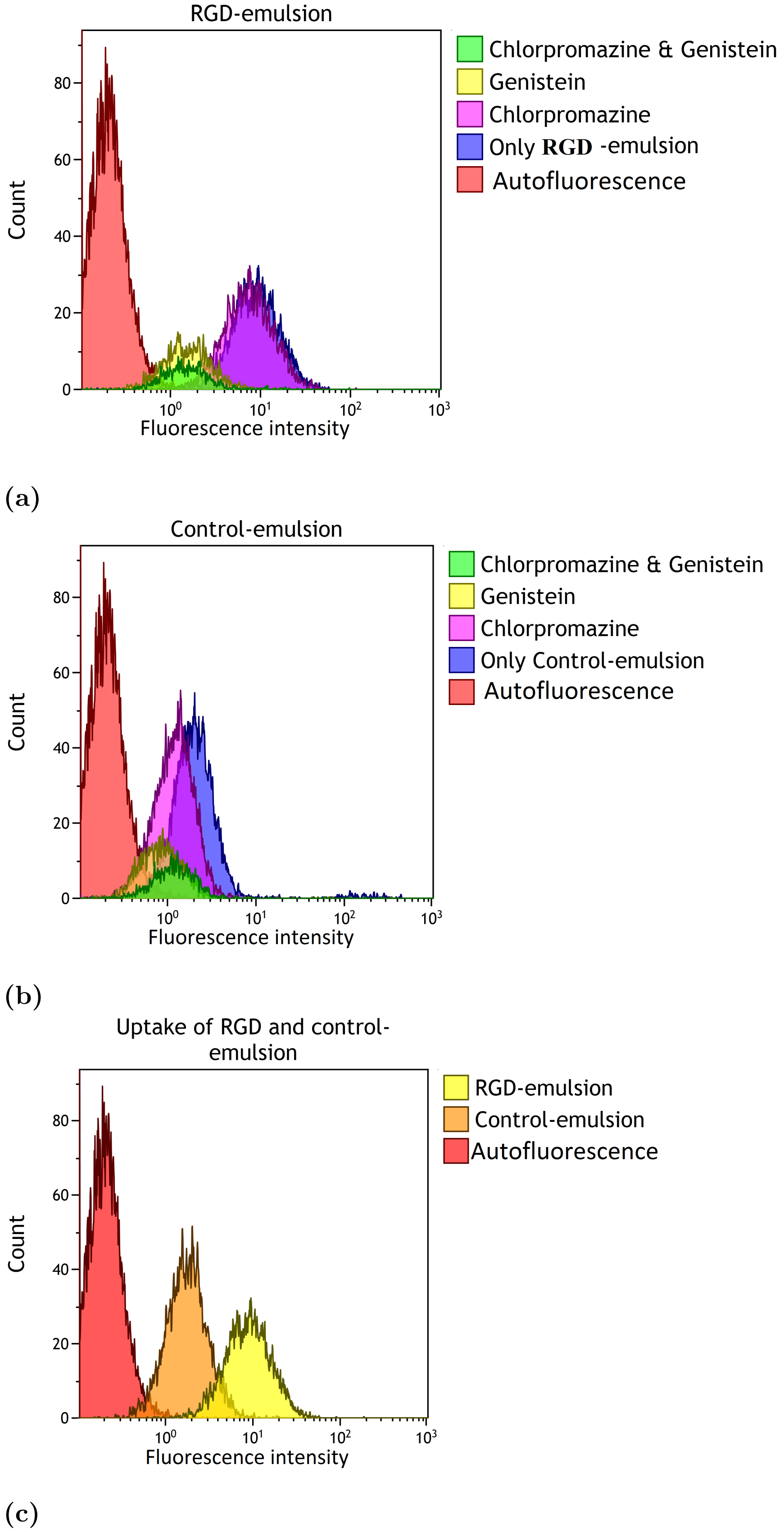

Figure 4.17: Representative histograms obtained in flow cytometry from cells incubated with RGD-emulsion and inhibitors (a), and control-emulsion and inhibitors (b). Histograms that show the difference in uptake of RGD and control-emulsion are also included (c).

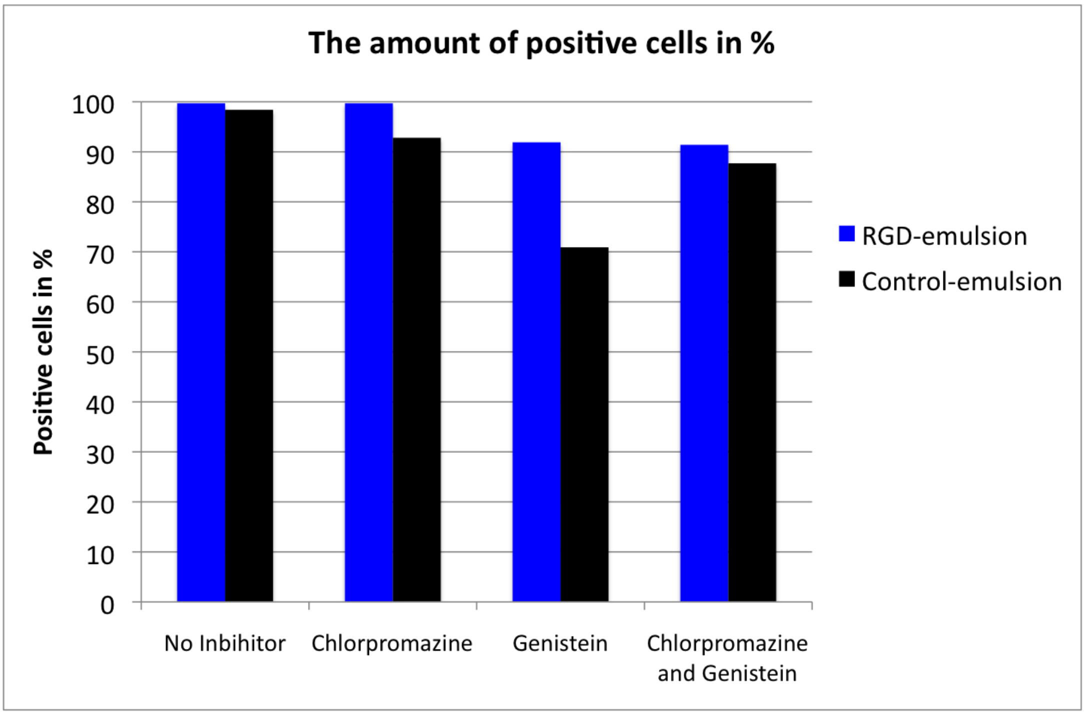

Figure 4.18: The amount of positive cells in each sample type relative to the total number of cells in the sample, in %. The number of positive cells in samples with control-emulsion is more greatly affected by inhibitors than for samples with RGD-emulsions. The percentage of positive cells is reduced to 70.9 % for control-emulsion/genistein, which means that approximately 27 % of all cells are completely inhibited by genistein in this sample.

Table 4.2: *Overview over the purpose and results of different experiments conducted, with reference to correlated figures.*

Experiment	**Purpose**	**Result**	**Reference**
DLS	Size & PDI characterization	Mean peak diameters from 109-121 nm. Some emulsions with PDI above 0.2.	Table 4.1
CLSM			
Test Experiment for Studying Em.Upt.	Visualize nucleus & cell membrane in combination with emulsions	Emulsions mainly localized in the peri-nuclear region. Lower uptake of control-em.	Figure 4.2
Inv. Optimal Incubation times	Find optimal incubation times for RDG and cont. emulsion	Sufficient inc.times of 20 min for RGD and approx. 3 hours for control-em.	Figure 4.3 and 4.4
Lysosome Staining	Investigate colocalization of emulsions with lysosomes	Larger coloc. for control-em. 5 min-2 h after inc. Similar coloc. for RGD and cont.em. after 24 h.	Figure 4.5, 4.6 and 4.7
Early E. Staining w/Rab5-GFP	Investigate coloc. of emulsions w/early endosomes	Rab5a-GFP marking affected emulsion uptake. No coloc.	Figure 4.8
Early E. Staining w/Transferrin Alexa Fluor	Investigate coloc. of emulsions w/early endosomes	Little colocalization	Figure 4.9 and 4.10
Cells Inc. w/ Both Emulsion Types Simultaneously	Coloc. of the two emulsion-types	Little coloc., but increases w/ time	Figure 4.11, 4.12 and 4.13
Flow Cytometry			
Inv. the Effect of RGD-Dialysis	Uptake amount of dialysed vs. non-dialysed RGD-emulsion	Uptake of dialysed RGD-emulsion substantially higher	Figure 4.14 and 4.15 and
Chlorpromazine and Genistein Endocytic Inhibition	Investigate uptake in response to inhibition of uptake pathways	Genistein largest inhibitory effect on uptake amount	Figure 4.16, 4.17 and 4.18

Chapter 5

Discussion

5.1 Characterization by DLS

DLS was done to assess the size and polydispersity of the different emulsion batches. All batches showed mean peak diameters between 93 nm and 130 nm, which was acceptable in aspect of expected size around 100 nm. However, some batches showed PDIs slightly above 0.2, which points to a larger spread in the size distributions for these batches. In these batches the amount of lipids used was higher, however the volume of hydration buffer was the same as for the other preparations. This indicated that with the used preparation method, nanoemulsions with a PDI below 0.2 can only reproducibly be prepared at lipid concentrations of 10 mM or below.

5.2 CLSM Experiments

5.2.1 Investigating Optimal Incubation times of RGD versus Control Emulsions

By incubating RGD and control-emulsions with cells for different periods of time, it was confirmed that the RGD-emulsions are taken up faster and more extensively by the cells than control-emulsions. Thus a shorter incubation time was sufficient for substantial RGD-emulsion uptake. The aim was to find incubation times that resulted in similar uptake amount for control and RGD-emulsions, and that was more realistic compared to *in vivo* uptake. The uptake of RDG-emulsion was present in nearly all cells throughout different samples after 20 minutes of incubation or less, and this incubation time was therefore concluded to be sufficient for further experiments. For the control-emulsion the uptake was qualitatively similar to that of 20 minutes incubation with RGD-emulsion after approximately 3 hours. As a consequence, those incubation times were applied for further experiments.

A cause of the larger uptake of RGD-emulsions at earlier time points is that the RGD-emulsion is more quickly taken up by cells due to receptor-mediated endocytosis. In literature, the uptake and recycling of $\alpha_v\beta_3$ integrins is described as a fast process [107]. Other studies have found that the number of $\alpha_v\beta_3$ integrins on HUVECs are (2.63 ± 0.08) x 10^5 per cell, and that the number of integrins expressed on cells correlates well to the amount of RGD peptide taken up. Furthermore, the uptake dynamics of RGD peptides compared to control peptides has been elucidated with flow cytometry at 37 C° over a time period of 2 hours. The mean fluorescence intensity of RGD peptides in HUVECs was more than 2.5 larger than for control peptides after 2000 seconds [108]. Uptake was also investigated with fluorescent peptides in CLSM, and it was found that RGD peptides could be clearly visualized within HUVECs after only 15 minutes of incubation, while the control version could not be visualized at all at this incubation time [108]. This is perfectly in agreement with our findings for the RGD-emulsion.

The difference in uptake for RGD-conjugated NPs and non-conjugated NPs has been reported previously. For example, it has been found that RGD-conjugated PLGA nanoparticles of approximately 200 nm showed more than three times larger uptake than the non-conjugated control NP in HUVECs after only 30 minutes of incubation [72]

5.2.2 Trafficking to Lysosomes

From the lysosome staining experiments, it was seen that a larger amount of control-emulsion than RGD-emulsion was colocalized with lysosomes from 5 minutes to 3 hours after incubation. After 24 hours, the colocalization was more similar for both emulsion types. The colocalization was investigated both visually and quantitatively, and the results clearly indicate that RGD-emulsions avoid the lysosomes to a large degree than control-emulsions *at least* the three first hours after incubation.

Others have performed similar experiments with the use of lysosome staining plus RGD-conjugated and non-conjugated NPs. Some reports support our findings [90], while others find different results. For example, RGD-conjugated PLGA NPs had substantial colocalization with lysosomes after 30 minutes of incubation, and the same trend was seen for RGD-nanogels, RGD-PEO-b-PCL micelles and RGD-nanoribbons [72, 109, 110, 111]. Additionally, the RGD-nanogel study show that the colocalization decreases substantially after 24 hours, which means that the RGD-nanogel exits the lysosomes within 24 hours [110]. As the internalization of these constructs were proven to be facilitated by the same receptor-mediated endocytosis with integrins, their trafficking and destiny must be determined by other factors once inside the cell. The sizes of the different NPs were in completely different ranges: the nanogels were of 30-40 nm size, the PEO-b-PCL micelles of 60-90 nm, the PLGA NPs approximately 200 nm and the nanoribbons between hundreds of nm and up to μm. This means that deviating results compared to the RGD-emulsion in question must be determined by other factors than size, for example by the chemical composition or surface charge of the emulsion particles.

For the control-emulsion, it is more likely that the size of the particles affects the uptake mechanism, as it does not interact with specific receptors. The already mentioned study with ligand-devoid latex beads of 50 to 1000 nm can emphasize this. Beads below 200 nm were preferably taken up by clathrin-mediated mechanisms and trafficked to lysosomes, whereas caveolae-mediated uptake of beads that avoided lysosomes was utilized once the bead were of 500 nm [89]. However, size does not solely determine the uptake and trafficking, and there are plenty of examples that show caveolae-mediated uptake of particles below 200 nm. Polymeric micelles with cross-linked core (around 100 nm), Doxil liposomes (86 nm) and CdSe/ZnS quantum dots (18 nm) are internalized by caveolae. Their common denominator is a negative surface charge [82], and the surface charge of the emulsions is also believed to be slightly negative although experiments have not been done to validate this.

An experiment that showed results that were partially in agreement with lysosome colocalization for nanoemulsions comes from Oba et al. The experiment was performed with RGD-PEG-polylysine micelles and its non-conjugated version. Although a substantial fraction of the RGD-micelles were colocalized with lysosomes, the colocalization was approximately 1/3 larger for control-micelles [90]. In that matter, the results suggest that at least some fraction of the RGD-micelles were not transported to the lysosomes.

An issue that needs to be discussed in context of the lysosome staining experiment is the different incubation times for RGD and control-emulsions. As control-emulsions were incubated for a substantially longer time (3 hours), the first emulsion particles that enter the cell had in theory been trafficked for over 3 hours inside the cell at the time of imaging. This means that it in reality has not been investigated where these emulsion particles are localized at the same time points as for the RGD-emulsion (for example at 20 min incubation + 5 min). As the uptake of control-emulsion was small after 20 minutes (discussed in section 5.2.1), it would not have been possible to directly compare findings at these early times. However, at 3 hours after incubation of the RGD-emulsion, little of the emulsion particles were colocalized with the lysosomes. This latter observation strongly indicates that our observations are valid and that the trafficking to the lysosomes are indeed slower for RGD-emulsions than for control-emulsions.

As a last point it should be mentioned that small errors could have occured for all colocalization studies conducted in this thesis, as the colocalization analysis was not performed in 3 dimensions (only generated from 2-dimensional images). Even though CLSM suppresses signals not related to the confocal plane, it is not able to eliminate spatially unrelated signals completely. This is because the diffraction pattern of light is 3-dimensional, with axial symmetry along the z-axis. In that matter, distortion along the z-axis occurs because of imbalance between the lateral and axial resolution. Colocalization analysis of 3-dimensional z-stacks are therefore more accurate than single 2-dimensional images [112].

5.2.3 Trafficking to Early Endosomes

The experiment with expression of Rab5-GFP was performed in order to assess emulsion localization within early endosomes. Results showed little or no colocalization of emulsions in early endosomes (not quantitatively assessed), and furthermore the uptake amount of emulsion was decreased substantially for RGD-emulsions but also somewhat for control-emulsions.

Rab5 is a GTPase enzyme that can be switched on and off by interaction with other proteins and effectors. For example, Rab5 can become active by binding to caveolin-1 in caveolae, as this binding presumably recruits guanine exchange factors or maintain GTPase activity by other methods [113]. Active Rab5 principally contributes to the formation of endocytic vesicles, the trafficking of vesicles to early endosomes, and the fusion of endocytic vesicles with early endosomes [113, 114]. It is known that genetic modifications performed in order to express Rab5a-GFP results in Rab5 overexpression [115]. This means that the balance between endocytic regulators in the cell may become disturbed. For example, there could be too much Rab5 contained within existing early endosomes. Rab5 is normally converted to Rab7 to form late endosomes, but if there are increased amounts of Rab5 in the early endosomes effectors may not able to convert all of it into Rab7 [116]. The process is consequentially halted. One *possible* explanation for the reduced uptake of emulsions may be that factors that are to be reused in uptake mechanisms are "stuck" in halted Rab5 endosomes, and that new uptake is limited because other factors are *not* overexpressed. This would mean that systems that facilitate emulsion uptake use factors that are also used in the Rab5 pathway. Yet, little or no colocalization of emulsions and early endosomes was seen.

Staining of early endosomes with transferrin-Alexa Fluor 488 was done as an alternative to the Rab5-GFP experiment. In agreement with the Rab5-GFP experiment, results showed little colocalization for both emulsion types. This indicates that the emulsions are not *mainly* trafficked to the early endosomes after internalization, at least not within the first hour after incubation when the imaging took place.

Based upon information from literature, an illustration scheme that summarizes events along pathways for clathrin-mediated, caveolae-mediated and clathrin and caveolae independent uptake was made (figure 5.1). It can be seen that Rab5 contributes to formation of both caveolae and clathrin vesicles, and also fusion of these vesicles with early endosomes [113, 114]. However, the fusion of caveolae with caveosomes is Rab5 independent [117]. Transferrin is taken up by clathrin-mediated mechanisms and transported to the early endosomes [83, 115]. As virtually no colocalization was seen in the Rab5-GFP experiment nor in the transferrin-Alexa Fluor 488 experiment, the pathway from caveolae to caveosomes represent a possibility for early endosome escape. If overexpression of Rab5 affects the uptake dynamics as previously depicted, this would mean that slow caveolae formation (and hence slow emulsion uptake) can occur even if no colocalization with early endosomes are seen, as long as the emulsions go to caveosomes. As the RGD-emulsion was shown to quickly accumulate in the perinuclear area of the cells, possible trafficking from caveosomes may be to Golgi or to the ER [83, 117]. A setback for the caveosome trafficking theory is that the existence of caveosomes recently has been questioned [118].

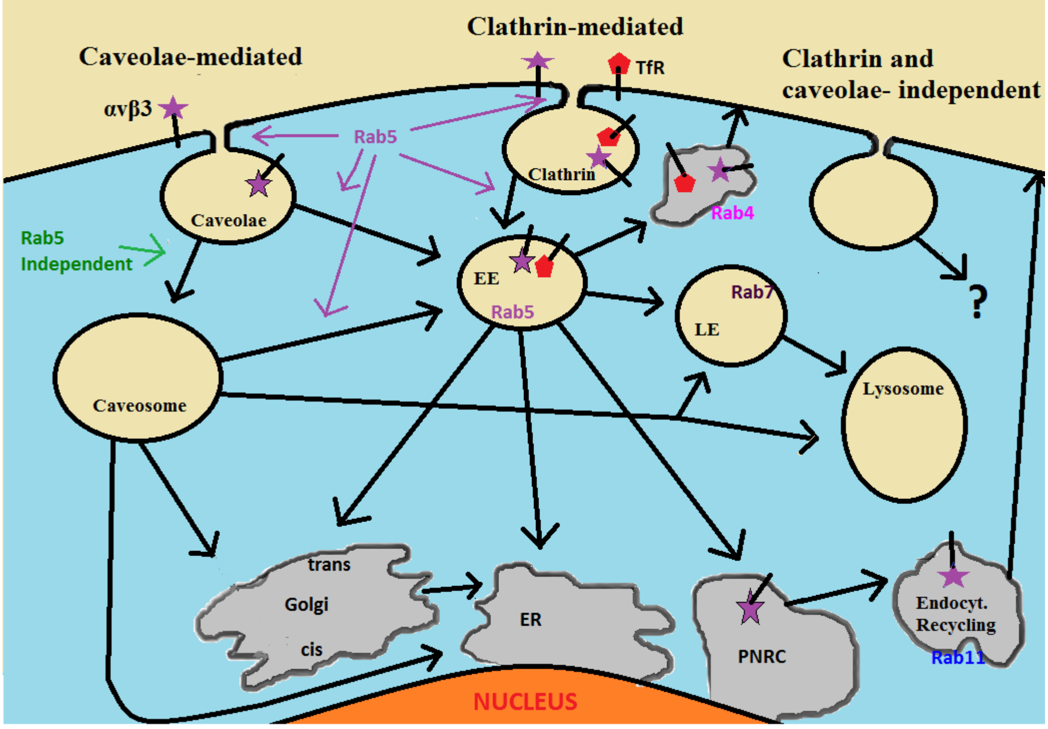
Caveolae-mediated
Clathrin-mediated
Clathrin and caveolae- independent
αvβ3
TfR
Rab5
Clathrin
Caveolae
Rab4
Rab5 Independent
EE
Rab5
Rab7
LE
?
Caveosome
Lysosome
trans
Golgi
cis
ER
PNRC
Endocyt. Recycling
Rab11
NUCLEUS

Figure 5.1: Illustration that summarize events along the endocytosis pathways of caveolae-mediated, clathrin-mediated and clathrin and caveolae independent endocytosis. The trafficking pathways of the transferrin receptor (TfR) and $\alpha_v\beta_3$ integrin receptor are included. Abbreviations: EE=early endosomes, LE=late endosomes, ER=endoplasmatic reticulum, PNRC= perinuclear recycling compartment.

A second theory of emulsion uptake can be proposed for clathrin and caveolae independent endocytosis. It has been found that substances taken up by these mechanisms can bypass Rab5 positive early endosomes. However, little is known about the subsequent trafficking pathways, and substances that utilize them are also taken up by other mechanisms, such as clathrin or caveolae mediated endocytosis [82]. This makes it hard to assess the probability of emulsion uptake by clathrin and caveolae independent endocytosis although quantitative colocalization analysis did show *small* values of colocalization with early endosomes.

The trafficking pathway of $\alpha_v\beta_3$ integrins should also be mentioned, as this is relevant for RGD-emulsions. It is known that these integrins are taken up by caveolae-mediated endocytosis and/or clathrin-mediated endocytosis and subsequentially transported to early endosomes. Further, the $\alpha_v\beta_3$ integrin basically follows two pathways, whereas one is a short recycling pathway (half-life of 3 minutes, shown as Rab4 dependent sorting in the illustration) and the other is a long pathway to the perinuclear recycling compartment (PNRC) with subsequent trafficking to an endocytic recycling compartment (half-life of 10 minutes, shown as Rab11 dependent sorting) [107, 119]. This could be an alternative pathway for the RGD-emulsions, since small amounts of colocalization in early endosomes were found quantitatively. Also, the long trafficking pathway of the $\alpha_v\beta_3$ integrin would in theory involve RGD-emulsion trafficking to the PNRC within approximately 5 minutes after uptake, and this is consistent with findings of RGD-emulsion in the perinuclear region within a short time after incubation. However, the trafficking route of a ligand conjugated NP may differ from the trafficking route of the ligand alone [120], which may also very well be the case for RGD-emulsions.

5.2.4 Cells Incubated with Both Emulsion Types Simultaneously

Cells were incubated with control-emulsion (marked by rhodamine) and RGD-emulsion (marked by NIR) simultaneously in order to assess differences in uptake and trafficking for the two types of emulsions. Quantitatively, it was shown that the colocalization was relatively low but present, and t-tests showed that a larger fraction of the RGD-emulsion was colocalized with control-emulsion than vice versa. Furthermore, the colocalization increased with time. Qualitatively, it was seen that the control emulsion was dispersed in smaller vesicles closer to the periphery of the cell (but also somewhat in the perinuclear region), while the RGD-emulsion were mainly contained in larger vesicles in the perinuclear region when imaged directly after incubation.

The data and images obtained indicate that the two types of emulsions are either taken up by different mechanisms or taken up by the same mechanisms but internalized or sorted into distinct vesicles. This is reasonable because it was seen, especially in 3-dimensional images, that RGD and control-emulsions were localized in separate vesicles towards the periphery of the cell. In either case, the vesicles they reside in seem to fuse together with time. This is in agreement with the lysosome trafficking experiments, as it was seen that only the control-emulsion was colocalized with lysosomes initially, but that both emulsion types were colocalized with lysosomes after 24 hours. The early endosome experiments points to the caveolae-mediated uptake as the most probable mechanism for uptake of both emulsion types. If so is the case, there must be some process inside the cell that decide the trafficking route for the respective emulsions after initial uptake. The question of uptake mechanism for the respective emulsion types will be more thoroughly discussed in the section 5.3.2.

The size of vesicles containing-control emulsion versus vesicles containing RGD-emulsions is logical considering findings in section 5.2.1 that control-emulsions are more slowly taken up than RGD-emulsions. As RGD-emulsions most probably are bound to integrin receptors, they are likely to be more concentrated so that more emulsion resides in each vesicle. Whether such vesicles are formed directly after initial uptake or after sorting and fusion processes is not known. The control-emulsions are most likely taken up by non-specific interactions with the cell membrane or by fluid phase endocytosis, and this would lead to a slower uptake with less concentrated amounts of emulsion in each vesicle [71]. Hence, these vesicles appear smaller compared to vesicles of RGD-emulsion.

The findings that control-emulsions are dispersed towards the periphery of the cell to a larger extent than RGD-emulsions is in agreement with results from by Oba et al.

with RGD-conjugated and non-conjugated micelles. It was found that non-conjugated micelles were mainly residing at locations towards the periphery of the cell, while RGD-micelles accumulated faster in the perinuclear region. Furthermore, it was found that the two types of micelles were contained in distinct vesicles after a short incubation time. The colocalization subsequently increased with time and was substantial 24 hours after incubation [90]. This is in excellent agreement with the results for emulsions, although in this case the cells were not investigated 24 hours after incubation.

5.3 Flow Cytometry Experiments

5.3.1 Investigating the Effect of RGD-Dialysis

From experiments with dialyzed and non-dialyzed RGD-emulsions, it was seen that the uptake of emulsion in cells was greatly enhanced for the dialyzed emulsion. This is reasonable, as free RGD peptides may bind and induce internalization of $\alpha_v\beta_3$ integrins.

Similar experiments have been done, for example for PLGA NPs. It was shown that addition of excess cRGD molecules competitively decreased cellular uptake of RGD-PLGA NPs but not of non-conjugated PLGA NPs [72].

Besides from indicating a more optimal way of preparing emulsions, the results show that specific receptors are indeed involved in the uptake of RGD-emulsions and that uptake of RGD and control-emulsions most likely differ because of this.

5.3.2 Chlorpromazine and Genistein Endocytic Inhibition

Uptake studies of cells incubated with emulsions in the presence of endocytic inhibitors chlorpromazine and genistein were done to obtain more knowledge about the uptake mechanisms for the different emulsions. Of the two inhibitors, genistein showed the greatest inhibitory effect for uptake amount of both emulsion types. However, the effect was substantially larger for the RGD-emulsion than for the control-emulsion. Additionally, the increased uptake of RGD-emulsion compared to control-emulsion was indeed confirmed from samples with no inhibitors, as the uptake of RGD-emulsion was approximately 4.5 times larger than that of the control-emulsion (figure 4.16 and image (c) in figure 4.17).

Results suggest that both emulsion types were *mainly* taken up by the aid of caveolae-mediated endocytosis. This was also indicated in experiments with early endosome staining, if the theory concerning trafficking to caveosomes is correct. A much larger fraction of the RGD-emulsion uptake was inhibited by genistein compared to the control-emulsion (shown by t-tests). This suggests that the RGD-peptide facilitates a fast receptor-mediated uptake through the caveolae, while the control-emulsion is possibly taken up by caveolae through non-specific interactions with receptors or other membrane components. For example, the PEG chains on the surface of the emulsion particles might interact with plasma membrane components through hydrophobic interaction or through a bridge of hydrated water molecules [90]. It should be mentioned that the number of cells measured in the flow cytometer in samples incubated with genistein was lower than that of samples incubated with chlorpromazine (figure 4.17). This is most probably due to toxicity of genistein, and might affect the calculated statistics. Cytotoxicity of genistein and chlorpromazine has been assessed by others [121], and results show a general higher toxicity of chlorpromazine compared to genistein. The opposite seemed to be true for our experiments. However, it is known that the cytotoxicity of different inhibitors varies with cell line [121].

Even though trafficking to lysosomes normally is associated with the clathrin-mediated pathway, studies with non-conjugated polymeric micelles have shown that NPs taken up by caveolae can bypass the early endosomes and still reach the lysosomes within a short period of time after incubation [122]. This may be the case for control-emulsion taken up by caveolae, as control-emulsion was seen in lysosomes to a much greater extent than RGD-emulsions directly after incubation (section 5.2.2).

Chlorpromazine also showed some inhibitory effect for both emulsions, which means that a small part of the emulsion is taken up by the clathrin-mediated mechanism. However, the number of positive cells decreased the most for control-emulsions in response to chlorpromazine, and this might suggest that clathrin-mediated endocytosis play a larger role for control-emulsion uptake than for RGD-emulsion uptake. Clathrin-mediated uptake involves subsequent trafficking to the early endosomes as depicted in figure 5.1. It was seen from CLSM studies that the emulsions were not mainly in early endosomes, but quantitative colocalization *did* show some small values for colocalization. This indicates that clathrin-mediated uptake found by flow cytometry is reasonable, although it was not qualitatively seen in images.

Concerning samples incubated with both inhibitors simultaneously, it can be seen that the uptake was not decreased below that of genistein inhibition. In fact, the uptake seemed to increase by a small amount for control-emulsions. There can be several reasons for this effect. Firstly, it has been shown that endocytic inhibition with chlorpromazine can upregulate other uptake mechanisms [96, 97]. This might mean that clathrin-mediated endocytosis participates to a greater extent for control-emulsions than for RGD-emulsions, which was also indicated by the lower percentage of positive cells in those samples. Secondly, the number of cells in these samples was decreased substantially due to the toxicity of the inhibitors. The latter means that the amount of cells might not have been sufficient to compare average findings with that of average findings for other samples. Most importantly, the results indicate that some fraction of the emulsions is taken up by neither caveolae-mediated endocytosis *nor* clathrin-mediated endocytosis. Other possibilities then include macropinocytosis and/or clathrin and caveolae independent endocytosis, or other yet unknown mechanisms.

Finally, it should be mentioned that the ability of the inhibitors to block uptake mechanisms is far from perfect, and it is also dependent on the cell type utilized [121]. This means that it is hard to assess whether emulsion uptake in presence of inhibitors is exclusively due to uptake by other mechanisms or due to inability of the inhibitors to block endocytosis. In aspect of this, the interpretation of results is not necessarily 100% in agreement with reality, but might give an indication concerning key aspects.

5.4 Overview of Possible Trafficking Pathways

Based on results obtained in this thesis and in literature, possible uptake mechanisms and trafficking pathways for RGD and control-emulsions can be proposed. However, a substantial amount of work still remains to get a clearer picture. The proposal explanations below are illustrated in fig 5.2.

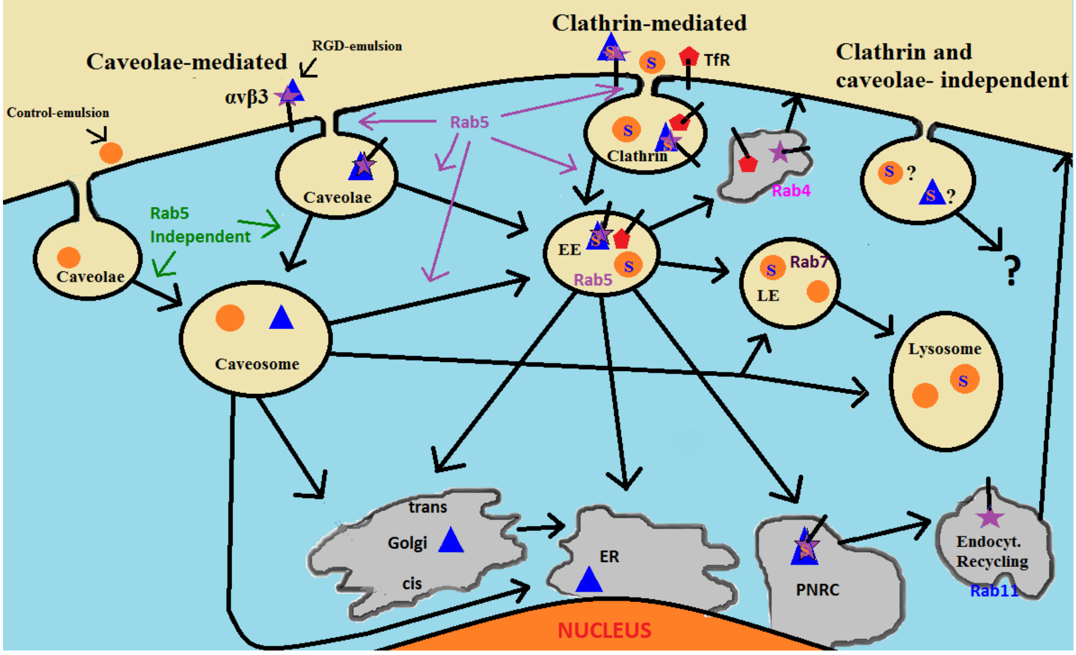
Clathrin-mediated
Caveolae-mediated
RGD-emulsion
αvβ3
TfR
Clathrin and caveolae- independent
Control-emulsion
Rab5
Caveolae
Clathrin
Rab4
S
?
Rab5 Independent
Caveolae
EE
Rab5
Rab7
LE
?
Caveosome
Lysosome
trans
Golgi
cis
ER
PNRC
Endocyt. Recycling
Rab11
NUCLEUS

Figure 5.2: Illustration that summarize events along the endocytosis pathways of caveolae-mediated, clathrin-mediated and clathrin and caveolae independent endocytosis, and that indicate possible uptake and trafficking pathways for RGD and control-emulsions. The trafficking pathways of the transferrin receptor (TfR) and $\alpha_v\beta_3$ integrin receptor are included. Symbols containing an S (small) indicate that this involves only small amounts of emulsion. Abbreviations: EE=early endosomes, LE=late endosomes, ER=endoplasmatic reticulum, PNRC= perinuclear recycling compartment.

Experiments with staining of early endosomes and endocytic inhibitors suggest that the largest parts of RGD and control-emulsions are taken up through caveolae-mediated endocytosis. However, they might be internalized or sorted into different vesicles, as experiments with NIR-RGD-emulsion and rho-control-emulsion showed that they mainly resided in separate vesicles. The interaction of the RGD-emulsion with the $\alpha_v\beta_3$ integrins is a probable explanation of the sorting of RGD-emulsion into distinct vesicles. The delayed uptake of emulsions in Rab5 experiments is most likely caused by Rab5 overexpression, because Rab5 regulates internalization of caveolae vesicles as well as clathrin vesicles. As emulsions are not mainly seen in early endosomes, they are somehow sorted to avoid this. Based on literature, the most likely trafficking pathway from caveolae is Rab5-independent fusion with caveosomes. Furthermore, control-emulsions showed quite large colocalization with lysosomes already 5 minutes after incubation. It is possible that they are sorted from caveosomes and into late endosomes and/or lysosomes [122, 123], while the RGD-emulsion remains in caveosomes for extended periods of time, or is further trafficked to ER or Golgi [83]. At some, later time point, the RGD-emulsion is also trafficked to lysosomes by unknown mechanisms.

As uptake studies with endocytic inhibitors showed a small uptake also in clathrin-vesicles, while small colocalization values were found for transferrin-Alexa Fluor 488, it can be assumed that some small portion of the emulsions might be taken up by clathrin-mediated endocytosis (small portions of emulsion is marked by S in the illustration). Based on literature and the lysosome staining experiment, it is further likely that the control-emulsion follows the maturation pathway of early endosomes- late endosomes-lysosomes [57, 80, 81]. However, for the RGD-emulsion it is possible that it follows the long pathway of the $\alpha_v\beta_3$ integrins that are taken up by the clathrin-mediated mechanism, which involves further trafficking to the perinuclear recycling compartment within approximately 5 minutes (discussed in section 5.2.3).

In flow cytometric uptake studies it was shown that some parts of the emulsion are not taken up by neither clathrin-mediated mechanism nor caveolae-mediated mechanism. Macropinocytosis and/or clathrin and caveolae independent endocytosis are possibilities, or other unknown mechanisms. Uptake by clathrin and caveolae independent endocytosis have been shown to bypass the lysosomes, but details about these mechanism are scarce, so this possibility is denoted by question marks in the illustration.

5.5 Implications and Further Work

In this thesis it has been shown that the targeting of nanoemulsions with RGD enhances the uptake in HUVECs substantially compared to the non-targeted version. Furthermore, the RGD-emulsion avoids the lysosomes, which can improve the efficiency of drug delivery immensely. The emulsions are made up of biocompatible and biodegradable compounds approved by the FDA, and in light of this the emulsions have a great potential for reaching clinical trials.

Further work must be invested to elucidate the uptake and trafficking pathways of the emulsions to greater detail. For example, plasmids encoding for fluorescent proteins associated with the ER and Golgi can be used to investigate if the RGD-emulsions indeed end up here in live cells. Caveolae can be stained to support the theory of caveolae-mediated uptake. It would also be preferable to repeat the early endosome staining experiments to see if optimization of the protocol can affect the results. Repetition of the NIR-RGD and Rho-control emulsion experiments could be done to investigate what happens after 24 hours, and compare this to the lysosome colocalization. Moreover, the dynamics and stability of the emulsions inside the cells should be assessed. As an example, knowledge about the timing of emulsion degradation in the cells can be obtained. If the time frame of degradation is known, the results can be compared to other experiments, such as the time frame of RGD-emulsion colocalization in lysosomes.

Currently, coworkers are conducting *in vivo* work with emulsions as probes for molecular imaging of angiogenesis. It has been shown that the RGD-emulsions bind to endothelial cells in tumor vessel walls in mice to a much greater extent than the control-emulsion. Furthermore, this binding sustains for prolonged periods of time, up to 48 hours post injection. This emphasizes the value of nanoemulsions not only for drug delivery purposes, but also for imaging and multimodality purposes.

Chapter 6

Conclusion

Through experiments conducted in this thesis it is clear that endocytic uptake and trafficking is highly complex and that single factors alone do not determine uptake mechanism and destiny of internalized emulsions. However, CLSM and flow cytometry studies did elucidate certain aspects concerning RGD and control-emulsion uptake and trafficking.

First of all, it was found that RGD-emulsions are taken up by HUVECs mainly due to interaction with $\alpha_v\beta_3$ integrins. The uptake amount was approximately 4.5 times larger than that of control-emulsions, and control-emulsions are most probably taken up by non-specific interaction with cell membrane components. Moreover, both emulsion types are *mainly* taken up by caveolae-mediated endocytosis, but also to a small extent by clathrin-mediated endocytosis and other unidentified processes. Results further indicate that both emulsions avoid the early endosomes to a great extent, but that control-emulsions reach the lysosomes shortly after incubation. RGD-emulsion colocalization with lysosomes was not observed until 24 hours after incubation. Although both emulsions are taken up by caveolae-mediated mechanisms, they are not taken up/sorted into the same vesicles. This was seen from experiments with NIR-RGD-emulsions and Rho-control-emulsions. However, they do fuse with time, especially in the perinuclear region of the cells.

A simplified proposal can be suggested concerning the *main* uptake and trafficking pathway for emulsions: both RGD and control-emulsions are taken up by caveolae-mediated mechanisms, however, they are taken up or sorted into distinct vesicles due to RGD-emulsion interaction with $\alpha_v\beta_3$ integrins. Further, both emulsions are trafficked to caveosomes. From caveosomes, the control-emulsion is transported to the late endosomes or lysosomes, whereas RGD-emulsion may be transported to Golgi or ER. Finally, the RGD-emulsion is also trafficked to the lysosomes.

Bibliography

[1] V. Wagner, A. Dullaart, A-K. Bock and A. Zweck. *The Emerging Nanomedicine Landscape.* Nature Biotechnology, 2006; 24; 10; 1211-1217

[2] Y. Malam, M. Loizidou, A. M. Seifalian, *Liposomes and Nanoparticles: Nanosized Vehicles for Drug Delivery in Cancer.* Trends in Pharmacological Sciences, 2000 ;30; 11; 592-599

[3] C.J. Sunderland, M. Steiert, J.E. Talmadge, A.M. Derfus, S.E. Barry, *Targeted Nanoparticles for Detecting and Treating Cancer.* Drug. Dev. Res., 2006; 67; 70-93

[4] Y. Liu, H. Miyoshi, M. Nakamura, *Nanomedicine for Drug Delivery and Imaging: A Promising Avenue for Cancer Therapy and Diagnosis Using Targeted Functional Nanoparticles* Int. J. Cancer, 2007; 120; 2527-2537

[5] E. Blanco, C. W. Kessinger, B. D. Sumer, J. Gao, *Multifunctional Micellar Nanomedicine for Cancer Therapy.* Exp. Biol. Med., 2009; 234; 2; 123-131

[6] L. Zhang, F. X. Gu, J. M. Chan, A. Z. Wang, R. S. Langer, O. C. Farokhzad, *Nanoparticles in Medicine: Therapeutic Applications and Developments.* Clinical Pharmacology & Therapeutics, 2008; 83; 5; 761-769

[7] J. Panyam, V. Labhasetwar, *Biodegradable Nanoparticles for Drug and Gene Delivery to Cells and Tissue.* Advanced Drug Delivery Reviews, 2003; 55; 329-347

[8] H. Chen, L. Wang, J. Yeh, X. Wu, Z. Cao, Y. A. Wang, M. Zhang, L. Yang, H. Mao, *Reducing Non-specific Binding and Uptake of Nanoparticles and Improving Cell Targeting with an Antifouling PEO-b-PgMPS Copolymer Coating.* Biomaterials, 2010; 31; 5397-5407

[9] K. Park, S. Lee, E. Kang, K. Kim, K. Choi, I. C. Kwon, *New Generation of Multifunctional Nanoparticles for Cancer Imaging and Therapy.* Adv. Funct. Mater., 2009; 19; 1553-1566

[10] A. Gianella, P. A. Jarzyna, V. Mani, S. Ramachandran, C. Calcagno, J. Tang, B. Kann, W. J. R. Dijk, V. L. Thijssen, A. W. Griffioen, G. Storm, Z. A. Fayad, W. J. M. Mulder, *Multifunctional Nanoemulsion Platform for Imaging Guided Therapy Evaluated in Experimental Cancer.* ACS Nano, 2011 May 25. [Epub ahead of print]

[11] P. A. Jarzyna, T. Skajaa, A. Gianella, D. P. Cormode, D. D. Samber, S. D. Dickson, W. Chen, A. W. Griffioen, Z. A. Fayad. W. J.M. Mulder, *Iron Oxide Core Oil-in-water Emulsions as a Multifunctional Nanoparticle Platform for Tumor Targeting and Imaging.* Biomaterials, 2009; 30; 6947-6954

[12] S. Hak, H. M. H. F. Sanders, G. J. Strijkers, K. Nicolay, *Lipid-Based Nanoparticles as MRI Contrast Agents: Characterization and Application* Encyclopedia of Nanoscience and Nanotechnology, 2009; X; 1-24

[13] O. V. Salata, *Applications of nanoparticles in biology and medicine.* Journal of Nanobiotechnology, 2004;2;3

[14] J. F. Kukowska-Latallo, K. A. Candido, Z. Cao, S. S. Nigavekar, I. J. Majoros, T. P. Thomas, L. P. Balogh, M. K. Khan, J. R. Baker Jr., *Nanoparticle Targeting of Anticancer Drug Improves Therapeutic Response in Animal Model of Human Epithelial Cancer.* Cancer Res., 2005; 65; 5217-5324

[15] D. Bhadra, S. Bhadra, N. K. Jain, *PEGylated Peptide Dendrimeric Carriers for the Delivery of Antimalarial Drug Chloroquine Phosphate.* Pharm. Res., 2006; 23; 623-633

[16] H. L. Wong, A. M. Rauth, R. Benadayan, X. Y. Wu, *In vivo Evaluation of a new Polymer-lipid Hybrid Nanoparticle (PLN) Formulation of Doxorubicin in a Murine Solid Tumor Model.* Eur. J. Pharm. Biopharm., 2007; 65; 300-308

[17] A. Scnyder, S. Krahenbuhl, J. Drewe, J. Huwyler, *Targeting of Daunomycin Using Biotinylated Immunoliposomes: Pharmacokinetics, Tissue Distribution and in vitro Pharmacological Effects.* J. Drug Target, 2005; 13; 325-335

[18] S. de Jong, G. Chikh, L. Sekirov, S. Raney, S. Semple, S. Klimuk, N. Yuan, M. Hope, P. Cullis, Y. Tam, *Encapsulation in Liposomal Nanoparticle Enhances the Immunostimulatory, Adjuvant and Anti-tumor Activity of Subcutaneously Administered CpG ODN.* Cancer Immunol. Immunother., 2007; 56(8);1251-64.

[19] A. Pal, S. Khan, Y. Wang, N. Kamath, A. K. Sarkar, A. Ahmad, S. Sheikh, S. Ali, D. Carbonaro, A. Zhang, I. Ahmad, *Clinical Safety, Pharmacokinetics and Antitumor Efficacy Profile of Liposome-entrapped SN-38 Formulation.* Anticancer Research, 2005; 25;331-342

[20] R. Singh, K. T. Al-Jamal, L. Lacerda, K. Kostarelos, *Nanoengineering Artificial Lipid Envelopes Around Adenovirus by Self-Assembly.* ACS NANO, 2008; 2; 5; 1040-1050

[21] M. Everts, V. Saini, J. L. Leddon, R. J. Kok, M. Stoff-Khalili, M. A. Preuss, C. L. Millican, G. Perkins, J. M. Brown, H. Bagaria, D. E. Nikles, D. T. Johnson, V. P. Zharov, D. T. Curiel, *Covalently Linked Au Nanoparticles to a Viral Vector: Potential for Combined Photothermal and Gene Cancer Therapy.* Lett., 2006; 6; 587-591

[22] S. P. Strand, S. Lelu, N. K. Reitan, C. de Lange Davies, P. Artursson, K. M. Vårum, *Molecular Design of Chitosan Gene Delivery Systems with an Optimized Balance between Polyplex Stability and Polyplex Unpacking.* Biomaterials, 2010; 31; 975-987

[23] A. G. Ziady, M. Kotlarchyk, L. Bryant, M. McShane, Z. Lee, *Bioluminescent Imaging of Reporter Gene Expression in the Lungs of Wildtype and Model Mice Following the Administration of PEG-Stabilized DNA Nanoparticles.* Microscopy Research and Technique, 2010; 73; 918-928

[24] L. R. Hirsch, R. J. Stafford, J. A. Bankson, S. R. Sershen, B. Rivera, R. E. Price, J. D. Hazle, N. J. Halas, J. L. West, *Nanoshell-mediated Near-infrared Thermal Therapy of Tumors under Magnetic Resonance Guidance.* Proc. Natl. Acad. Sci., 2003; 100; 13549-13554

[25] Q. Huo, J. Liu, L.-Q. Wang, Y. Jiang,T. N. Lambert, E. Fang, *A New Class of Silica Cross-linked Micellar Core-Shell Nanoparticles.* J. Am. Chem. Soc., 2006; 128; 6447-6453

[26] M. E. Davis, Z. G. Chen, M. Gurbuz, T. M. Simone, and S. A. Mousa. *Nanoparticle therapeutics: an emerging treatment modality for cancer.* Nat. Rev. Drug Discov., 2008; 7; 771-82

[27] X. Yan, G.L. Scherphof, J.A. Kamps, *Liposome opsonization.* J. Liposome Res. 2005;15:10939

[28] T. M. Allen, P. R. Cullis, *Drug Delivery Systems: Entering the Mainstream.* Science, 2004; 303; 1808- 1822

[29] W. C. Russell, *Update on adenovirus and its vectors.* Journal of general Virology, 2000; 81; 2573-2604

[30] J. M. Wilson, *Lessons learned from the gene therapy trial for ornithine transcarbamylase deficiency.* Molecular Genetics and Metabolism, 2009; 96; 151-157

[31] X. Huang, P. K. Jain, I. H. El-Sayed, M. A. El-Sayed, *Plasmonic photothermal therapy (PPTT) using gold nanoparticles.* Laser. Med. Sci., 2008; 23; 217-228

[32] F. Zhou, D. Xing, Z. Ou, B. Wu, *Cancer photothermal therapy in the near-infrared region using single-walled carbon nanotubes.* Journal of Biomedical Optics, 2009; 14; 021009-1 - 021009-7

[33] J. Liu, J. Li, T. J. Rosol. X. Pan, J. L. Voorhees, *Biodegradable Nanoparticles for Targeted Ultrasound Imaging of Breast Cancer Cells* in vitro. Phys. Med. Biol., 2007; 4739-4747

[34] M. Liong, J. Lu, M. Kovochich, T. Xia, S. G. Ruehm, A. E. Nel, F. Tamanoi, J. I. Zink, *Multifunctional Inorganic Nanoparticles for Imaging, Targeting, and Drug Delivery.* ACS Nano, 2008; 2; 5; 889-896

[35] D. L. J. Thorek, A. K. Chen, J. Czupryna, A. Tsourkas, *Superparamagnetic Iron Oxide Nanoparticle Probes for Molecular Imaging.* Annals of Biomedical Engineering, 2006; 34; 1; 22-38

[36] G. M. Lanza, K. D. Wallace, M. J. Scott, W. P. Cacheris, D. R. Abendschein, D. H. Christy, A. M. Sharkey, J. G. Miller, P. J. Gaffney, S. A. Wickline, *A Novel Site-targeted Ultrasonic Contrast Agent with Broad Biomedical Application.* Circulation, 1996; 94; 3334-3340

[37] C. M. Moran, J. A. Ross, C. Cunningham, M. Butler, T. Anderson, D. Newby, K. A. Fox, W. N. McDicken, *Manufacture and Acoustical Characterization of a High-frequency Contrast Agent for Targeting Applications.* Ultrasound Med. Biol., 2006; 32; 421-428

[38] M. A. Wheatley, F. Forsberg, N. Dube, M. Patel, B. E. Oeffinger, *Surfactant-Stabilized Contrast Agent on the Nanoscale for Diagnostic Ultrasound Imaging.* Ultrasound Med. Biol., 2006; 32; 83-93

[39] N. Sanvicens, M. P. Marco, *Multifunctional nanoparticles - properties and prospects for their use in human medicine.* Trends in Biotechnology, 2008; 26; 8

[40] E. Helgesen, Project paper: *Characterization of Lipid-based Nanoparticles.* Norwegian University of Science and Technology, Institute of Physics, 2010.

[41] M.C. Sandstrom, E. Johansson, K. Edwards, *Structure of Mixed Micelles Formed in PEG-Lipid/Lipid Dispersions.* Langmuir 2007; 23; 4192-4198

[42] R. Brasseur, B. de Kruijff, J-M. Ruysschaert, *Mode of organization of lipid aggregates: A conformational analysis.* Bioscience Reports, 1984; 4; 259-267

[43] V. Degiorgio and M. Corti, *Physics of Amphiphiles: Micelles, Vesicles, Microemulsions.* North-Holland Physics Publishing, 1985.

[44] Philip Nelson *Biological Physics. Energy, Information, Life.* Updated First Edition, W. H. Freeman and Company, New York, 2008.

[45] S-W. Hui, A. Sen, *Effects of lipid packing on polymorphic phase behavior and membrane properties.* Proc. Natl. Acad. Sci., 1989; 86; 5825-5829

[46] M. Antonietti, S. Förster, *Vesicles and Liposomes: A Self-Assembly Principle Beyond Lipids.* Adv. Mater., 2003; 15; 16; 1323- 1333

[47] N. J. Vogel, C. L. Vogel, I. C. Henderson, *The Role of Liposomal Anthracyclines and Other Systemic Therapies in Management of Advanced Breast Cancer.* Semin. Oncol., 2004; 31; 106-146

[48] A. D. Bangham, *Liposomes: the Babraham connection.* Chemistry and Physics of Lipids, 1993; 64; 275- 285

[49] G. Sessa, G. Weissmann, *Incorporation of Lysozyme into Liposomes.* The Journal of Biological Chemistry, 1970; 245; 13; 3295- 3301

[50] G. Gregoriadis, B. E. Ryman, *Liposomes as Carriers of Enzymes or Drugs: a New Approach to the Treatment of Storage Diseases.* Biochem. J.; 5; 124; 58P

[51] M. de Silva, B. L. Hazleman, D. P. Page Thomas, P. Wraight, *Liposomes in Arthritis: a New Approach.* The Lancet, 1979; June 23; 1320- 1322

[52] D. D. Lasic, F. J. Martin, A. Gabizon, S. K. Huang, D. Papahadjopoulos, *Sterically Stabilized Liposomes: a Hypothesis on the Molecular Origin of th Extended Circulation Times.* Biochimica et Biophysica Acta, 1991; 1070; 187- 192

[53] K.L. Mittal, B. Lindman (Eds.), *Surfactants in Solution.* Vols. 13, Plenum Press, New York, 1991; Vols. 1-3

[54] V. Weissig, K.R. Whiteman, V.P. Torchilin, *Accumulation of liposomal- and micellar-bound protein in solid tumor.* Pharm. Res., 1998; 15; 15521556.

[55] T. G. Mason, J. N. Wilking, K. Meleson, C. B. Chang, S. M. Graves, *Nanoemulsions: formation, structure, and physical properties.* J. Phys.: Condens. Matter 18, 2006

[56] S. Hak, *Combined in vivo confocal laser scanning microscopy and magnetic resonance imaging to study an* $\alpha_v\beta_3$ *–integrin targeted nanoemulsion.* Poster for World Molecular Imaging Congress, 2011, San Diego

[57] W. M. Becker, L. J. Kleinsmith, J. Hardin, G. P. Bertoni *The World of the Cell.* Seventh Edition. Pearson, San Francisco, 2009.

[58] Edited by Morton Rosoff, *Vesicles.* Surfactant science series, Marcel Dekker New York, 1996; volume 62

[59] S.Raffy, J. Teissie, *Control of Lipid Membrane Stability by Cholesterol Content.* Biophysical Journal, 1999; 76; 2072-2080

[60] D. R. Senger, L. Van De Water, L. F. Brown, J. A. Nagy, K. Yeo, T. Yeo, B. Berse, R. W. Jackman, A. M. Dvorak, H. F. Dvorak, *Vascular permeability factor (VPF, VEGF) in tumor biology.* Cancer and Metastasis Reviews, 1993; 12; 303-324

[61] H. Maeda, J. Wu, T. Sawa, Y. Matsumura, K. Hori, *Tumor Vascular Permeability and the EPR Effect in Macromolecular Therapeutics: A Review.* Journal of Controlled Release, 2000; 65; 271-284

[62] D. Bovelli, G. Plataniotis, F. Roila, *Cardiotoxicity of chemotherapeutic agents and radiotherapy-related heart disease: ESMO Clinical Practice Guidelines.* Annals of Oncology, 2010; 21, 277- 282

[63] S.K Hobbs, W. L. Monsky, F. Yuan, W.G. Roberts, L. Griffith, V.P. Torchilin, R.K. Jain, *Regulation of transport pathways in tumor vessels: Role of tumor type and microenvironment.* Proc. Natl. Acad. Sci. USA, 1998; 95; 4607-4612

[64] D. Uyar, B. Kulp, G. Peterson, K. Zanotti, M. Markman, J. Belinson, *Cardiac Safety Profile of Prolonged (¿6 cycles) Pegylated Liposomal Doxorubicin Administration in Patients with Gynecologic Malignancies.* Gynecol. Oncol., 2004; 94; 147-151

[65] K. Egami, T. Murohara, M. Aoki, T. Matsuishi, *Ischemia-induced Angiogenesis: Role of Inflammatory Response Mediated by P-selectin.* Journal of Leukocyte Biology, 2006; 79; 971-976

[66] G. McMahon, *VEGF Receptor Signaling in Tumor Angiogenesis.* The Oncologist, 2000; 5; 3-10

[67] K. Pietras, T. Sjöblom, K. Rubin. C-H. Heldin, A. Östman, *PDGF Receptors as Cancer Drug Targets.* Cancer Cell, 2003; 3; 439-443

[68] R. Stupp, M. E. Hegi, B. Neyns, R. Goldbrunner, U. Schlegel, P. M. J. Clement, G. G. Grabenbauer, A. F. Ochsenbein, M. Simon, P-Y. Dietrich, T. Pietsch, C. Hicking, J-C. Tonn, A-C. Diserens, A. Pica, M. Hermisson, S. Krueger, M. Picard, M. Weller, *Phase I/IIa Study of Cilengitide and Temozolomide With Concomitant Radiotherapy Followed by Cilengitide and Temozolomide Maintenance Therapy in Patients With Newly Diagnosed Glioblastoma.* Journal of Clinical Oncology, 2010; 28; 2712-2718

[69] J. S. Desgrosellier, D. A. Cheresh, *Integrins in Cancer: Biological Implications and Therapeutic Opportunities.* Nature Reviews Cancer, 2010; 10; 9-19

[70] M. C. Chamberlain, *What Role Should Cilengitide Have in the Treatment of Glioblastoma.* Journal of Clinical Oncology, 2010; 28; 695

[71] M. Oba, S. Fukushima, N. Kanayama, K. Aoyagi, N. Nishiyama, H. Koyama, K. Kataoka, *Cyclic RGD Peptide-Conjugated Polyplex Micelles as a Targetable Gene Delivery System Directed to Cells Possessing* $\alpha_v\beta_3$ *and* $\alpha_v\beta_5$ *Integrins.* Bioconjugate Chem., 2007; 18; 1415-1423

[72] U. S. Toti, B. R. Guru, A. E. Grill, J. Panyam, *Interfacial Activity Assisted Surface Functionalization: A Novel Approach To Incorporate Maleimide Functional Groups and cRGD Peptide on Polymeric Nanoparticles for Targeted Drug Delivery.* Molcular Pharmaceutics, 2010; 7; 4; 1108-1117

[73] R. Nallamothu, G. C. Wood, C. B. Pattillo, R. C. Scott, M. F. Kiani, B. M. Moore, L. A. Thoma, *A Tumor Vasculature Targeted Liposome Delivery System for Combretastatin A4: Design, Characterization, and In Vitro Evaluation.* AAPS PharmSciTech 2006; 7 (2) Article 32

[74] P. A. Netti, D. A. Berk, M. A. Swartz, A. J. Grodizinsky, R. K. Jain, *Role of Extracellular Matrix Assembly in Interstitial Transport in Solid Tumors.* Cancer Research, 2000; 60; 2497- 2503

[75] K. B. Neeves, A. J. Sawyer, C. P. Foley, W. Mark Saltzman, W. L. Olbricht, *Dilation and Degradation of the Brain Extracellular Matrix Enhances Penetration of Infused Polymer Nanoparticles.* Brain Research, 2007; 1180; 121-132

[76] W. P. Daley, S. B. Peters, M. Larsen, *Extracellular Matrix Dynamics in Development and Regenerative Medicine* Journal of Cell Science, 2008; 255-264

[77] P. J. K. Kuppen, M. M. van der Eb, L. E. Jonges, M. Hagenaars, M. E. Hokland, U. Nannmark, R. H. Goldfarb, P. H. Basse, G. J. Fleuren, R. C. Hoeben, C. J. H. van de Velde, *Tumor Structure and Extracellular Matrix as a Possible Barrier for Therapeutic Approaches Using Immune Cells or Adenoviruses in Colorectal Cancer.* Histochem. Cell. Biol., 2000; 115; 67-72

[78] S. Ramanujan, A. Pluen, T. D. McKee, E. B. Brown, Y. Boucher, R. K. Jain, *Diffusion and Convection in Collagen Gels: Implications for Transport in the Tumor Interstitium.* Biophysical Journal, 2002; 83; 1650-1669

[79] J. M. Besterman, R. B. Low, *Endocytosis: a review of mechanisms and plasma membrane dynamics.* Biochem. J., 1983; 210; 1-13

[80] S. D. Conner, S. L. Schmid, *Regulated Portals of Entry Into the Cell.* Nature, 2003; 422; 37- 44

[81] I. A. Khalil, K. Kogure, H. Akita, H. Harashima, *Uptake Pathways and Subsequent Intracellular Trafficking in Nonviral Gene Delivery.* Pharmocological Reviews, 2006; 58; 32-45

[82] G. Sahay, D. Y. Alakhova, A. V. Kabanov, *Endocytosis of Nanomedicines.* Journal of Controlled Release, 2010; 145; 182-195

[83] L. Pelkmans, A. Helenius, *Endocytosis via Caveolae.* Traffic, 2002; 3; 311-320

[84] G. E. Palade, *Fine structure of blood capillaries.* Journal of Applied Physics, 1953; 24; 1424

[85] E. Yamada, *The fine structure of the gall bladder epithelium of the mouse.* Journal of Biophys. Biochem. Cytol., 1955; 1; 445-458

[86] B. Razani, M. P. Lisanti, *Caveolin-deficient Mice: Insights into Caveolar Function and Human Disease.* J. Clin. Invest., 2001; 108; 1553-1561

[87] E-M. Damm, L. Pelkmans, J. Kartenbeck, A. Mezzacasa, T. Kurzchalia, A. Helenius, *Clathrin- and caveolin- 1- independent endocytosis: entry of simian virus 40 into cells devoid of caveolae.* The Journal of Cell Biology, 2005; 168; 3; 477-488

[88] V. Puri, R. Watanabe, R. D. Singh, M. Dominguez, J. C. Brown, C. L. Wheatley, D. L. Marks, R. E. Pagano, *Clathrin-dependent and -independent internalization of plasma membrane sphingolipids initiates two Golgi targeting pathways.* The Journal of Cell Biology, 2001; 154; 3; 535-547

[89] J. Rejman, V. Oberle, I. S. Zuhorn, D. Hoekstra, *Size-dependent Internalization of Particles via the Pathways of Clathrin- and Caveolae-mediated Endocytosis.* Biochem. J., 2004; 377; 159-169

[90] M. Oba, K. Aoyagi, K. Miyata, Y. Matsumoto, K. Itaka, N. Nishiyama, Y. Yamasaki, H. Koyama, K. Kataoka, *Polyplex Micelles with Cyclic RGD Peptide Ligands and Disulfide Cross-Links Directing to the Enhanced Transfection via Controlled Intracellular Trafficking.* Molcular Pharmaceutics, 2008; 5; 6; 1080-1092

[91] *LysoTracker® and LysoSensor™ Probes.* Invitrogen Detection Technologies, Revised: 15-October-2007; MP 07525. Available at invitrogen.com

[92] *Transferrin Conjugates* Invitrogen Detection Technologies, Revised: 19-June-2007; MP 02871. Available at invitrogen.com

[93] M. Lakadamyali, M. J. Rust, X. Zhuang, *Ligands for Clathrin-Mediated Endocytosis Are Differentially Sorted into Distinct Populations of Early Endosomes.* Cell, 2006; 124; 997-1009

[94] *CellLight™ Reagents ∗BacMam 2.0∗.* Invitrogen Detection Technologies, Revised: 6-January-2011; MP 10582. Available at invitrogen.com

[95] V. Zinchuk, O. Zinchuk, T. Okada, *Quantitative Colocalization Analysis of Multicolor Confocal Immunofluorescence Microscopy Images: Pushing Pixels to Explore Biological Phenomena.* Acta histochem., 2007; 40; 101-111

[96] L-H. Wang, K. G. Rothberg, R. G. W. Anderson, *Mis-Assembly of Clathrin Lattices on Endosomes Reveals a Regulatory Switch for Coated Pit Formation.* The Journal of Cell Biology, 1993; 123; 1107-1117

[97] S-F. Peng, M. T. Tseng, Y-C. Ho, M-C. Wei, Z-X. Liao, H-W. Sung, *Mechanisms of Cellular Uptake and Intracellular Trafficking with Chitosan/DNA/poly(γ-glutamic acid) Complexes as a Gene Delivery Vector.* Biomaterials, 2011; 32; 239-248

[98] R. G. Parton, B. Jogerst, K. Simons, *Regulated internalization of caveolae.* The Journal of Cell Biology, 1994; 127; 1199-1215

[99] I. R. Nabi, P. U. Le, *Caveolae/raft dependent endocytosis.* The Journal of Cell Biology, 2003; 161; 4; 673-677

[100] Malvern Instruments Ltd., *Zetasizer Nano Series User Manual.* Malvern, Worcestershire, MANO317, Issue 2.1, July 2004.

[101] R. Pecora, *Dynamic Light Scattering From Macromolecules.* Department of Chemistry, Stanford University, 1993; SPIE Vol. 1884,

[102] N. S. Claxton, T. J. Fellers, M. W. Davidson, *Laser Scanning Confocal Microscopy.* Department of Optical Microscopy and Digital Imaging, National High Magnetic Field Laboratory, The florida State University (http://olympusfluoview.com)

[103] J. B. Pawley, *Handbook of Biological Confocal Microscopy.* Third Edition, Springer Science + Business Media, LCC, 2006

[104] D. Murphy, *Differential interference contrast (DIC) microscopy and modulation contrast microscopy.* Fundamentals of Light Microscopy and Digital Imaging, Wiley-Liss, New York, 2001; 153168

[105] P. N. Prasad, *Introduction to Biophotonics.* John Wiley and Sons, Inc, New Jersey, 2003

[106] M. Rahman, *Introduction to Flow Cytometry.* SeroTec, Ltd, 2006

[107] P. T. Caswell, J. C. Norman, *Integrin Trafficking and the Control of Cell Migration.* Traffic, 2006; 7; 14-21

[108] S. Cressman, Y. Sun, E. J. Maxwell, N. Fang, D. D. Y. Chen, P. R. Cullis, *BInding and Uptake of RGD-Containing Ligands to Cellular $\alpha_v\beta_3$ Integrins.* Int. J. Pept. Res. Ther., 2009; 15; 49-59

[109] X-B. Xiong, Z. Ma, R. Lai, A. Lavasanifar, *Therapeutic Response to Multifunctional Polymeric Nano-conjugates in the Targeted Cellular and Subcellular Delivery of Doxorubicin.* Biomaterials, 2010; 757-768

[110] S. Shimoda, S. Sawada, K. Akiyoshi, *Cell Specific Peptide-Conjugated Polysaccharide Nanogels for Protein Delivery.* Macromol. Biosci., 2011; 11; 000-000 (early publication, no side numbers)

[111] Y-B. Lim, O-J. Kwon, E. Lee, P-H. Kim, C-O. Yun, M. Lee, *A Cyclic RGD-Coated Peptide Nanoribbon as a Selective Intracellular Nanocarrier.* Org. Biomol. Chem., 2008; 6; 1944-1948

[112] S. Bolte, F. P. Cordelieres, *A guided Tour into Subcellular Colocalization Analysis in Light Microscopy.* Journal of Microscopy, 2006; 224; 213-232

[113] M. Hagiwara, Y. Shirai, R. Nomura, M. Sasaki, K. Kobayashi, T. Tadokoro, Y. Yamamoto, *Caveolin-1 Activates Rab5 and Enhances Endocytosis through Direct Interaction.* Biochem. Biophys. Res. Commun, 2009; 378;73-78

[114] J. L. Seachrist, P. H. Anborgh, S.S.G. Ferguson, *β_2-Adrenergic Receptor Internalization, Endosomal Sorting, and Plasma Membrane Recycling Are Regulated by Rab GTPases.* The Journal of Biological Chemistry, 2000; 275; 35;27221-27228

[115] B. Sönnichsen, S. De Renzis, E. Nielsen, J. Rietdorf, M. Zerial, *Distinct Membrane Domains on Endosomes in the Recycling Pathway Visualized by Multicolor Imaging of Rab4, Rab5, and Rab11.* The Journal of Cell Biology, 2000; 149; 4; 901-913

[116] J. Rink, E. Ghigo, Y. Kalaidzisis, M. Zerial, *Rab Conversion as a Mechanism of Progression from Early to Late Endosomes.* Cell, 2005; 122; 735-749

[117] R. G. Parton, *Caveolae Meet Endosomes: A Stable Relationship?.* Developmental Cell, 2004; 7; 4; 458-460

[118] R. G. Parton, M. T. Howes, *Revisiting Caveolin Trafficking: The End of The Caveosome.* J. Cell Biol., 2010; 191; 3; 439-441

[119] P. Caswell, J. Norman, *Endocytic Transport of Integrins During Cell Migration and Invasion.* Trends in Cell Biology, 2008; 18; 6; 257-263

[120] C. Tekle, B. van Deurs, K. Sandvig, T-G. Iversen, *Cellular Trafficking of Quantum Dot-Ligand Bioconjugates and Their Induction of Changes in Normal Routing of Unconjugated Ligands.* Nano Letters, 2008; 8; 7; 1858-1865

[121] D. Vercauteren, R. E. Vandenbroucke, A. T. Jones, J. Rejman, J. Demeester, S. C. de Smedt, N. N. Sanders, K.Braeckmans, *The Use of Inhibitors to Study Endocytic Pathways of Gene Carriers: Optimization and Pitfalls.* Molecular Therapy, 2010; 18; 3; 561-569

[122] G. Sahay, J. O. Kim, A.V. Kabanov, T. K. Bronich, *The Exploitation of Differential Endocytic Pathways in Normal and Tumor Cells in the Selective Targeting of Nanoparticulate Chemotherapeutic Agents.* Biomaterials, 2010; 31; 923-933

[123] D. K. Sharma, A. Choudhury, R. D. Singh, C. L. Whealey, D. L. Marks, R. E. Pagano, *Glycosphingolipids Internalized via Caveolar-related Endocytosis Rapidly Merge with the Clathrin Pathway in Early Endosomes and Form Microdomains for Recycling.* The Journal of Biological Chemistry, 2003; 278; 9; 7564-7572

Appendix

Flow Cytometry Figures

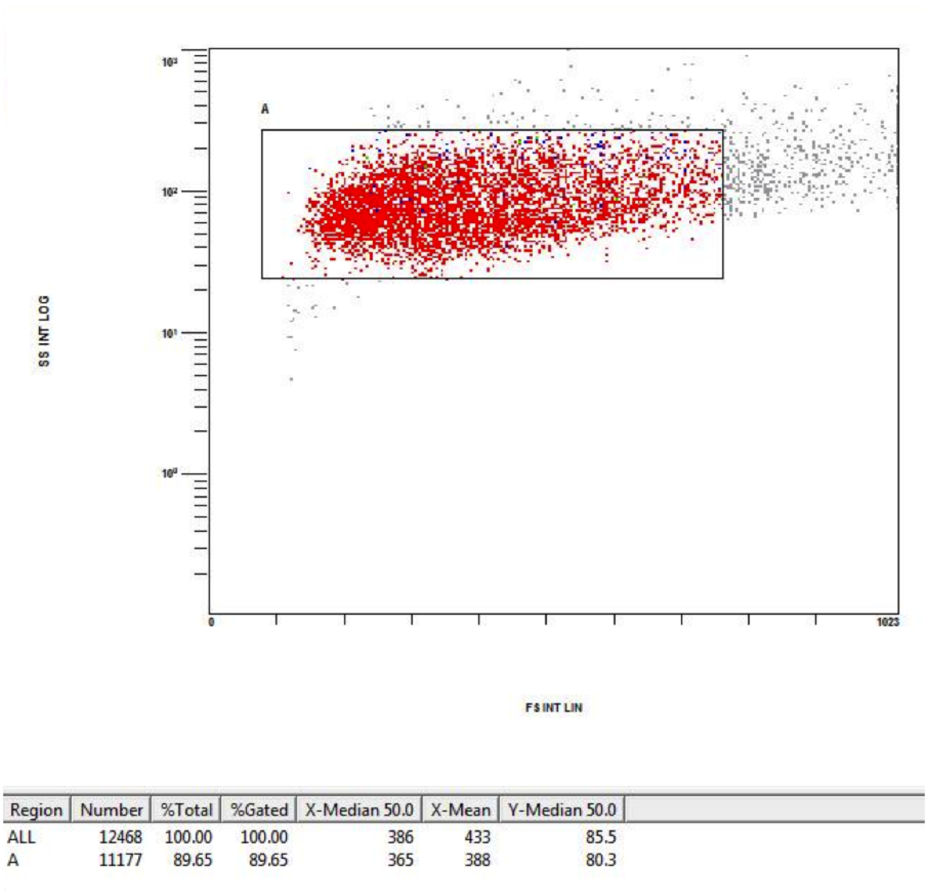

Region	Number	%Total	%Gated	X-Median 50.0	X-Mean	Y-Median 50.0
ALL	12468	100.00	100.00	386	433	85.5
A	11177	89.65	89.65	365	388	80.3

Figure 6.1: Scatterplot of FS vs. SS that shows how cells were gated to avoid dead cells, debris and cell clusters in results for flow cytometry experiments. Approximately 90% of all cells were gated.

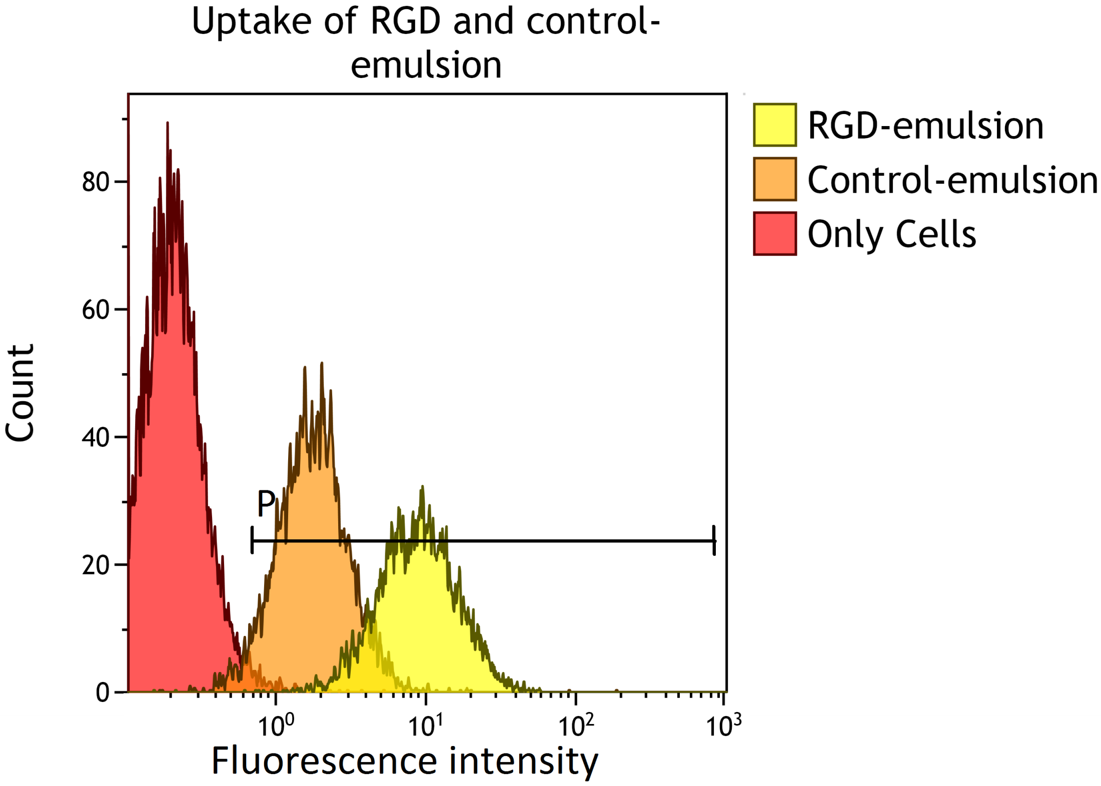

Figure 6.2: Histograms of fluorescence intensity vs. count that show how a boundary line was set to define cells that were positive for emulsion uptake (positive cells lie within the line marked by P). The threshold for the line was set to approximately 6-7 in fluorescence intensity. Fluorescence intensity below the line was considered to be autofluorescence.